PULSED N.M.R. DIFFUSION STUDIES IN BINARY LIQUID MIXTURES.

by

R.B.DAWSON, B.Sc., A.R.C.S.

A thesis submitted for the degree of Doctor of Philosophy of The University of London.

October 1973.

Department of Chemistry,
Imperial College of Science and Technology,
London, S.W.7 2AY.

ABSTRACT.

Self diffusion coefficients are reported for the protonated component in the following systems; benzene/carbon tetrachloride, n-hexane/carbon tetrachloride, octamethylcyclotetrasiloxane/perdeutero-benzene, tetraphenyltetramethylcyclotetrasiloxane/carbon tetrachloride, and polypropylene glycol/carbon tetrachloride, all at 25 C; benzene/perdeutero-chloroform and chloroform/perdeutero-benzene at 15 C.

Measurements were made at different compositions by the n.m.r. spin echo method using a pulsed field gradient. An expression has been derived which describes the evolution of the spin echo with time, which lends itself to a clear demonstration of the effects of unequal field gradient pulses.

Where sufficient data is available the self diffusion data have been compared with the predictions of the equation

$$D_{12} = D_{11}(\partial \ln a_1 / \partial \ln c_1)_{TP}$$

and the predictions of a hard sphere model based on Enskog's equations for diffusion in a dense, hard sphere fluid.

DEDICATED TO

VERONICA

AND MY

PARENTS.

ACKNOWLEDGEMENT.

My best thanks are due to J.A. Barrie and Dick Sheppard for their continued interest, support, and assistance.

Thanks are due to the technical staff in the mechanical, glass blowing, and electrical workshops.

Financial support was provided by the Science Research Council through the award of a Research Studentship.

Finally, I should like to say a special thank you to my wife for her patient support over the past three years.

CONTENTS.

	page
Chapter 1: INTRODUCTION.	8
Chapter 2: TRANSLATIONAL DIFFUSION MEASURED BY N.M.R. METHODS.	11
2-1 Introduction.	11
2-2 Nuclear Magnetic Energy Levels and the Net Magnetization Vector.	12
2-3 The Bloch Equations.	15
2-4 The Rotating Frame of Reference.	16
2-5 Pulse Methods.	18
2-6 The Effect of Diffusion in the Presence of a Steady Field Gradient.	20
2-7 The Effect of Diffusion in the Presence of a Pulsed Field Gradient.	21
2-8 The Stimulated Echo.	23
2-9 Derivation of the Diffusion Attenuation Term in the Pulsed Field Gradient Experiment.	25
2-10 The Determination of the Self Diffusion Coefficient by Following the Variation of $T_{1\rho}$ with H_1.	33
2-11 A Comparison of the N.M.R. Method with Other Methods for the Determination of Self Diffusion Coefficients.	35
Chapter 3: A SUMMARY OF DIFFUSION THEORY RELEVANT TO THE TREATMENT OF THE EXPERIMENTAL RESULTS.	39
3-1 Introduction.	39
3-2 Fick's Laws.	39
3-3 The Phenomenological Description of Diffusion.	42
3-4 The Statistical Mechanical Theory of Bearman.	52
3-5 Enskog's Theory for Diffusion in a Dense Hard Sphere System.	55

page

3-6 The Radial Distribution Function. 58

Chapter 4: N.M.R. INSTRUMENTATION. 60

4-1 Introduction. 60

4-2 Pulsed and Continuous Wave N.M.R. Spectrometers. 60

4-3 The Bruker B-KR304s. 62

4-4 Other Instrumental Methods. 74

Chapter 5: EXPERIMENTAL PROCEDURE AND SOURCES OF ERROR. 77

5-1 Introduction. 77

5-2 Preparation of Samples. 77

5-3 Positioning the Probe in the Magnetic Field. 78

5-4 Tuning the Spectrometer. 78

5-5 Adjusting the 90 and 180 Degree Pulses. 79

5-6 Positioning the Field Gradient Pulses. 79

5-7 Determination of the Diffusion Coefficient. 80

5-8 Calibration Procedure. 82

5-9 The Effect of Convection. 84

5-10 The Effect of Unequal Gradient Pulses. 85

5-11 Non Linearity of the Diode Detector at Low Signal Strengths. 97

5-12 Errors in Measurement. 98

5-13 Computer Programmes. 100

Chapter 6: EXPERIMENTAL RESULTS. 104

6-1 Introduction. 104

6-2 Materials. 105

6-3 Approximating the Molecules to Hard Spheres. 106

6-4 The Benzene-Carbon Tetrachloride System. 108

6-5 The n-Hexane-Carbon Tetrachloride System. 116

6-6 The Benzene-Chloroform System. 124

page

6-7 The Octamethylcyclotetrasiloxane-Benzene System. 129

6-8 The Tetraphenyltetramethylcyclotetrasiloxane -Carbon Tetrachloride System. 137

6-9 The Polypropylene Glycol-Carbon Tetrachloride System. 141

6-10 Discussion. 143

Appendix A: THE EVALUATION OF $\langle \varphi'^2 \rangle$. 148

Appendix B: DIFFUSION MEASUREMENTS IN NON-ELECTROLYTE LIQUID SYSTEMS BY MEANS OF THE N.M.R. SPIN ECHO METHOD. 151

BIBLIOGRAPHY. 178

Chapter 1: INTRODUCTION.

Since the first successful demonstrations of nuclear magnetic resonance phenomenon (1,2) the topic has grown at an enormous rate. Of prime importance to the chemist has been the development of high resolution instruments capable of resolving spectra to reveal chemical shifts. However, before the advent of Fourier transform n.m.r. most chemists took little interest in pulsed n.m.r. techniques.

Pulse experiments (3,4) involve subjecting the nuclei to short, intense pulses of radio frequency power and observing the subsequent behaviour of the signal induced by the nuclei. The decay of the signal provides useful information about the relaxation of the excited nuclei back to equilibrium. In liquid samples diffusion of nuclei to different parts of the polarizing magnetic field causes a rapid decay of the nuclear signal, often masking the effect of other relaxation processes. Methods were devised by Carr and Purcell (5) to reduce this diffusive effect so that other relaxation processes could be studied. At the same time it became apparent that here was an elegant method for the direct determination of self diffusion coefficients which had certain advantages over more traditional methods. The method depends on measuring the attenuation due to diffusion in a linear magnetic field gradient of the signal called the spin echo . In a later development the field gradient is pulsed on and off during the experiment (10,11). This is the method used in this work.

In this thesis the self diffusion coefficients of

components in binary liquid mixtures have been determined across the composition range. In binary liquid mixtures there are three principal diffusion coefficients which characterise translational motion of the molecules. In the appropriate reference frame a single mutual diffusion coefficient describes diffusion under the non-equilibrium condition of a concentration gradient. Two self diffusion coefficients describe the random motion of the molecules of the two components at equilibrium.

Many equations have been developed to relate these three diffusion coefficients, but all equations which can be applied to real systems involve a considerable degree of approximation either in the initial model used to describe the diffusion process or in the simplification of complex expressions to a tractable form.

One of the aims of this work has been to provide further data which can be compared with theoretical predictions. For this reason systems have been chosen for which other, necessary data are available. As far as is known none of the diffusion coefficients determined in this work has been previously measured by the n.m.r. spin echo method and only the self diffusion of benzene in carbon tetrachloride has been studied by other means.

In the following chapter the basic theory behind the n.m.r. method is presented. An alternative derivation to that of Tanner and Stejskal (10,11) of the effect of diffusion on the echo attenuation in the pulsed field gradient experiment is shown. The equation developed describes the evolution of

the spin echo with time for a cylindrical sample and lends itself to a clear demonstration of the effect of unequal magnetic field gradient pulses. In chapter 3 the diffusion theories necessary for an understanding of the results are presented. A description of pulsed n.m.r. instrumentation, with particular reference to the equipment used in these experiments, is given in chapter 4. The experimental procedures are described and particular sources of error are discussed in chapter 5. Finally, in chapter 6, the experimental results are presented and discussed.

Chapter 2: TRANSLATIONAL DIFFUSION MEASURED BY N.M.R. METHODS.

2-1 Introduction.

The self diffusion coefficient of a molecule can be measured directly by pulsed n.m.r. techniques provided that it contains a nucleus with non-zero magnetic moment. The usual technique is to impose a steady magnetic field gradient across the sample or to pulse the field gradient on and off during the experiment.

The steady field gradient method is capable of measuring self diffusion coefficients down to about 10^{-11} $m.^2$ s^{-1} and the pulsed field gradient method has extended this limit down to about 10^{-13} $m.^2 s.^{-1}$ Recently a third method has been described (6) which determines the self diffusion coefficient in viscous liquids by following the variation of the relaxation time in the rotating frame, $T_{1\rho}$, with the strength of the rotating magnetic field, H_1. For proton resonance this enables self diffusion coefficients in the range $10^{-12} m.^2 s.^{-1}$ to $5 \times 10^{-17} m.^2 s.^{-1}$ to be measured and both limits could be reduced by several orders of magnitude by applying the technique to other nuclei. These direct methods of determining the self diffusion coefficient are distinct from those n.m.r. methods which assume various relaxation mechanisms and relate experimentally determined correlation times with diffusion coefficients.

The following sections describe, in mainly classical terms, the basic n.m.r. theory that is relevant to an

understanding of how the self diffusion coefficient is determined directly by n.m.r. experiments. The methods are described and a theoretical expression for the evolution of the n.m.r. signal with time is deduced for the pulsed field gradient method. Finally a comparison is made between the n.m.r. method and other methods used for the determination of self diffusion coefficients.

2-2 Nuclear Magnetic Energy Levels and the Net Magnetization Vector.

Nuclei with a spin quantum number greater than zero have a magnetic moment, $\bar{M}$, proportional to and parallel with their angular momentum, $\bar{A}$:

$$\bar{M} = \gamma \bar{A} \ , \qquad (2\text{-}1)$$

where γ is the magnetogyric ratio.

The measurable components of angular momentum are intgral or half integral values of the modified Planck constant, $\not{h}$. The maximum component is given by $I\not{h}$, where I is the spin quantum number. The nucleus has 2I + 1 distinct states with component values I,I-1,...., -I. The magnetic moment, therefore, also has 2I + 1 states, the maximum component being designated $\bar{\mu}$. The complete set of observable values is given by $m\bar{\mu}/I$, where m, the magnetic quantum number, may have values I, I-1,....,-I.

In the absence of an external magnetic field these magnetic states all have the same energy. In the presence of a magnetic field they split.The amount of splitting is

proportional to the strength of the external field, $\bar{H}_o$. For nuclei with spin I = 1/2 the difference in energy between the lower and upper states is $2\mu H_o$.

From Planck's expression, $h\nu = \Delta E$, one can calculate the frequency of radiation required to excite nuclei from the lower to the upper energy state. $\bar{H}_o$ is typically of the order of one Tesla (10^4 gauss) which puts ν in the radio frequency region of the spectrum.

At equilibrium the nuclei are distributed among the different energy states according to a Boltzmann distribution. When disturbed from this equilibrium state the nuclear spin system returns to equilibrium by a first order relaxation process characterized by a time constant T_1. This is known as the spin–lattice relaxation time.

The n.m.r. phenomena of interest in this thesis can be adequately explained and can be more clearly visualised through a classical rather than a quantum mechanical treatment.

There will be an excess of nuclei in the lower energy state according to the Boltzmann distribution. The moments of this excess number of nuclei sum to produce an overall magnetic moment vector, $\bar{M}$, lying parallel to $\bar{H}_o$. This net magnetic moment is considered to be made up of many individual magnetic moments, sometimes called isochromatic moments, which each behave in a manner described by classical mechanics.

The torque exerted on a magnetic moment by a magnetic field inclined at an angle θ relative to the moment causes

the nuclear magnetic moment to precess about the direction of the field with a frequency given by the Larmor equation:

$$\bar{\omega}_o = -\gamma \bar{H}_o \ . \qquad (2\text{-}2)$$

This is shown in figure 2-1.

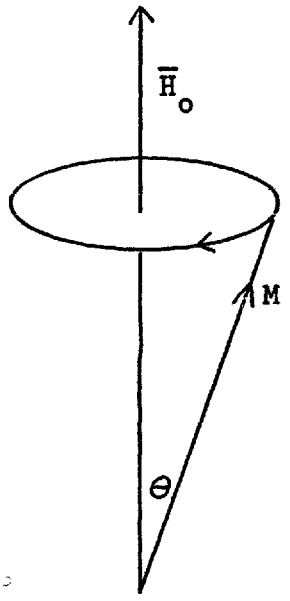


Figure 2-1: PRECESSION OF THE MAGNETIC MOMENT VECTOR $\bar{M}$ ABOUT THE MAGNETIC FIELD $\bar{H}_o$.

Experimentally, $\bar{M}$ is disturbed from its equilibrium direction by applying short radio frequency pulses to a coil surrounding the sample. This gives rise to an oscillating field $\bar{H}_x$ which is arranged to be at right angles to $\bar{H}_o$.

$$\bar{H}_x = 2\bar{H}_1 \cos \omega t. \qquad (2\text{-}3)$$

This can be considered to be the sum of two component fields of magnitude H_1 rotating in opposite directions with frequency ω.

2-3 The Bloch Equations.

The motion of the macroscopic magnetization vector, $\bar{M}$, can be explained in terms of a set of phenomenological differential equations. These are known as the Bloch equations.

The torque exerted on the moment $\bar{M}$ in the field $\bar{H}_o$ is given by:

$$\bar{M} \times \bar{H}_o = d\bar{A}/dt \ , \tag{2-4}$$

where the right hand side is the rate of change of angular momentum. Combining equations (2-1) and (2-4) one gets:

$$d\bar{M}/dt = \gamma \bar{M} \times \bar{H}_o \ . \tag{2-5}$$

Writing out the vector product in terms of components along the three cartesian axes we get:

$$\bar{M} \times \bar{H}_o = (M_y H_z - M_z H_y)\bar{i} + (M_z H_x - M_x H_z)\bar{j} + (M_x H_y - M_y H_x)\bar{k} \ . \tag{2-6}$$

When the circular frequency, ω , of the radio frequency field is in the neighbourhood of the resonance frequency, ω_o, then the actual oscillating field in the x direction can be effectively replaced by a field:

$$H_x = H_1 \cos \omega t,$$
$$H_y = \pm H_1 \sin \omega t. \tag{2-7}$$

The sense of rotation depending on the sign of γ.

Equations (2-5) to (2-7) may then be combined to give three equations for the time dependence of the components of $\bar{M}$:

$$dM_x/dt = \gamma(M_y H_o + M_z H_1 \sin \omega t) \ , \tag{2-8a}$$
$$dM_y/dt = \gamma(M_z H_1 \cos \omega t - M_x H_o) \ , \tag{2-8b}$$
$$dM_z/dt = -\gamma(M_x H_1 \sin \omega t - M_y H_1 \cos \omega t). \tag{2-8c}$$

Equations (2-8) are not yet complete because they do not take account of relaxation processes. Bloch (2) described relaxation by means of two first order processes with characteristic times T_1 and T_2. These are the time constants for the decay of the components of the magnetization vector along and perpendicular to $\bar{H}_o$ and so are sometimes known as the longitudinal and transverse relaxation times. Because of the processes involved in the relaxation, T_1 and T_2 are also known as the spin-lattice and spin-spin relaxation times. The Bloch equations then take the form:

$$dM_x/dt = \gamma(M_y H_o + M_z H_1 \sin \omega t) - M_x/T_2 \quad , \qquad (2\text{-}9a)$$

$$dM_y/dt = \gamma(M_z H_1 \cos \omega t - M_x H_o) - M_y/T_2 \quad , \qquad (2\text{-}9b)$$

$$dM_z/dt = -\gamma(M_x H_1 \sin \omega t + M_y H_1 \cos \omega t) - (M_z - M_o)/T_1 \quad , \qquad (2\text{-}9c)$$

where M_o is the equilibrium value of M_z.

These equations have been generalized by Torrey (9) to include terms due to the transfer of magnetization by diffusion. Essentially, the decay of the component of the magnetization vector perpendicular to H_o is now described by a relaxation time T_2^* given by:

$$1/T_2^* = 1/T_2 + \tfrac{1}{3} D\gamma^2 G^2 t^2 \quad , \qquad (2\text{-}10)$$

where D is the self diffusion coefficient and G is the magnetic field gradient.

2-4 The Rotating Frame of Reference.

The behaviour of the magnetic moment vector, $\bar{M}$, under the influence of external magnetic fields is most clearly

visualized with respect to a rotating frame of reference (x',y',z') rather than with respect to the laboratory frame (x,y,z). The rotating frame is such that z' lies parallel to z and x' and y' rotate about this direction at the Larmor frequency.

In the rotating frame the effective field in the z direction is given by:

$$\bar{H}_{eff} = \bar{H}_o + \bar{\omega}'/\gamma \quad , \qquad (2\text{-}11)$$

where ω' is the frequency of the rotating frame. At the Larmor frequency $\bar{\omega}' = \bar{\omega}_o = -\gamma\bar{H}_o$ and so the effective field in the z direction is zero. In a real magnetic field there will be inhomogeneities in the field and the consequence of this is that the effective field will be close to zero. Inhomogeneities are often treated as small linear gradients in the field strength. Diffusion in such a field causes attenuation of the signals following the application of r.f. pulses giving rise to such terms as that appearing in the right hand side of equation (2-10). It is this effect that forms the basis of the measurement of self diffusion coefficients.

When the r.f. pulses are applied, two magnetic fields rotating with frequencies + and - $\bar{\omega}$ in the laboratory frame are produced. When $\bar{\omega} = \bar{\omega}_o$, $\bar{H}_1$ is fixed in direction in the $x'y'$plane. It is convenient to consider $\bar{H}_1$ lying along the x' axis. The other field rotating with frequency $-\bar{\omega}$ has virtually no effect on the behaviour of the magnetization vector and can be ignored. This is because the direction of this field is changing very rapidly with respect to the magnetization vector .

2-5 Pulse Methods.

Pulse methods, first suggested by Bloch and co-workers (2), were initially demonstrated by Hahn (3). In these experiments the behaviour of a transient signal is observed after the application of short, intense radio frequency pulses. Many sequences of pulses have been described (3,4,5,14,15) but the most important for the determination of diffusion coefficients is the 90-180 degree pulse sequence first described by Hahn (4) and by Carr and Purcell (5).

In this experiment the oscillating field, H_1, is applied to the sample for two short periods such that the isochromatic moments making up the net magnetization vector are rotated through successive angles of 90 and 180 degrees about the x' axis. The behaviour of the system during and after the application of these pulses is illustrated in figure 2-2.

An r.f. pulse is applied at time zero for a period t_s. In the rotating frame there is effectively only the field H_1 produced by this pulse acting on the magnetization vector which rotates about H_1 at a frequency given by γH_1. t_s is set so that $\gamma H_1 t_s$ is equal to 90 degrees, thus $\bar{M}$ is rotated to lie along the y' axis (figure 2-2a). The componemts of $\bar{M}$ get out of phase due to the presence of the small inhomogeneities in the polarizing field causing the isochromatic moments to rotate about the z axis at slightly different frequencies (figure 2-2b). As the isochromatic moments get out of phase the net magnetization vector, $\bar{M}$, goes to zero and the induction signal following the 90 degree pulse decays to zero.

The second r.f. pulse is applied at time τ for a period $2t_s$. The components of $\bar{M}$ are flipped through 180 degrees about the x axis (figure 2-2c). This causes the components of $\bar{M}$ to start coming back into phase. As they come back into phase $\bar{M}$ increases, inducing a signal known as the spin echo with its maximum at time 2τ (figure 2-2d). After coming back into phase the isochromatic moments spread out once more and the spin echo dies away (figure 2-2e). The peak of the echo is smaller than that of the induction tail following the 90 degree pulse because of longitudinal and transverse relaxation processes and also because of the diffusion of nuclei to different parts of the polarizing field in the time interval 2τ .

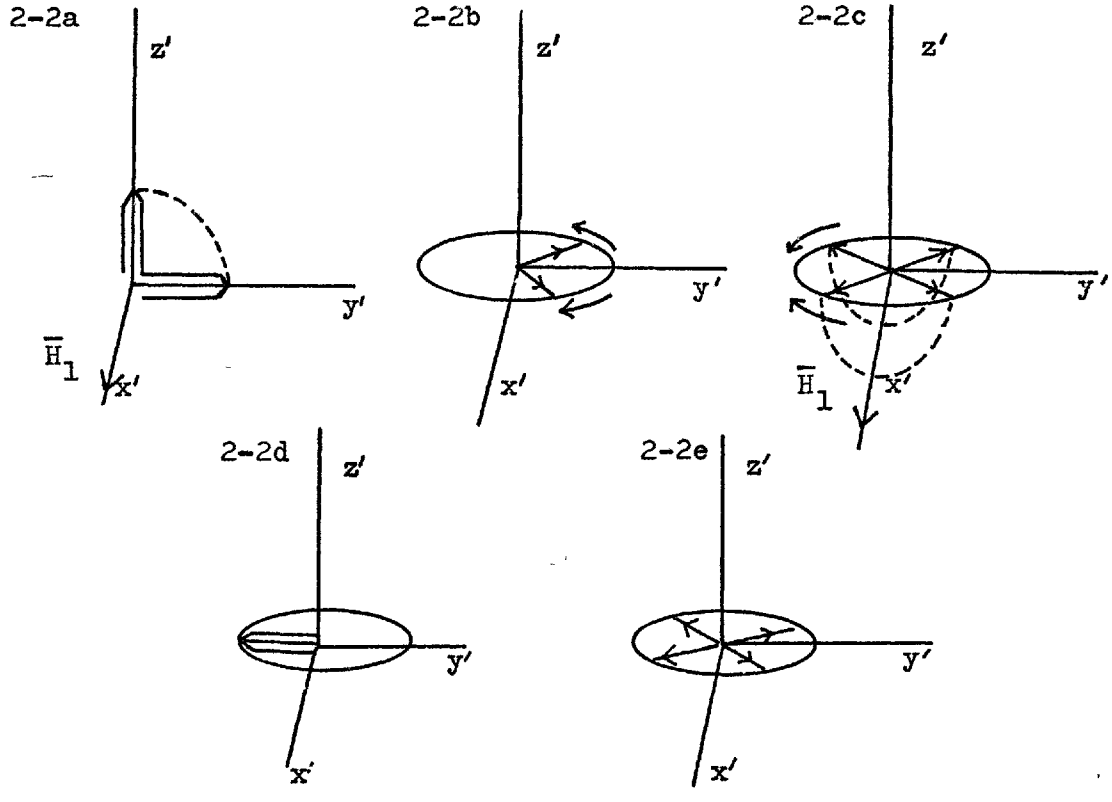


Figure 2-2: THE 90-180 DEGREE PULSE SEQUENCE AND SPIN ECHO FORMATION.

2-6 The Effect of Diffusion in the Presence of a Steady Field Gradient.

The effect of diffusion on the amplitude of the spin echo in the presence of a steady field gradient was first treated by Hahn (3), but he did not measure any diffusion coefficients. The first diffusion coefficient measured, using the spin echo method, was that of water by Carr and Purcell (5) using a steady, linear field gradient.

In their paper Carr and Purcell derive the following expression for the intensity of the echo maximum occuring at time t:

$$A(t) = A(0) \exp \left\{(-t/T_2) + (-\gamma^2 G^2 D t^3/12)\right\} \quad , \qquad (2\text{-}12)$$

for a single 90-180 degree pulse sequence. In equation (2-12) G represents the value of the field gradient and D represents the self diffusion coefficient. The effect of diffusion on the echo maximum at time 2τ is thus:

$$\exp(-2k\tau^3/3) \quad , \qquad (2\text{-}13)$$

where $k = \gamma^2 G^2 D$.

Other expressions derived by Hahn (3) and by Das and Saha (12) are in error over the numeric factor due to the manner in which they average to take into account the random motion of the molecules (7,8).

The self diffusion coefficient can thus be evaluated by measuring the attenuation of the echo signal as G or τ is varied. In practice it is simpler if G is varied since one does not then require explicit knowledge of the relaxation time T_2.

2-7 The Effect of Diffusion in the Presence of a Pulsed Field Gradient.

In order to measure smaller diffusion coefficients by the steady gradient method, it becomes necessary to increase the size of the field gradient. However this results in a narrowing of the echo and so the bandwidth of the receiver must be increased which decreases the signal to noise ratio. It is also necessary to increase the amplitude of the radio-frequency pulses so that the condition; $\gamma H_1 \gg \gamma \Delta H_z$ still holds. This latter condition is necessary if the isochromatic moments are to be in phase after the 90 degree pulse. These two conditions greatly increase the instrumental problems.

These problems can be overcome if the magnetic field gradient is turned on and off during the experiment so that it is absent when the spin echo is detected. This was first mentioned by Anderson and co-workers (18) but was largely developed by Stejskal and Tanner (10, 11, 16). The usual sequence of pulses is shown in figure 2-3. Stejskal and Tanner have analysed the effect of diffusion on the echo amplitude for rectangular field gradient pulses as shown in figure 2-3a. The expression they derived was:

$$\ln \frac{A(2\tau)}{Ao} = -\gamma^2 D \left\{ \frac{2}{3}\tau^3 \bar{G}_o^2 + \delta^2(\Delta - \frac{1}{3}\delta)\bar{G}^2 - \delta\left[(t_1^2 + t_2^2) + \delta(t_1+t_2) + \frac{2}{3}\delta^2 - 2\tau^2\right] \bar{G}.\bar{G}_o \right\} \quad (2\text{-}14)$$

where $A(2\tau)$ is the amplitude of the echo at time 2τ and Ao is the amplitude of the spin echo in the absence of

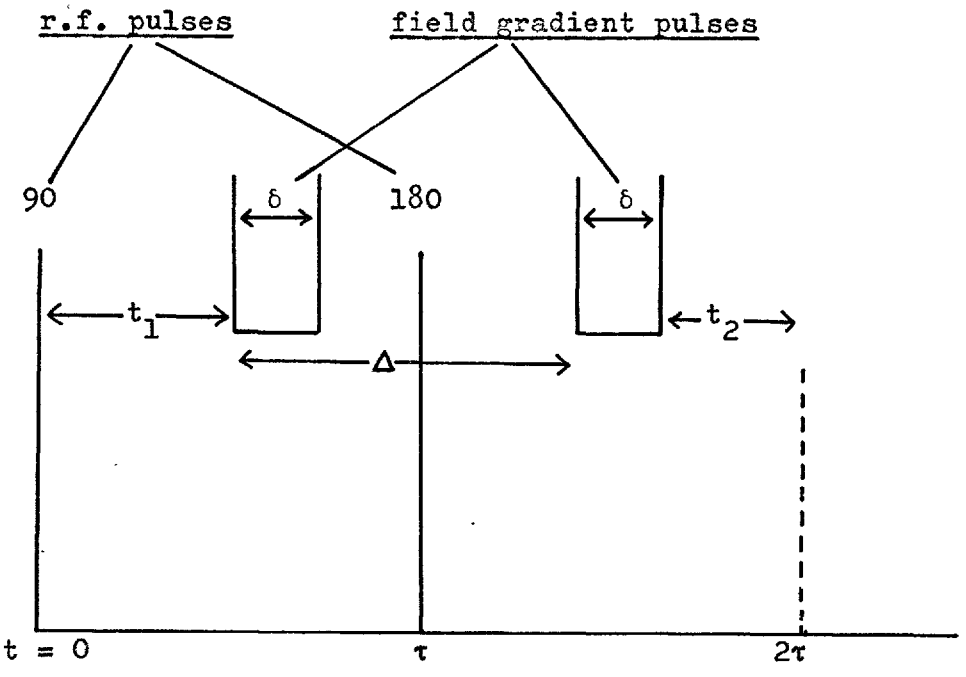


Figure 2-3a: TIME INTERVALS FOR 90-180 DEGREE SPIN ECHO EXPERIMENT. NOTATION OF TANNER AND STEJSKAL.

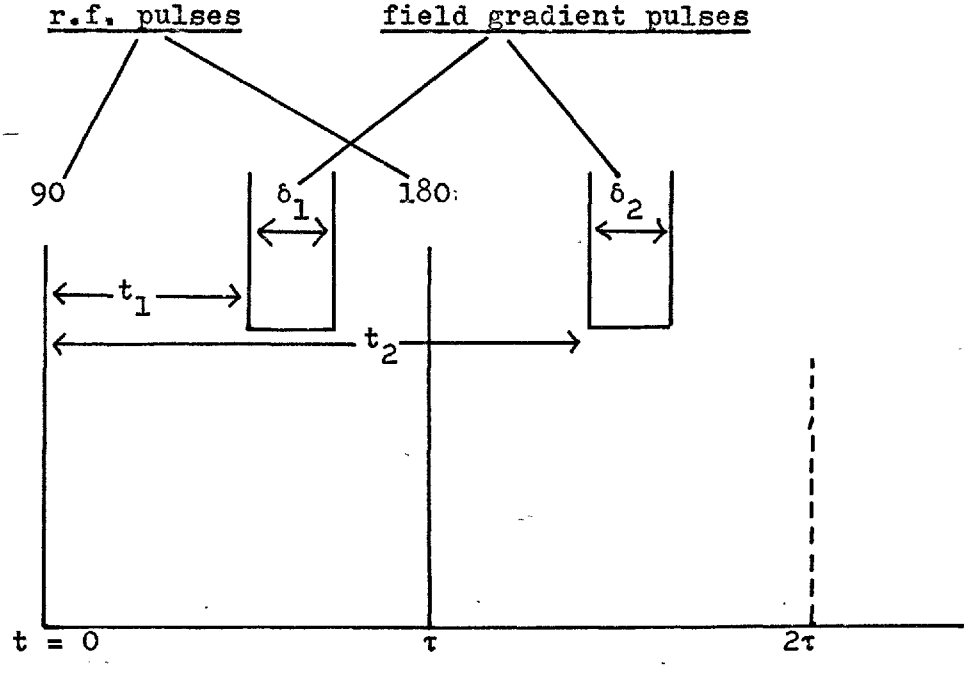


Figure 2-3b: TIME INTERVALS FOR 90-180 DEGREE SPIN ECHO EXPERIMENT. NOTATION OF SECTION 2-9.

the field gradient. G_o is any residual field gradient present in H_o and $t_2 = 2\tau - (t_1 + \Delta + \delta)$. If G is put equal to zero in equation (2-14) then

$$\ln \frac{A(2\tau)}{Ao} = -\gamma^2 D \frac{2}{3}\tau^3 G_o \,, \qquad (2\text{-}15)$$

which is the same as the result derived by Carr and Purcell (5). As G_o approaches zero only the term in G remains giving:

$$\ln \frac{A(2\tau)}{Ao} = -\gamma^2 D\delta^2(\Delta - \frac{\delta}{3})G^2. \qquad (2\text{-}16)$$

This expression can be simplified even further if $\delta \ll \Delta$ to give:

$$\ln \frac{A(2\tau)}{Ao} = -\gamma^2 D\delta^2 \Delta G^2 \qquad (2\text{-}17)$$

Stejskal and Tanner have also analysed the effect of diffusion for a time dependent field gradient of the form:

$$G(t) = G_o + G\left[1 - \cos(2\pi t/\tau)\right] \qquad (2\text{-}18)$$

and obtained:

$$-\ln \frac{A(2\tau)}{Ao} = -\gamma^2 D\tau^3 \left\{ \frac{2}{3}G_o^2 + (\frac{2}{3} + \frac{5}{4\pi^2})G^2 + (\frac{4}{3} + \frac{1}{\pi^2})G_o \cdot G \right\}. \qquad (2\text{-}19)$$

Most workers have used the rectangular pulses although the sinusoidal G(t) has been used (13).

2-8 The Stimulated Echo.

Echoes are obtainable from other pulse sequences beside the 90-180 degree sequence. In fact historically they were first observed using a 90-90 degree sequence (3).

If three 90 degree pulses are applied instead of the usual two pulse sequence then as many as five echoes may be observed. If τ_1 and τ_2 are the time intervals between the first and second r.f. pulse and the first and third r.f. pulse respectively, then an echo occurs at time $t = \tau_1 + \tau_2$. This echo is known as the stimulated echo.

It has been shown (3,14) that this echo is unique in that its relaxation attenuation has a T_1 dependence between the second and third r.f. pulses. The other echoes and also the echo produced by the 90-180 degree pulse sequence attenuate according to T_2 as their time of occurrence is delayed. Since T_1 may often be much larger than T_2, the use of this echo could have advantages in certain systems (15).

In the presence of a time independent magnetic field gradient, G_o, the attenuation of the stimulated echo is given by (15):

$$\ln \frac{A}{A(0)} = -\frac{(\tau_2-\tau_1)}{T_1} - \frac{2\tau_1}{T_2} - \ln 2 - \gamma^2 D G_o^2 \tau_1^2 (\tau_2 - \frac{\tau_1}{3}). \quad (2\text{-}20)$$

In the presence of rectangular field gradient pulses the attenuation due to diffusion is given by:

$$\ln \frac{A}{Ao} = -\gamma^2 D \left\{ \delta^2 (\Delta - \frac{\delta}{3}) G^2 + \tau_1^2 (\tau_2 - \frac{\tau_1}{3}) G_o^2 - \delta \left[t_1^2 + t_2^2 + \delta(t_1+t_2) + \frac{2\delta^2}{3} - 2\tau_1\tau_2 \right] G.G_o \right\} \quad (2\text{-}21)$$

This reduces to the term in equation (2-14) when $\tau_1 = \tau_2$.

The rectangular field gradient pulses are positioned between the first and second r.f. pulses and after the third r.f. pulse.

2-9 Derivation of the Diffusion Attenuation Term in the Pulsed Field Gradient Experiment.

The following derivation is an extension of the method used by Douglass and McCall (17) to derive the effect of diffusion on the echo amplitude in the presence of a steady field gradient. It will be seen that the result is equivalent to that derived by Stejskal and Tanner (10,11) who extended the method of Torrey (9) and the random walk model of Carr and Purcell (5). In the derivation presented here the case of gradient pulses of unequal length is explicitly considered and an expression for the evolution of the echo signal with time is obtained.

The specific case considered here is that of a cylindrical sample with time independent field gradients along and perpendicular to the cylinder's axis. At various times an extra field gradient across the cylinder's axis is pulsed on and off.

In this section the following notation is used:

t_1 : the time between the 90 degree r.f. pulse and the start of the first gradient pulse,

δ_1 : the width of the first gradient pulse,

τ : the time between the 90 and 180 degree pulses,

t_2 : the time between the 90 degree pulse and the second gradient pulse,

δ_2 : the width of the second gradient pulse,

G_o : the magnitude of the steady magnetic field gradient across the cylinder in the z direction, i.e. $(\partial H_z/\partial z)_x$,

G_x : the magnitude of the steady magnetic field gradient in the x direction, i.e. $(\partial H_z/\partial x)_z$,

G : the magnitude of the pulsed magnetic field gradient in the z direction,

$H(t)$: the magnitude of the polarizing magnetic field in the direction z that a magnetic moment finds itself in at time t,

H_o : the magnitude of the polarizing magnetic field in the z direction at the centre of the sample being studied. This notation is different to that used by Stejskal and Tanner (10,11). The differences can be seen by comparing figures 2-3a and 2-3b.

Since the two field gradient pulses are considered to have the same polarity, it is necessary that the 180 degree pulse occurs between the two gradient pulses for the production of spin echoes. This restriction could be dispensed with if gradient pulses of the opposite polarity were available.

The phase accumulated by a precessing magnetic moment at time t greater than τ is given by:

$$\varphi = \gamma \left\{ \int_o^{\tau} H(t)\, dt - \int_{\tau}^{t} H(t)\, dt \right\} . \qquad (2\text{-}22)$$

The gradient pulses are rectangular and so $H(t)$ has the form:

$$\begin{aligned}
H(t) &= H_o + G_o z(t) + G_x x(t) , && 0 < t < t_1 , \\
H(t) &= H_o + (G_o + G) z(t) + G_x x(t) , && t_1 < t < t_1 + \delta_1 , \\
H(t) &= H_o + G_o z(t) + G_x x(t) , && t_1 + \delta_1 < t < t_2 , \\
H(t) &= H_o + (G_o + G) z(t) + G_x x(t) , && t_2 < t < t_2 + \delta_2 , \\
H(t) &= H_o + G_o z(t) + G_x x(t) , && t_2 + \delta_2 < t ,
\end{aligned} \qquad (2\text{-}23)$$

where $x(t)$ and $z(t)$ give the position of the moment at time t.

So at time t greater than $t_2 + \delta_2$ we get:

$$\varphi = \gamma G_o \left\{ \int_o^{t_1} z(t)\,dt + \int_{t_1+\delta_1}^{\tau} z(t)\,dt - \int_{\tau}^{t_2} z(t)\,dt - \int_{t_2+\delta_2}^{t} z(t)\,dt \right\}$$
$$+ \gamma G_x \left\{ \int_o^{\tau} x(t)\,dt - \int_{\tau}^{t} x(t)\,dt \right\}$$
$$+ \gamma (G_o + G) \left\{ \int_{t_1}^{t_1+\delta_1} z(t)\,dt - \int_{t_2}^{t_2+\delta_2} z(t)\,dt \right\}$$
$$+ \gamma H_o (2\tau - t) \quad . \qquad (2\text{-}24)$$

If one goes into the rotating frame with frequency γH_o then the term in H_o disappears from the above equation. From here onwards φ represents the phase of the magnetic moment relative to the rotating frame.

The signal produced in the spectrometer coil is proportional to the resultant magnetic moment made up of all the individual moments. The resultant moment is given by:

$$M = M_o \int_{-\infty}^{\infty} p(\varphi)\cos(\varphi)\,d\varphi \quad , \qquad (2\text{-}25)$$

where $p(\varphi)$ is the probability density of moments having relative phase φ.

If one substitutes $Z(t) = z(t) - z_o$ and $X(t) = x(t) - x_o$ then:

$$\varphi = \gamma G_o \left\{ \int_o^{t_1} Z(t)\,dt + \int_{t_1+\delta_1}^{\tau} Z(t)\,dt - \int_{\tau}^{t_2} Z(t)\,dt - \int_{t_2+\delta_2}^{t} Z(t)\,dt \right\}$$
$$+ \gamma G_x \left\{ \int_o^{\tau} X(t)\,dt - \int_{\tau}^{t} X(t)\,dt \right\}$$
$$+ \gamma (G_o + G) \left\{ \int_{t_1}^{t_1+\delta_1} Z(t)\,dt - \int_{t_2}^{t_2+\delta_2} Z(t)\,dt \right\}$$
$$+ \gamma G_o z_o (2\tau - t) + \gamma G z_o (\delta_1 - \delta_2)$$
$$+ \gamma G_x x_o (2\tau - t) \quad . \qquad (2\text{-}26)$$

This can be written as:

$$\varphi = \varphi' + \gamma G_o z_o(2\tau - t) + \gamma G z_o(\delta_1 - \delta_2) + \gamma G_x x_o(2\tau - t). \quad (2\text{-}27)$$

For the sample shape being considered φ', x_o, and z_o are independent variables and so:

$$p(\varphi) = q(\varphi')h(z_o)j(x_o), \quad (2\text{-}28)$$

where $q(\varphi')$, $h(z_o)$, $j(x_o)$ are the appropriate probability densities.

It can be shown (17) that $q(\varphi')$ is Gaussian:

$$q(\varphi') = (2\pi\langle\varphi'^2\rangle)^{-1/2} \exp(-\varphi'^2/2\langle\varphi'^2\rangle), \quad (2\text{-}29)$$

where $\langle\varphi'^2\rangle$ represents the mean square of φ'.

For the sample geometry being considered, $h(z_o)$ is given by:

$$h(z_o) = (2/\pi a^2)(a^2 - z_o^2)^{1/2} \quad \text{for } |z_o| < a,$$
$$= 0 \quad \text{for } |z_o| > a \quad (2\text{-}30)$$

and $j(x_o)$ is given by:

$$j(x_o) = 1/L \quad \text{for } |x_o| < L/2,$$
$$= 0 \quad \text{for } |x_o| > L/2, \quad (2\text{-}31)$$

where a is the radius of the cylindrical sample and L is its height.

Using equations (2-27) and (2-28) the resultant moment is now given by:

$$M = M_o \int_{-\infty}^{\infty}\int_{-\infty}^{\infty}\int_{-\infty}^{\infty} q(\varphi')h(z_o)j(x_o)\cos(\varphi' + k_1 z_o + k_2 x_o)dz_o dx_o d\varphi' \quad (2\text{-}32)$$

where k_1 represents $\gamma(G_o(2\tau - t) + G(\delta_1 - \delta_2))$ and k_2 represents $\gamma G_x(2\tau - t)$.

When the cosine term is expanded, the integrals over the sine terms between the limits given above disappear since these are even functions. So we have:

$$M = M_o \int_{-\infty}^{\infty}\int_{-\infty}^{\infty}\int_{-\infty}^{\infty} q(\varphi')\cos(\varphi')h(z_o)\cos(k_1 z_o)\, j(x_o)\cos(k_2 x_o)\, dz_o dx_o d\varphi \quad . \qquad (2\text{-}33)$$

The evaluation of the above integrals gives:

$$M = M_o \exp(-\langle\varphi'^2\rangle/2)\, 2J_1(a\gamma(G_o(2\tau - t) + G(\delta_1 - \delta_2)))\,/\,(a\gamma(G_o(2\tau - t) + G(\delta_1 - \delta_2)))$$

$$\cdot \frac{2\sin(\gamma G_x(2\tau - t)L/2)}{\gamma G_x(2\tau - t)L} \qquad (2\text{-}34)$$

where J_1 is the Bessel coefficient of order one.

Taking into account transverse relaxation we obtain for the amplitude of the spectrometer signal at time t:

$$A(t) = A(0)\exp(-t/T_2)\exp(-\langle\varphi'^2\rangle/2)$$

$$\cdot 2J_1(a\gamma(G_o(2\tau - t) + G(\delta_1 - \delta_2)))\,/\,(a\gamma(G_o(2\tau - t) + G(\delta_1 - \delta_2)))$$

$$\cdot 2\sin(\gamma G_x(2\tau - t)L/2)\,/\,(\gamma G_x(2\tau - t)L) \qquad (2\text{-}35)$$

The evaluation of $\langle\varphi'^2\rangle$ is outlined in appendix A. The final result is:

$$\begin{aligned}\langle\varphi'^2\rangle = 2\gamma^2 D \Big\{ & G_o^2(2\tau^3 + t^3/3 - 2\tau^2 t) \\ & + G_x^2(2\tau^3 + t^3/3 - 2\tau^2 t) \\ & + G^2(t_1\delta_1^2 + t_2\delta_2^2 + \delta_1^3/3 + \delta_2^3/3 \\ & \quad - 2\delta_1\delta_2 t_1 - \delta_1^2\delta_2) \\ & + G_o G(\delta_1(4t_1\tau - 2t_1 t - t_1^2) \\ & \quad + \delta_2(2t_2 t - t_2^2 - 2\tau^2) \\ & \quad + \delta_1^2(2\tau - t_1 - t) + \delta_2^2(t - t_2) \\ & \quad - (\delta_1^3 - \delta_2^3)/3)\Big\} \qquad (2\text{-}36)\end{aligned}$$

By substituting equation (2-36) into equation (2-35) an expression is obtained for the nuclear signal at any time greater than $t_2 + \delta_2$ for the particular sample under consideration. The equation derived by Stejskal and Tanner (10,11) refers specifically to the case when G_x is zero, δ_1 and δ_2 are equal, and t is equal to 2τ. In this case equation (2-35) reduces to:

$$\frac{A(2\tau)}{A_o} = \exp(-\langle\varphi'^2\rangle/2)$$

or

$$\ln(A(2\tau)/A_o) = -\langle\varphi'^2\rangle/2 \qquad (2\text{-}37)$$

where A_o equals $A(0)\exp(-2\tau/T_2)$.

Substituting equation (2-36) for $\langle\varphi'^2\rangle$ putting G_x equals zero, δ_1 equal to δ_2, and t equal to 2τ one gets:

$$\ln(A(2\tau)/A_o) = -\gamma^2 D \left\{2G_o^2\tau^3/3 + G^2\delta^2(t_2 - t_1 - \delta/3) + G_oG\delta((4t_2\tau - t_1^2 - t_2^2 - 2\tau^2) + \delta(2\tau - t_1 - t_2) - 2\delta^2/3)\right\} \qquad (2\text{-}38)$$

Equation (2-38) is the same as that of Stejskal and Tanner when one takes into account the differences of notation.

The evolution of the echo signal with time as given by equation (2-35) for the case where G_x is zero and the two gradient pulses are equal is shown in figure 2-4. The values given to the parameters in equation (2-35) are given at the end of this section.

The successive echoes plotted in figure 2-4 are for G values of 0, 20, 40, 60, and 80 gauss per centimetre and gradient pulse widths of 1 millisecond. The echo peaks all

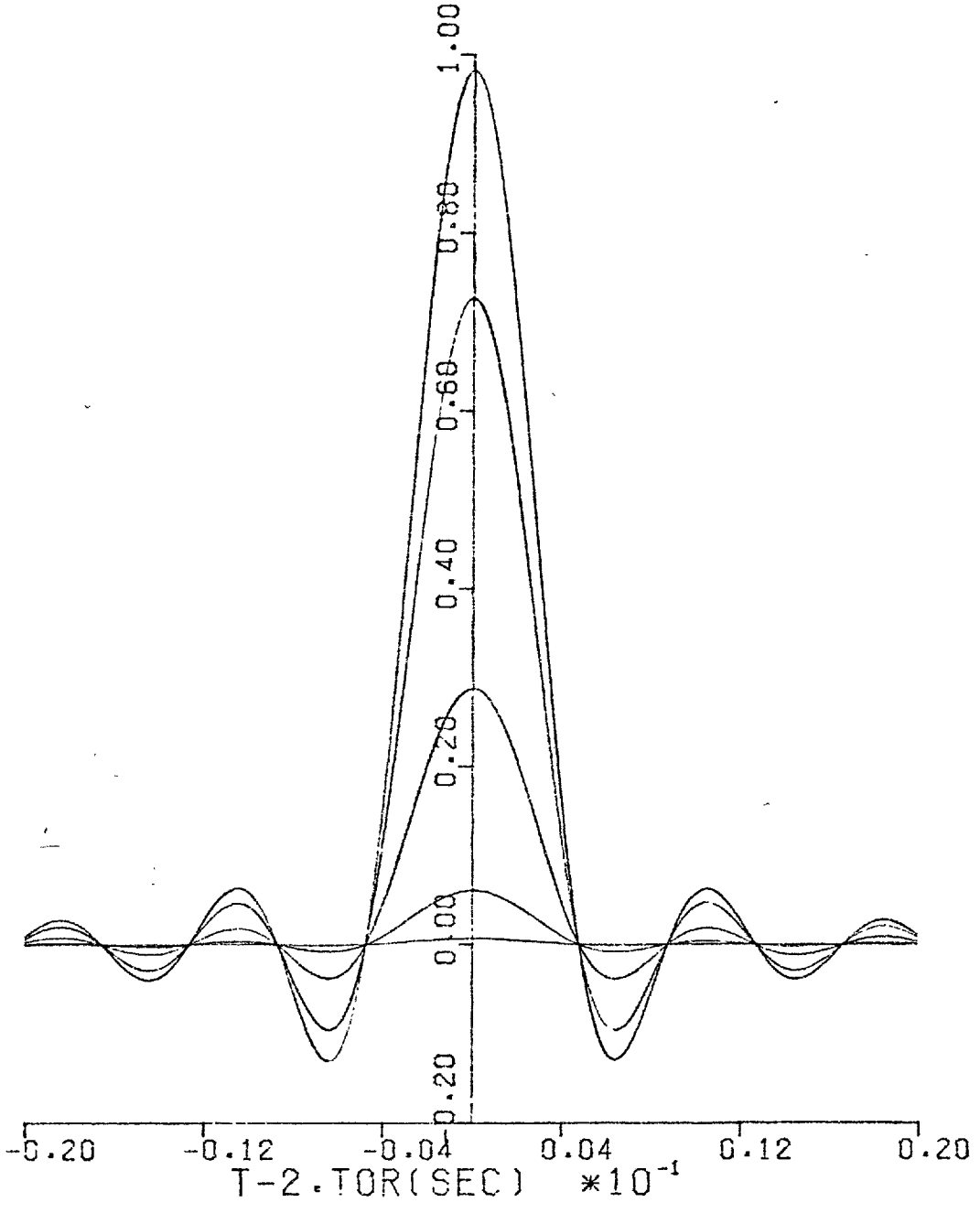


Figure 2-4: THEORETICAL SPIN ECHOES. EQUAL GRADIENT PULSES AND G_x EQUAL TO ZERO.

occur at time 2τ and the echoes are virtually symmetric about this point.

It should be mentioned here that signals such as those depicted in figure 2-4 will only be observed in spectrometers employing phase sensitive detection. If the spectrometer employs diode detection then the negative parts of the signal appear positive and hence all minima become maxima.

In chapter 5 the equations developed in this section are used to demonstrate the effects of unequal gradient pulses.

Parameters in equation (2-35) were given the following values in producing figure 2-4:

$\gamma = 26755$ rad. s.$^{-1}$ gauss^{-1} (appropriate for protons)

$D = 2{\cdot}2 \times 10^{-9}$ m.^{2} s.$^{-1}$ (appropriate for benzene)

$A(0) = 1$ volt

$T_2 = 20$ s.

$\tau = 50$ ms.

$t_1 = 20$ ms.

$t_2 = 70$ ms.

$G_o = 0{\cdot}1$ gauss cm.$^{-1}$

$a = 0{\cdot}3$ cm.

$L = 1$ cm.

2-10 The Determination of the Self Diffusion Coefficient by Following the Variation of $T_{1\rho}$ with H_1.

Recently the two field gradient methods of determining the self diffusion coefficient have been supplemented by a method described by Burnett and Harmon (6).

Before describing the method, the relaxation time $T_{1\rho}$ is defined. $T_{1\rho}$ is the relaxation time which describes the decay of the induction signal in what are known as spin-locking experiments. A 90 degree r.f. pulse with $\overline{H}_1$ along the x′ axis rotates $\overline{M}$ to the y′ axis. The phase of the r.f. signal is now changed by 90 degrees so that $\overline{H}_1$ also lies along the y′ axis. This effectively eliminates the effect of inhomogeneity in the Ho field on the decay of the induction signal. The spins are said to be locked along the y′ axis. The signal, however, still decays due to relaxation processes with the characteristic time constant $T_{1\rho}$.

The method of Burnett and Harmon depends on the fact that in viscous, dipolar liquids the dependence of $T_{1\rho}$ upon frequency becomes experimentally significant when the self diffusion coefficient is less than 10^{-12} m.^{2}s.$^{-1}$. This method allows the determination of self diffusion coefficients down to as low as 5×10^{-17} m.^{2}s.$^{-1}$ for proton resonance and even lower for other nuclei because of their different magnetogyric ratios. This method is distinct from other magnetic resonance techniques (97) which measure the correlation time for molecular diffusion, τ_D, instead of D.

It can be shown that for spin 1/2 nuclei (6):

$$\Delta_1 \equiv (1/T_2 - 1/T_1) = (2\sqrt{2}-1)\gamma^4 \hbar^2 \pi n u_o^{1/2}/20D^{3/2} \qquad (2\text{-}39)$$

and

$$\Delta_2 \equiv (1/T_2 - 1/T_{1\rho}) = \sqrt{2}\gamma^4 \hbar^2 \pi n u_1^{1/2}/20D^{3/2}. \qquad (2\text{-}40)$$

Hence:

$$1/T_{1\rho} = -(\sqrt{2}\gamma^4 \hbar^2 \pi n u_1^{1/2}/20D^{3/2}) + 1/T_2 \qquad (2\text{-}41)$$

from which:

$$\frac{d(1/T_{1\rho})}{d(u_1^{1/2})} = -\sqrt{2}\gamma^4 \hbar^2 \pi n/20D^{3/2} \qquad (2\text{-}42)$$

where n is the number density of resonant nuclei, $\overline{u}_o$ is the Larmor frequency and $\overline{u}_1$ equals $\gamma\overline{H}_1$.

The frequency dependence in the above equations is approximate and for an accuracy of five per cent in Δ_1 and Δ_2 it is necessary that the parameter $(u\sigma^2/D)^{1/2}$ be less than about two. In this expression σ represents the molecular diameter and u represents either u_o or u_1 depending on whether T_1 or $T_{1\rho}$ is measured. If $(u\sigma^2/D)^{1/2}$ is much greater than two, then the above equations are incorrect. This restriction implies that self diffusion constants inferred from a measure of Δ_1 are limited to the range where the diffusion coefficient is greater than 10^{-13} m.^{2} s.$^{-1}$.

The advantage of using the rotating frame measurement lies in the fact that u_1 can be made very much smaller than u_o, allowing correspondingly smaller diffusion coefficients to be measured. The lower limit on the size of the diffusion coefficient that can be measured depends the nucleus under study, its number density, n, and its molecular diameter, σ.

The condition $\omega_1 > \gamma H_{loc}$, where H_{loc} is the local field due to dipolar broadening, sets the limit on the value of ω_1.

Initial work with this method (6) has determined the self diffusion coefficient of glycerol at 270·7K to be $(9{\cdot}61 \pm 0{\cdot}38) \times 10^{-14} m.^2 s.^{-1}$.

2-11 A Comparison of the N.M.R. Method with other Methods for the Determination of Self Diffusion Coefficients.

Self diffusion coefficients are determined by measuring the mutual diffusion of labelled and non-labelled molecules. The diffusion coefficient so determined is taken to be the self diffusion coefficient of the species provided that the labelling does not affect the properties of the molecule. There are two major methods of labelling molecules for diffusion measurements, these are by isotopic substitution and by the phase of the nuclear magnetic moments. The latter method is as near to ideal labelling as can be envisaged, but the former alters the mass of the molecule and so the diffusion properties of the labelled molecule must be slightly different to those of the non-labelled molecule. As experimental procedures have been improved interest in an isotope effect on diffusion coefficients has grown (100,101,160). It has been pointed out (102) that the n.m.r. spin echo method measures the true self diffusion coefficient as long as quantum effects are negligible, but the diffusion coefficient measured by using isotopically labelled molecules only approaches the true self diffusion coefficient as the concentration of the labelled

molecule goes to zero. Comparisons (24,61,100,101) between n.m.r. and isotopic measurements generally show good agreement.

Methods used for measuring self diffusion coeficients by use of isotopically labelled molecules are basically the same as those used for measuring the mutual diffusion of different molecular species. The most commonly used methods are the diaphragm cell (103,104,105,106) and the capillary cell (107,108). The use of optical methods is made difficult by the usually very small difference in refractive index. The self diffusion coefficient of water has, however, been determined by an optical method (109). Recently a further technique based on the line broadening of a reflected laser beam has been described (110). This technique is particularly applicable to studying the diffusion of macromolecules in solution.

The n.m.r. spin echo method has several distinct practical advantages over isotopic methods. It is possible to perform experiments rapidly and repeatedly. The amount of sample required is small and different samples can be conveniently stored in sealed n.m.r. tubes. It is relatively simple to vary the temperature of the sample and the pressure above the sample. The period over which diffusion is measured is very short, usually of the order of tens of milliseconds. This lends the technique to the study of restricted diffusion phenomena. The pulsed field gradient method is of particular value here since the time over which diffusion is measured is essentially the time between the two gradient pulses, Δ, which can be

easily varied. The pulsed field gradient method also has the advantage over the steady gradient method in that there is a greater choice of the parameter which can be varied to determine the self diffusion coefficient. The n.m.r. method is also capable of the absolute determination of diffusion coefficients, but it is better to calibrate the instrument against a species of known diffusion coefficient. This is discussed further in chapter 5.

The major disadvantages of the spin echo method are that it requires quite a high concentration of n.m.r. active nuclei to get a large enough signal and generally, in a mixture, only one component should contain the nucleus under study. Normally one is limited to nuclei with spin 1/2 amd for many elements the isotopic abundance of such nuclei is low. The apparatus required is costly and complex and inevitably this causes instrumental problems.

Appendix B lists the the non-electrolyte liquid systems that have been studied by means of the n.m.r. spin echo technique since about 1963. Measurements prior to that have been summarized elsewhere (91). The experimental accuracy is normally about ± 5 per cent going down to ± 10 or 15 per cent at low concentrations of nuclei. A few workers, however, do claim better accuracies of up to ± 1 per cent. The method has also been applied to the study of restricted diffusion in numerous systems (11,28,44,45,46,64,71,73,74,75,84), to diffusion in gases (37,82,83) and to electrolyte solutions (47,70).

Isotopic methods are less restrictive in the molecular systems that can be studied but the experiments are considerably longer. The capillary method determines absolute diffusion coefficients with a typical accuracy of about 2 per cent although this has been improved on (111,112). The diaphragm cell technique has been developed to a high degree of accuracy (105,106) and provides the most accurate method available today (to about ·1 per cent). The technique is, however, not absolute and each cell has to be calibrated against salt solutions.

In conclusion it can be said that the n.m.r. spin echo technique has not yet been developed enough for its accuracy to match that of the best isotopic methods, but its speed and convenience make it a most attractive method. Its accuracy will improve with the use of more advanced instrumentation, but it is unlikely to supercede isotopic methods because of the limited number of suitable n.m.r. active nuclei. Rather, it is likely that both techniques will continue to be used to complement each other.

Chapter 3: A SUMMARY OF DIFFUSION THEORY RELEVANT TO THE TREATMENT OF THE EXPERIMENTAL RESULTS.

3-1 Introduction.

This chapter presents a summary of that part of diffusion theory which is relevant to an understanding of the treatment of the experimental results presented later.

Initially the mutual and self diffusion coefficients of components in a binary liquid system are defined. The relationship between these diffusion coefficients is then developed following Laity's treatment (113) based on the phenomenological theory of Onsager (114,115,116). The results of Bearman's statistical approach (117) are outlined. Enskog's theory (118) for diffusion in dense hard sphere systems is then used to obtain expressions for the friction coefficients arising from the phenomenological treatment (119).

3-2 Fick's Laws.

The basic relationship which defines the diffusion coefficient is Fick's first law, which can be written as:

$$\bar{J} = -D(\overline{\partial c}/\partial x)_{T,P} \quad , \qquad (3\text{-}1)$$

where $\bar{J}$ is the flux per unit area in the presence of a concentration gradient. The particular units used in defining $\bar{J}$ and the concentration gradient will determine the units of the diffusion coefficient, D.

Fick's first law can be used in the derivation of the expression known as Fick's second law:

$$\frac{\partial c}{\partial t} = \frac{\partial}{\partial x}\left(D\frac{\partial c}{\partial x}\right)_{T,P} \quad . \qquad (3\text{-}2)$$

This equation forms the basis for the determination of the diffusion coefficient by methods which follow the change of concentration with time.

The diffusion coefficient, as defined by equation (3-1), is usually a function of concentration and its value is also dependent on the frame of reference with respect to which $\bar{J}$ is defined.

In a binary system consisting of components 1 and 2 an expression can be written for the flux of each component according to equation (3-1):

$$\bar{J}_1 = -D_{12}\left(\partial \bar{c}_1 / \partial x\right)_{T,P} \quad , \qquad (3\text{-}3a)$$

$$\bar{J}_2 = -D_{21}\left(\partial \bar{c}_2 / \partial x\right)_{T,P} \quad . \qquad (3\text{-}3b)$$

If $\bar{J}_1$ and $\bar{J}_2$ are measured with respect to a plane across which there is no net transport of volume then we have the condition:

$$\bar{J}_1 V_1 + \bar{J}_2 V_2 = 0 \quad , \qquad (3\text{-}4)$$

where V_1 and V_2 are the volumes of species 1 and 2 transported across the plane per unit flux. The following condition also holds:

$$V_1 c_1 + V_2 c_2 = 1 \quad . \qquad (3\text{-}5)$$

This is so because $V_1 c_1$ and $V_2 c_2$ represent the volumes of species 1 and 2 per unit total volume and the mixture consists only of these species.

Differentiating equation (3-5) and combining with equations (3-3) and (3-4) leads to the condition:

$$D_{12}^{V} = D_{21}^{V} \quad , \qquad (3\text{-}6)$$

where the superscript denotes the reference frame. Thus under

these conditions the diffusion process is described by a single diffusion coefficient known as the mutual diffusion coefficient. In other frames of reference this is not the case unless the units of distance are redefined (120).

Since the diffusion coefficient usually varies with concentration, mutual diffusion coefficients are normally measured under conditions such that concentration differences in the experiment are kept very small. The differential diffusion coefficient measured in this way may be identified with the mutual diffusion coefficient at the mean experimental concentration. If the concentration varies significantly during an experiment then the diffusion coefficient so determined is known as an integral diffusion coefficient. This is an average mutual diffusion coefficient over the concentration range.

Although the diffusion coefficient is defined in terms of a bulk flow of components under non-equilibrium conditions, molecular motion is still taking place when the system is at equilibrium and there is no net bulk flow. The molecules move about at random and the mean square distance moved in time t is related to a diffusion coefficient by the classical Einstein Smoluchowski equation:

$$D = \langle x^2 \rangle / 2t \quad . \qquad (3\text{-}7)$$

This is known as the self diffusion coefficient. In a binary system each component will moving about at random and each will have its own self diffusion coefficient. It has been suggested that the term self diffusion coefficient should be reserved for single component liquids and that the term

intradiffusion coefficient is more appropriate in mixtures (121). However, in this thesis the term self diffusion coefficient is used. In a binary system the self diffusion coefficient of either species is usually a function of composition.

Measurements of the self diffusion coefficient are normally made by labelling the molecules in some way so that their motion may be detected. In the case of isotopically labelled molecules the diffusion coefficient can still be considered as being defined by the gradient of labelled species. In the n.m.r. experiment the definition of the self diffusion coefficient in terms of a concentration gradient is rather more difficult since in this case each layer of molecules in the direction of the field gradient is uniquely tagged by the phase of its net magnetic moment vector. One can consider the concentration gradient of molecules from each layer as defining the diffusion coefficient. In the derivation of the effect of random motion on the spin echo amplitude the diffusion coefficient was introduced by means of equation (3-7) rather than equation (3-1). In this case it might be more appropriate to regard equation (3-7) as defining the self diffusion coefficient.

3-3 The Phenomenolgical Description of Diffusion.

The phenomenological theory of transport processes assumes that, under conditions not too far removed from equilibrium, a flux, J, is directly proportional to a driving force, X. Thus Ohm's law tells us that the flux of electrons is proportional to the difference in electric potential and Fourier's law relates heat flux to the temperature gradient.

The diffusion coefficient defined by Fick's first law can be regarded as a phenomenological coefficient relating a mass flux to a concentration gradient, but, as we shall see later, the concentration gradient is not the most appropriate driving force for diffusion.

When two or more irreversible transport processes take place simultaneously they may interfere with one another in that each flux is not only linearly dependent on its own driving force but also on the other driving forces. Thus we have:

$$\begin{aligned} J_1 &= L_{11}X_1 + L_{12}X_2 + L_{13}X_3 + \cdots\cdots + L_{1n}X_n \\ J_2 &= L_{21}X_1 + L_{22}X_2 + L_{23}X_3 + \cdots\cdots + L_{2n}X_n \\ &\cdot \qquad\qquad\qquad\qquad\qquad\qquad \cdot \\ &\cdot \qquad\qquad\qquad\qquad\qquad\qquad \cdot \\ Jn &= L_{n1}X_1 + L_{n2}X_2 + L_{n3}X_3 + \cdots\cdots + L_{nn}X_n \end{aligned} \qquad (3\text{-}8)$$

or:

$$\begin{aligned} X_1 &= R_{11}J_1 + R_{12}J_2 + R_{13}J_3 + \cdots\cdots + R_{1n}J_n \\ X_2 &= R_{21}J_1 + R_{22}J_2 + R_{23}J_3 + \cdots\cdots + R_{2n}J_n \\ &\cdot \qquad\qquad\qquad\qquad\qquad\qquad \cdot \\ &\cdot \qquad\qquad\qquad\qquad\qquad\qquad \cdot \\ X_n &= R_{n1}J_1 + R_{n2}J_2 + R_{n3}J_3 + \cdots\cdots + R_{nn}Jn \end{aligned} \qquad (3\text{-}9)$$

The Rs and the Ls are the phenomenological coefficients. The matrix of the R coefficients is the inverse of the matrix of the L coefficients. The R coefficients are known as friction coefficients although it has been suggested that they might more correctly be called resistances.

Onsager (114) has argued that, under certain conditions, these matrices are symmetric, that is $R_{ij} = R_{ji}$ and $L_{ij} = L_{ji}$. These relationships are known as Onsager's reciprocal relations (O.R.R.). In order that the O.R.R. hold, the fluxes and forces must satisfy certain thermodynamic conditions. For an irreversible process one starts off by writing Gibbs's equation for a unit volume of the system under consideration in terms of partial time derivatives and writing for each such term an appropriate balance equation:

$$\frac{\partial \rho_p}{\partial t} = -\nabla J_p + \text{production term} \quad , \qquad (3\text{-}10)$$

where ρ_p is the amount of property p per unit volume and J_p is the flux of property p. It is a fundamental assumption of the theory that Gibbs's equation may be applied to a system not at equilibrium . Appropriate expressions are substituted for the fluxes and an expression for the entropy production, β, is singled out. This expression is multiplied by the temperature, T, to obtain the energy dissipation and rearranged to the form:

$$T\beta = J_1X_1 + J_2X_2 + \cdots\cdots + J_nX_n \qquad (3\text{-}11)$$

The fluxes and forces in equation (3-11) are those for which the O.R.R. hold. The choice of flows or forces is to some extent arbitrary, but once one set is chosen the others are fixed by equation (3-11). In the case of diffusion the flux is defined in terms of amount of species per unit area per second. In order that the product of flux and driving force should have units of energy dissipation the driving force should have units of energy per unit length per amount of species. Thus, rather than concentration gradient, the

gradient of chemical potential is a more appropriate driving force for diffusion.

The O.R.R. have generally been confirmed within the limits of experimental error (122), but some authorities do have reservations as to their significance (123,124).

Consider, now, the diffusive fluxes in an n component system at constant temperature and pressure. In general we have for the driving forces:

$$X_i = \sum_k R_{ik} J_k \quad . \tag{3-12}$$

By the second law of thermodynamics we have the relation:

$$T\beta \geqslant 0 \quad , \tag{3-13}$$

the equals sign applying when all particle velocities are the same. In terms of the R coefficients this leads to the relationship:

$$\sum_k R_{ik} c_k = 0 \quad . \tag{3-14}$$

Condition (3-13) also limits the values which the R coefficients may take. As an example, for a two component system:

$$T\beta = J_1 X_1 + J_2 X_2 \geqslant 0 \quad . \tag{3-15}$$

Hence:

$$R_{11} J_1^{\,2} + (R_{12} + R_{21}) J_1 J_2 + R_{22} J_2^{\,2} \geqslant 0 \quad , \tag{3-16}$$

which with the O.R.R. puts the following constraints on the R coefficients :

$$R_{11} \text{ and } R_{22} \geqslant 0 \quad \text{and} \quad R_{12}^{\,2} \leqslant R_{11} R_{22} \tag{3-17}$$

Multiplying equation (3-14) by J_i/c_i we get:

$$\sum_k R_{ik} c_k J_i / c_i = 0 \tag{3-18}$$

Subtracting equation (3-18) from equation (3-12) we get:

$$X_i = \sum R_{ik}(J_k - J_i c_k/c_i) \qquad (3\text{-}19)$$

$$= \sum R_{ik} c_k (v_k - v_i) \ , \qquad (3\text{-}20)$$

where the v_j represents the velocity of the jth species. Thus we get for diffusive flow, where the appropriate driving force is the negative gradient of chemical potential:

$$-\nabla \mu_i = \sum R_{ik} c_k (v_k - v_i) \ . \qquad (3\text{-}21)$$

The advantage of this formalism is that the friction coefficients are independent of the reference frame since they only depend on relative velocities. It is also to be noted that the diagonal components of the R matrix, the R_{ii}, do not contribute to equation (3-21).

The theory is now developed by linking v_k and v_i through their frame of reference. For a binary system the simplest relationship is with reference to a frame of reference such that:

$$c_1 v_1^m + c_2 v_2^m = 0 \ . \qquad (3\text{-}22)$$

If the concentration is in moles per unit volume there is no net transport in the number of moles across a reference plane. The velocities measured with respect to this frame are distinguished by the superscript m. Laity (113) now continues by defining a thermodynamic mutual diffusion coefficient by the equation:

$$J_1 = -D_{12}(c_1/a_1)\nabla a_1 \ , \qquad (3\text{-}23)$$

where a_1 is the activity of species 1. This seems to be

rather unnecessary and somewhat confusing since diffusion coefficients are normally defined through Fick's law. Here we proceed in terms of the mutual diffusion coefficients, defined by Fick's law, appropriate to the mole fixed frame of reference:

$$J_1^m = -D_{12}^m \nabla c_1 \tag{3-24a}$$

$$J_2^m = -D_{21}^m \nabla c_2 \tag{3-24b}$$

Note that in this frame D_{12}^m does not equal D_{21}^m.

Dealing with the flux of species 1 equation (3-24a) leads to:

$$v_1^m = -D_{12}^m \nabla \ln c_1 \tag{3-25}$$

$$= -D_{12}^m \nabla \ln a_1 \left(\partial \ln c_1 / \partial \ln a_1\right)_{TP} \tag{3-26}$$

$$= -\frac{D_{12}^m}{RT} \nabla \mu_1 \left(\partial \ln c_1 / \partial \ln a_1\right)_{TP} \tag{3-27}$$

Combining equations (3-22) and (3-21) to eliminate v_2^m we get:

$$-\nabla \mu_1 = -R_{12} v_1^m (c_1 + c_2) \tag{3-28}$$

$$= -R_{12} v_1^m / V \ , \tag{3-29}$$

where V represents the molar volume of the solution. Comparing equations (3-27) and (3-29) leads to the result:

$$D_{12}^m = -\frac{VRT}{R_{12}} \left(\partial \ln a_1 / \partial \ln c_1\right)_{TP} . \tag{3-30}$$

Similarly for component 2 one gets:

$$D_{21}^m = -\frac{VRT}{R_{21}} \left(\partial \ln a_2 / \partial \ln c_2\right)_{TP} \tag{3-31}$$

Normally mutual diffusion coefficients are measured with reference to a laboratory fixed frame under conditions

that make this virtually a volume fixed frame. In this frame we have:

$$J_1^v V_1 + J_2^v V_2 = 0 \quad , \tag{3-32}$$

where V_1 and V_2 are the partial molar volumes of the components. The diffusion coefficients are defined by:

$$J_1^v = -D_{12}^v \nabla c_1 \tag{3-33a}$$

$$J_2^v = -D_{21}^v \nabla c_2 \quad . \tag{3-33b}$$

In the mole fixed frame the transport of volume across unit area plane per unit time is:

$$J_1^m (V_1 - V_2) \quad . \tag{3-34}$$

In the volume fixed frame the unit area plane moves with this volume flow so that there is no net volume exchange. Hence, velocities in the mole fixed frame, v_1^m, are related to those in the volume fixed frame, v_1^v, by:

$$v_1^m = v_1^v + J_1^m (V_1 - V_2) \tag{3-35}$$

hence:

$$-D_{12}^m \nabla \ln c_1 = -D_{12}^v \nabla \ln c_1 - D_{12}^m c_1 \nabla \ln c_1 (V_1 - V_2) \tag{3-36}$$

and so:

$$D_{12}^v = D_{12}^m (1 - c_1 (V_1 - V_2)) \tag{3-37}$$

and using equation (3-30):

$$D_{12}^v = -\frac{VRT}{R_{12}} (\partial \ln a_1 / \partial \ln c_1)_{TP} (1 - c_1 (V_1 - V_2)) \tag{3-38}$$

Now

$$\left(\frac{\partial \ln a_1}{\partial \ln c_1}\right) = \left(\frac{\partial \ln a_1}{\partial \ln x_1}\right) \frac{V}{V_2} \tag{3-39}$$

where x_1 represents the mole fraction of species 1.

$$\therefore \quad D_{12}^v = -\frac{VRT}{R_{12}} \left(\frac{\partial \ln a_1}{\partial \ln x_1}\right) \frac{V}{V_2} (1 - c_1 (V_1 - V_2)) \tag{3-40}$$

which simplifies to:

$$D_{12}^{V} = \frac{-VRT}{R_{12}}(\partial \ln a_1/\partial \ln x_1)_{TP} \cdot \qquad (3\text{-}41)$$

Similarly if one considers the flux of component 2 one gets:

$$D_{21}^{V} = \frac{-VRT}{R_{12}}(\partial \ln a_2/\partial \ln x_2)_{TP} , \qquad (3\text{-}42)$$

confirming the result of section 3-2 that in the volume fixed frame $D_{12}^{V} = D_{21}^{V}$.

Self diffusion in a single component system can be envisaged as mutual diffusion in a binary system of species 1 and 3, where 1 and 3 are identical except for some distinguishing tag. In this case equation (3-41) becomes:

$$D_{13} = \frac{-VRT}{R_{13}} \qquad (3\text{-}43)$$

since the mixture is ideal. D_{13} is taken to be equal to the self diffusion coefficient D_{11}. Laity (113) identifies R_{13} with the R_{11} which dropped out of equation (3-21). This is not so and the practice of labelling the R_{13} as R_{11} can lead to confusion. However, the subscript 11 is of value and so R_{13} is identified as R_{11}^{*}.

Self diffusion coefficients in a binary mixture may be be introduced by considering a 3 component system, where two components, 1 and 3, are identical except for the distinguishing tag and where there is no concentration gradient of species 2. Equation (3-21) gives:

$$-\nabla\mu_1 = R_{12}c_2(V_2 - V_1) + R_{13}c_3(V_3 - V_1) \qquad (3\text{-}44a)$$

$$-\nabla\mu_2 = R_{21}c_1(V_1 - V_2) + R_{23}c_3(V_3 - V_2) = 0 \qquad (3\text{-}44b)$$

Since 3 is taken to be chemically identical with 1, R_{12} is identified with R_{32}. Because of the ideality of mixtures of 1 and 3 at constant concentration of 2 one gets:

$$v_1^v = -D_{11}^v \nabla \mu_1 \quad . \tag{3-45}$$

In this case the mole fixed and volume fixed frames coincide and so $c_1 v_1^v + c_3 v_3^v = 0$. From now on the superscript v is dropped and all diffusion coefficients are to be taken as measured in the volume fixed frame. Solving equations (3-44) for v_1:

$$v_1 = \nabla \mu_1 / (R_{12} c_2 + R_{13} c_1) \tag{3-46}$$

where c_1 now represents the total concentration of species 1 and 3. Comparison with equation (3-45) leads to:

$$D_{11} = -VRT/(R_{12} x_2 + R_{11}^* x_1) \tag{3-47}$$

and similarly we get:

$$D_{22} = -VRT/(R_{22}^* x_2 + R_{12} x_1) \quad . \tag{3-48}$$

Combinations of equations (3-42), (3-47), and (3-48) lead to relationships between the three diffusion coefficients. It can be seen that as x_1 goes to zero then D_{11} becomes identical with D_{12} and that as x_2 goes to zero so D_{22} becomes identical with D_{12}. This gives the limiting behaviour of the diffusion coefficients in a binary mixture. The self and mutual diffusion coefficients are also related across the composition range by:

$$D_{11}Q = D_{12} \left\{ \frac{R_{12}}{x_1 R_{11}^* + x_2 R_{12}} \right\} \tag{3-49}$$

$$D_{22}Q = D_{12} \left\{ \frac{R_{12}}{x_1 R_{12} + x_2 R_{22}^*} \right\} \tag{3-50}$$

where Q is defined as $(\partial \ln a_1 / \partial \ln x_1)_{TP}$.

Equations (3-49) and (3-50) can be combined to yield numerous relationships between the three diffusion coefficients. The most interesting is that obtained by multiplying equation (3-49) by the mole fraction of species 2, x_2, and equation (3-50) by the mole fraction of species 1, x_1, and adding to give:

$$(x_1 D_{22} + x_2 D_{11})Q = D_{12} \left\{ \frac{x_1 R_{12}}{x_1 R_{12} + x_2 R_{22}^*} + \frac{x_2 R_{12}}{x_2 R_{12} + x_1 R_{11}^*} \right\} \quad (3\text{-}51)$$

When the friction coefficients are such that:

$$R_{11}^* R_{22}^* = R_{12}^2 \quad (3\text{-}52)$$

then equation (3-51) reduces to:

$$D_{12} = (x_1 D_{22} + x_2 D_{11})Q \quad (3\text{-}53)$$

Equation (3-53) has been frequently tested against experimental data (24,125,126) and is often referred to as the Hartly-Crank(120) or Darken equation (127).

It is also interesting to consider equations (3-49) and (3-50) in relation to the following equations:

$$D_{12} = D_{11}(\partial \ln a_1 / \partial \ln c_1)_{TP} \quad (3\text{-}54)$$

$$= D_{11}\frac{V}{V_2}(\partial \ln a_1 / \partial \ln x_1)_{TP} \quad (3\text{-}55)$$

and similarly for the self diffusion coefficient of species 2:

$$D_{12} = D_{22}\frac{V}{V_1}(\partial \ln a_2 / \partial \ln x_2)_{TP} \quad (3\text{-}56)$$

From equations (3-55) and (3-56) we see that $D_{11}/D_{22} = V_2/V_1$. Comparing equation (3-49) with (3-55) we see that for equation (3-55) to hold then:

$$R_{12} / (x_1 R_{11}^* + x_2 R_{12}) = V_2 / (x_1 V_1 + x_2 V_2) \quad (3\text{-}57)$$

and so:

$$R_{11}^{*}/R_{12} = V_1/V_2 \cdot \qquad (3\text{-}58)$$

Similarly, comparing equations (3-50) and (3-56) the condition for (3-56) to hold is:

$$R_{22}^{*}/R_{12} = V_2/V_1 \qquad (3\text{-}59)$$

When equations (3-55) and (3-56) hold then equation (3-53) holds and we have:

$$R_{11}^{*}/R_{12} = R_{12}/R_{22}^{*} = V_1/V_2 = D_{22}/D_{11} \qquad (3\text{-}60)$$

This relationship has previously been obtained by Tyrrel (128) from a consideration of the equations deduced by Bearman (117).

3-4 The Statistical Mechanical Theory of Bearman.

As a result of a series of papers (117) dealing with transport processes in liquid solutions, Bearman and Kirkwood have derived an expression for the mean frictional force acting on a molecule of species i in a n component system undergoing one dimensional, isothermal, isobaric diffusion, $\bar{F}_i^{(1,1)}$:

$$\bar{F}_i^{(1,1)} = \frac{1}{2} \sum_{j=1}^{n} \int c_j (\bar{r}/r) \frac{d\phi_{ij}}{dr} (g_{ij}^{(2,1)} - g_{ji}^{(2,1)}) \, d^3r \qquad (3\text{-}61)$$

where c_j is the concentration of species j in molecules per unit volume, ϕ_{ij} is the intermolecular potential between molecules i and j, assumed to depend only on the the magnitude of the vector distance, $\bar{r}$, separating the molecules. $g_{ij}^{(2,1)}$ is the non-equilibrium perturbation function which is the difference between the equilibrium radial distribution function, $g_{ij}^{(2,0)}$, and the non-equilibrium pair correlation function, $g_{ij}^{(2)}$.

The theory is developed in such a way that the

microscopic equations lead to the phenomenological relations for matter flux. Thus the results of the theory are not independent of the phenomenological approach. The non-equilibrium perturbation is written in terms of the equilibrium radial distribution as follows:

$$g_{ij}^{(2,1)}/g_{ij}^{(2,0)} = \alpha_{ij}^{(1)} \frac{\bar{r}}{r}.(v_j - v_i) + \text{higher order terms} \quad (3\text{-}62)$$

which combines with equation (3-61) to give:

$$\nabla \mu_i = \bar{F}_i^{(1,1)} = - \sum R_{ij} c_j (v_j - v_i) \quad (3\text{-}63)$$

where the R_{ij} are defined by:

$$R_{ij} = -\frac{1}{6} \int g_{ij}^{(2,0)} \frac{d\phi_{ij}}{dr} (\alpha_{ij}^{(1)} + \alpha_{ji}^{(1)}) \, d^3r \quad . \quad (3\text{-}64)$$

The theory can not predict the magnitude of the friction coefficients but leads to expressions for their ratios. In a binary system the theory gives:

$$\frac{R_{11}^* VRT}{x_1 R_{11}^* + x_2 R_{12}} = -\frac{1}{6} \int \frac{d\phi_{11}}{dr} g_{11}^{(2,0)} \alpha_{11} \, d^3r \quad (3\text{-}65)$$

$$R_{12} VRT(1/(x_1 R_{11} + x_2 R_{12}) + 1/(x_1 R_{12} + x_2 R_{22})) = -\frac{1}{3} \int \frac{d\phi_{12}}{dr} g_{12}^{(2,0)} \alpha_{12} \, d^3r \quad (3\text{-}66)$$

$$\frac{R_{22}^* VRT}{x_1 R_{12} + x_2 R_{22}^*} = -\frac{1}{6} \int \frac{d\phi_{22}}{dr} g_{22}^{(2,0)} \alpha_{22} \, d^3r \quad (3\text{-}67)$$

where $\alpha_{ij} = \alpha_{ij}^{(1)} D_{ij}$

The evaluation of the integrals on the right hand side of these equations is too complicated a task except for the simplest cases. Bearman (117) considered the case where the integrals are independent of concentration. This is true for solutions where the radial distribution function is independent

of concentration and where there is no excess volume of mixing. By considering the limits of the concentration range, equations (3-65) and (3-67) lead to:

$$R_{11}^{*}/R_{12} = R_{12}/R_{22}^{*} = V_1^{o}/V_2^{o} \qquad (3\text{-}68)$$

where V_1^{o} and V_2^{o} are the molar volumes of the pure species 1 and 2. Equation (3-53) will clearly hold for such solutions which are called regular by Bearman (117). Equation (3-68) is a particular case of equation (3-60) when the excess volume of mixing is zero.

In order for the geometric mean relationship, equation (3-52), to hold for the friction coefficients it is necessary for the following relationship to hold:

$$\int \frac{d\phi_{11}}{dr}\alpha_{11}g_{11}^{(2,0)}d^3r + \int \frac{d\phi_{22}}{dr}\alpha_{22}g_{22}^{(2,0)}d^3r = 2\int \frac{d\phi_{12}}{dr}\alpha_{12}g_{12}^{(2,0)}d^3r \; . \qquad (3\text{-}69)$$

The general theory also shows that for a regular solution $D_{11}\eta$, where η is the coefficient of shear viscosity, is independent of composition. This condition is in agreement with the Stokes-Einstein and related equations. When $D_{11}\eta$ is a constant then we have:

$$D_{11}^{o}\eta_1 = D_{11}\eta = D_{11}^{\infty}\eta_2 \; . \qquad (3\text{-}70)$$

Equation (3-53) is then transformable to the Carman-Stein equation (129):

$$D_{12}\eta = (D_{11}^{\infty}x_2\eta_2 + D_{22}^{\infty}x_1\eta_1)Q \qquad (3\text{-}71)$$

3-5 Enskog's Theory for Diffusion in a Dense Hard Sphere System.

The kinetic theory of gases at low pressures is sufficiently well developed to enable reasonable estimates of transport coefficients to be made. At present there is no analogous theory giving a satisfactory description of transport processes in dense fluids. The fundamental problem is to develop a realistic description of the molecular motion in the force field provide by molecular interactions. Since an adequate description of intermolecular forces is still in its infancy, it can be appreciated that a solution to this problem is not to be expected for a considerable time.

The model of a dense fluid made up of hard spheres has received considerable attention. The reason for this is that hard sphere fluids exhibit several simplifying features which make their theoretical treatment more tractable. For example, the assumption of pairwise additivity for the configuration energy is exact for a hard sphere fluid and thermodynamic and transport properties depend only on the value of the radial distribution function, $g(r)$, at the point of contact. In the dense hard sphere fluid it is possible to assume binary collisions only and the theory can be developed in a similar way to that for dilute gases. The probability of a three body collision is negligible since a binary collision is an instantaneous event. The theoretical predictions for the model can also be compared with the results of machine calculations.

For dilute monatomic gases the Chapman-Enskog theory (118) gives rigorous relations between the transport properties

and the intermolecular potential, $\phi(r)$. Provided that $\phi(r)$ is known, transport properties can be predicted to within a few per cent. For polyatomic molecules the exact theory is not fully developed, but the simple theory gives reasonable predictions for the coefficients of shear viscosity and diffusion.

The Enskog theory of diffusion in dense hard sphere systems is developed from dilute gas theory. The important assumptions in the development of the dilute gas theory are that binary collisions need only be taken into account and that there is no correlation between succeeding collisions, i.e. there is molecular chaos. In a real dense fluid neither of these assumptions is particularly good, but a hard sphere model meets the first condition exactly. Enskog now proposed that a molecular chaos of velocities, but not position, was a reasonable approximation. At sufficiently high densities this approximation breaks down.

The result of the theory is that the diffusion coefficient for a dense, hard sphere fluid is related to that at low density, D_g, by the expression:

$$D = D_g/g(\sigma), \qquad (3\text{-}72)$$

where $g(\sigma)$ is the value of the radial distribution function at contact. For a one component dilute hard sphere fluid, the first approximation of Enskog (118) to the diffusion coefficient is given by:

$$D = 3(kT/\pi m_1)^{1/2} V_1^{\circ}/8\sigma_{11}^2 \quad , \qquad (3\text{-}73)$$

where V_1° is the volume per sphere in the fluid, σ_{11} is the diameter of the sphere, and m_1 is its mass. For a dense hard

sphere fluid we have:

$$D_{11} = 3\,(kT/\pi m_1)^{1/2} V_1^o / 8\sigma_{11}^2 g_{11}(\sigma_{11}). \quad (3\text{-}74)$$

In a dilute hard sphere fluid of components 1 and 2 the first approximation of Enskog (118) to the mutual diffusion coefficient is given by:

$$D_{12} = 3(kT/2\pi\mu_{12})^{1/2} V/8\sigma_{12}^2 , \quad (3\text{-}75)$$

where V is the average volume per molecule and $\sigma_{12} = (\sigma_{11} + \sigma_{22})/2$. μ_{12} is the reduced mass of spheres 1 and 2. For a dense hard sphere fluid one gets:

$$D_{12} = 3(kT/2\pi\mu_{12})^{1/2} V/8\sigma_{12}^2 g_{12}(\sigma_{12}) . \quad (3\text{-}76)$$

The phenomenolgical theory gives the following results for the hard sphere systems described above:

$$D_{11} = -kTV/R_{11}^* , \quad (3\text{-}77)$$

$$D_{12} = -kTV/R_{12}^* . \quad (3\text{-}78)$$

Comparing equations (3-77) and (3-78) with equations (3-74) and (3-76) one gets the following expressions for the friction coefficients in a dense hard sphere fluid:

$$R_{11}^* = -\frac{8}{3}\sigma_{11}^2 (\pi m_1 kT)^{1/2} g_{11}(\sigma_{11}) , \quad (3\text{-}79)$$

$$R_{12} = -\frac{8}{3}\sigma_{12}^2 (2\pi\mu_{12} kT)^{1/2} g_{12}(\sigma_{12}) , \quad (3\text{-}80)$$

and similarly:

$$R_{22}^* = -\frac{8}{3}\sigma_{22}^2 (\pi m_2 kT)^{1/2} g_{22}(\sigma_{22}) . \quad (3\text{-}81)$$

It is interesting to compare the geometric mean rule for the friction coefficients, equation (3-52), with the result from the above equations:

$$R_{11}^{*}R_{22}^{*} = R_{12}^{2}\,\frac{\sigma_{11}^{2}+\sigma_{22}^{2}}{\sigma_{12}^{4}}\,\frac{(m_1+m_2)}{2(m_1m_2)^{1/2}}\,\frac{g_{11}(\sigma_{11})g_{22}(\sigma_{22})}{g_{12}(\sigma_{12})^{2}} \qquad (3\text{-}82)$$

Thus the geometric mean rule does not generally hold for this model except for the case where $\sigma_{11} = \sigma_{22}$ and $m_1 = m_2$, that is for identical molecules as far as the model is concerned.

Thus the Enskog theory for a dense fluid of hard spheres leads to expressions for the friction coefficients which can be evaluated if σ_{11}, σ_{22}, m_1, m_2, $g_{11}(\sigma_{11})$, $g_{12}(\sigma_{12})$, and $g_{22}(\sigma_{22})$ are known. The above treatment is based on that of McLaughlin (119).

3-6 The Radial Distribution Function.

When the assumption of pairwise additivity is valid, then a theoretical description of the fluid state may be developed in terms of the radial distribution function. The radial distribution function, which is a function of distance, density, and temperature, gives the ratio of the local number density at a distance r from a reference molecule to the bulk number density:

$$g(r) = \varrho(r)/\varrho. \qquad (3\text{-}83)$$

For a mixture the radial distribution function also depends on the composition.

For a hard sphere fluid there are several theoretical and empirical relations for the radial distribution function. Notable amongst these are the Percus-Yevick equation (130) and the Carnahan-Starling equation (131,132).

The Percus-Yevick equation is:

$$g(r_{12})\exp\left[\frac{\phi(r_{12})}{kT}\right] = 1 + \int\left[g(r_{23}) - 1\right] g(r_{13}) \left[1 - \exp\frac{\phi(r_{13})}{kT}\right] d\bar{r}_3 \quad (3\text{-}84)$$

This has been solved (133) for a mixture of hard spheres to give at the point of contact:

$$g_{12}(\sigma_{12}) = \frac{1}{(1-\varepsilon_3)} + \frac{3\sigma_{11}\sigma_{22}}{(\sigma_{11}+\sigma_{22})}\frac{\varepsilon_2}{(1-\varepsilon_3)^2} \quad , \quad (3\text{-}85)$$

where:

$$\varepsilon_i = \frac{\pi}{6}\sum \rho_j \sigma_j^i \quad . \quad (3\text{-}86)$$

$g_{11}(\sigma_{11})$ is obtained by putting 2 equal to 1 in equation (3-85). Equation (3-85) can also be written in the form:

$$2\sigma_{12}g_{12}(\sigma_{12}) = \sigma_{22}g_{11}(\sigma_{11}) + \sigma_{11}g_{22}(\sigma_{22}) \quad . \quad (3\text{-}87)$$

The Carnahan-Starling equation is an empirical equation which predicts the value of the radial distribution function at the point of contact only. Initially developed for a single component fluid, it has now been extended for the case of mixtures to give:

$$g_{12}(\sigma_{12}) = \frac{1}{(1-\varepsilon_3)} + \frac{3\sigma_{11}\sigma_{22}}{(\sigma_{11}+\sigma_{22})}\frac{\varepsilon_2}{(1-\varepsilon_3)^2} + 2\left(\frac{\sigma_{11}\sigma_{22}}{\sigma_{11}+\sigma_{22}}\right)^2 \frac{\varepsilon_3^2}{(1-\varepsilon_3)^2} \quad (3\text{-}88)$$

Again, $g_{11}(\sigma_{11})$ is obtained by making the necessary changes in the subscripts.

Chapter 4: N.M.R. INSTRUMENTATION.

4-1 Introduction.

The work reported in this thesis was carried out using a Bruker Pulsed N.M.R. Spectrometer, B-KR304s. The following sections describe in general terms the major differences between pulsed and continuous wave (c.w.) n.m.r. spectrometers; the Bruker instrument and particular problems that were encountered during this research; and finally a few comments are made on different instrumental techniques and developments that have been used in other spectrometer systems.

4-2 Pulsed and Continuous Wave N.M.R. Spectrometers.

The basic units of pulsed and c.w. spectrometers are superficially quite similar. Both require large magnetic fields to polarize the nuclear moments of the sample, an r.f. transmitter to generate the rotating H_1 field, an r.f. receiver to amplify and detect the signal from the sample and a probe to couple the transmitter and receiver to the sample.

On the magnet side there are few differences in the requirements. Magnets in high resolution c.w. and fourier transform n.m.r. require homogeneity of the order 1 part in 10^9, whereas wide line c.w. spectrometers and most pulsed spectrometers used for relaxation and diffusion studies have a homogeneity of about 1 part in 10^6. C.w. spectrometers operating at fixed radio frequency also require auxiliary sweep coils to vary the field strength throughout the range of resonance.

The transmitting requirements are, however, quite different. Pulsed spectrometers have to be capable of delivering short, high power pulses of r.f. signal to the probe, so creating the H_1 field. Typically, pulses are of the order of microseconds in length and H_1 fields up to several hundred gauss are produced which means that the power required is up to several kilowatts. C.w. spectrometers continuously transmit a much lower power signal. The H_1 field in a c.w. experiment may typically be as low as 10^{-4} gauss.

The receiver of a n.m.r. spectrometer needs to be sensitive to detect and amplify the weak nuclear signal. However, in a pulsed spectrometer the receiver must also be able to withstand large overloads during the transmission of an r.f. pulse and recover quickly enough to detect the signal produced. This problem does not arise in c.w. spectrometers where the transmitted power is much lower. Many of the problems in designing a pulsed spectrometer lie in meeting these two conflicting requirements. Much effort has gone into designing methods which isolate the transmitter and receiver from each other while linking both to the probe.

In general, it can be said that the design problems for a c.w. spectrometer are relatively simple compared to those for a pulsed spectrometer.

There is also a difference in the type of signal received from both types of spectrometer. In a c.w. experiment

the size of the nuclear signal as a function of frequency, or field strength, is determined for the sample under investigation. The pulsed experiment produces a signal which varies and decays away with time. The time domain function and the frequency domain function can be transformed into one another by means of Fourier analysis. This procedure allows the free induction decay following an r.f. pulse to be transformed into conventional n.m.r. spectra and forms the basis of Fourier transform n.m.r.

4-3 The Bruker B-KR304s.

The spectrometer used in these studies was manufactured by Bruker Physik AG, Kahlsruhe, Germany. The instrument was supplied in 1966 and since has been modified to produce a working system for measuring diffusion coefficients. A block diagram of the instrument is given in figure 4-1. The instrument has two operating frequencies of 15 MHz and 60 MHz. All measurements have been carried out at 60 MHz with a magnetic field strength of 1.409 Tesla for proton resonance.

In the following sections the units making up the spectrometer are described, then the magnet system and the pulsed field gradient unit are described.

A/ The Spectrometer.

i/ The Pulse Programmer.

The pulse programmer controls the position and duration of the radio frequency pulses transmitted to the

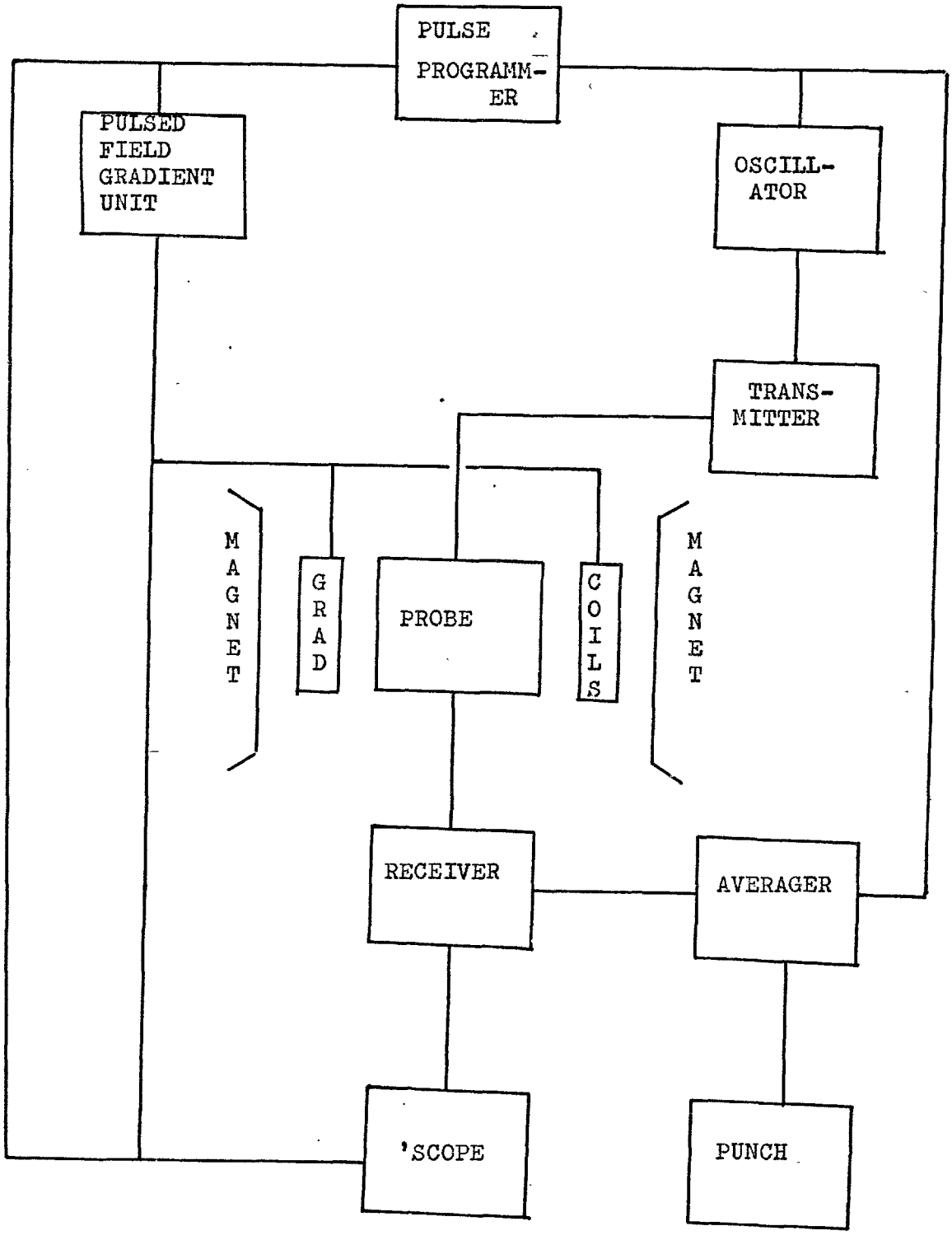


Figure 4-1: BLOCK DIAGRAM OF THE BRUKER PULSED N.M.R. SPECTROMETER.

probe. It also allows the selection of sequential or single pulse sequence operation, the former being used for setting up a Carr-Purcell sequence (5). All diffusion measurements are made in the single pulse mode.

The unit is designed to provide three independent r.f. pulses. In this work only pulses 1 and 2 were used to produce the 90 and 180 degree pulses. The position of the r.f. pulses in time, relative to an initial triggering pulse, are essentially monostable controlled, but the exact position is determined by clock pulses which are derived from and hence are synchronous with the master oscillator. In this way coherent operation is obtained. The r.f. pulse widths are also controlled by monostables which open r.f. gates in the oscillator unit allowing the 60 MHz r.f. signal into the transmitter and hence to the probe. The r.f. pulse widths are stable to 1 part in 10^3.

The pulse programmer also contains the 1 MHz crystal controlled oscillator which can be regarded as the heart of the instrument since it is from this oscillator that all the triggering pulses and the radio frequencies are derived. The short term stability of this oscillator is 1 part in 10^8.

ii/ The Oscillator Unit.

The unit labelled the oscillator produces the 15 and 60 MHz signals from the 1 MHz pulses of the master oscillator. This is achieved by frequency multipliers in steps of 5, 3, 2, and 2. This unit also contains the r.f. gates which when open allow the r.f. signals through to the transmitter. This is achieved by switching the polarity of valve grids via the

output of controlling monostables.

As well as providing the signal for the transmitter, the oscillator provides a 60 MHz signal which can be injected into the receiver. This heterodynes with the signal from the sample and by observing the beat frequency the field strength can be adjusted to bring the sample into resonance.

iii/ The Transmitter.

The transmitter amplifies the signal from the oscillator and transmits it to the probe. The maximum H_1 field produced by the transmitted signal at 60 MHz is about 60 gauss. The transmitter is of conventional design and operates in the class C region. Successive stages in the transmitter are transformer coupled and tuned to the resonant frequency so as to only allow that frequency signal through to the probe. After the replacement of any valves in this unit it was necessary to retune all the stages. Care has to be taken here not to distort the r.f. pulse shape. When switching to 15 MHz, transformer couplers tuned to this frequency are switched into circuit.

iv/ The Probe.

The probe used in these studies was of dural construction. The probe contains transmitter and receiver coils and associated tuning capacitors. The transmitter and receiver coils are both wound about the same axis. The sample tube when inserted into the probe rests on a teflon stopper. For samples of height less than 1 cm., the sample lies well within the transmitter coil, thus ensuring good homogeneity of H_1.

The temperature of the sample is controlled by means of a dural jacket which encloses the volume occupied by the coils. Thermostatted water is circulated through the jacket. The probe temperature, as indicated by a mercury in glass thermometer placed in the sample space, was constant to within 0.1 C over the period of a day. Most n.m.r. probes maintain temperature control by means of a gas flow over the sample, but,with this arrangement,it is difficult to get control to better than ± 1 C.

In our system the temperature of the water was controlled by a Churchill Laboratory Thermocirculator. The temperature in these devices is controlled by means of triac switching which unfortunately generated interference. This was supressed by an LC filter network.

v/ The Receiver.

The receiver amplifies the signal from the sample and demodulates it. The receiver bandwidth is 300 kHz. Filters can be switched into circuit to reduce the bandwidth to 100, 10, or 1 kHz. Most measurements were carried out at 10 kHz bandwidth. The receiver employs diode detection. The transfer characteristic of the receiver at full gain is shown in figure 4-2. With the instruments available it was not possible to investigate non-linearity at low input levels.

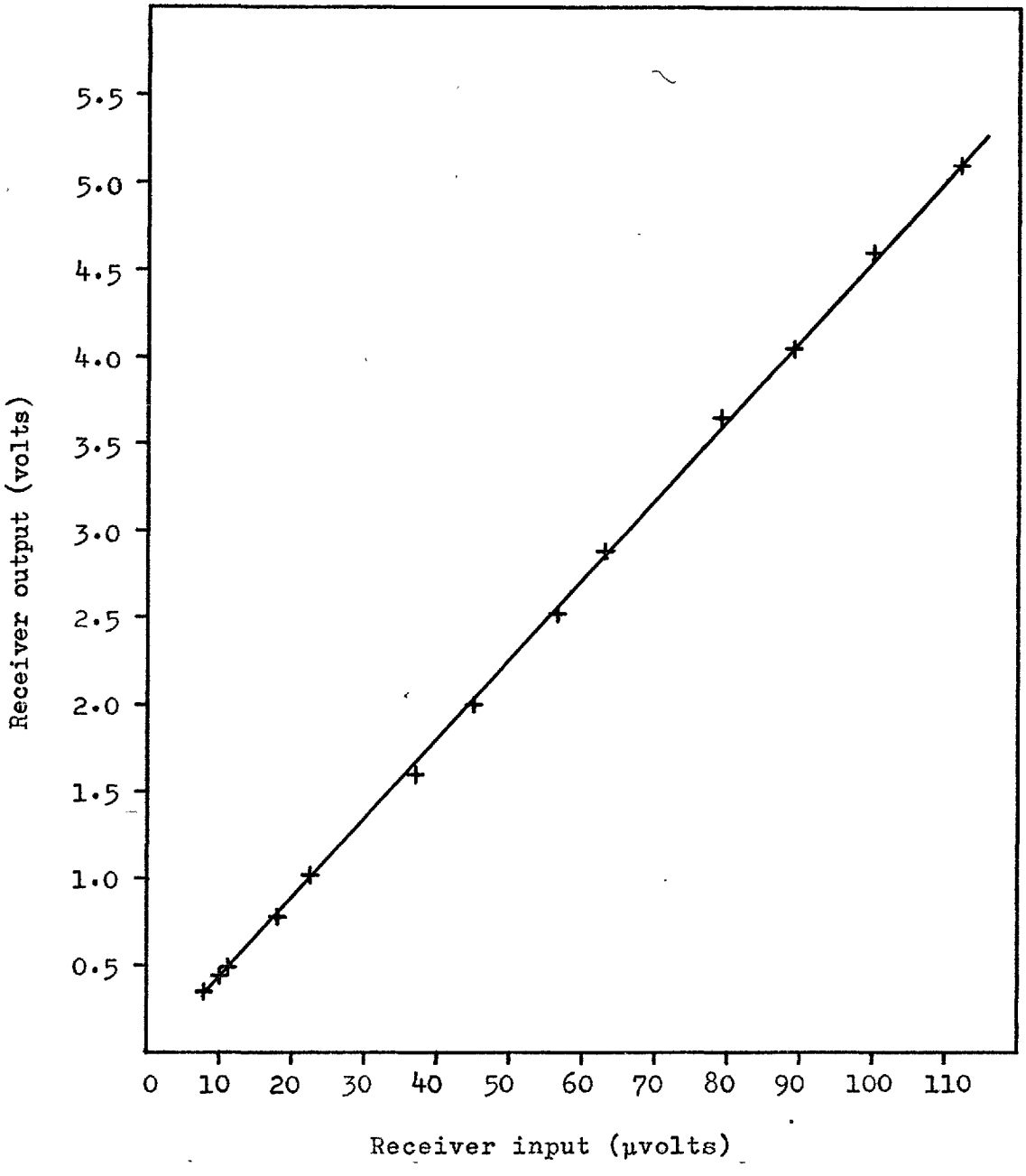


Figure 4-2: TRANSFER CHARACTERISTIC OF RECEIVER.

B/ The Magnet System.

i/ The Magnet.

A Bruker B-E25C8 elctro-magnet was used during this study. The magnet has 25 cm. poles and an adjustable air gap of 5 to 150 mm. Special pole caps were fitted to the magnet to improve field homogeneity, which was about 2 in 10^6. In operation the air gap was typically 35 mm. For proton resonance at 60 MHz. the current drawn by the magnet was about 18 amps.

The magnet is water cooled, each pole being cooled by three loops connected in parallel. The cooling circuit is a closed loop, heat being exchanged with tap water in a heat exchanger. The circuit incorporated two Rotameter flow sensors. One of the sensors detected the flow of distilled water in the cooling circuit, the other detected the flow of tap water through the heat exchanger. If either flow dropped to too low a level the magnet power supply turned off.

It was necessary to clean the magnet cooling coils out about every six months, otherwise they became blocked with debris picked up from pipe walls. It was often sufficient to vigorously push a length of 16 gauge copper wire in and out of the cooling coil exit. If this did not clear the coil then tap water was repeatedly forced through the coil in forward and reverse directions until it became unblocked.

ii/ The Magnet Power Supply.

Power to the magnet was supplied by a Bruker B-MN200/50 SI6N power supply unit. The power supply is air cooled. Normally the power supply current is stable to about 1 part in 10^6.

During the early part of this study the spectrometer was situated in very large laboratory and heat generated by the spectrometer did not appreciably affect the ambient temperature. However,after moving to a new laboratory it was found that the ambient temperature rose to 29 C when the spectrometer was turned on. At this temperature the power supply was not cooled sufficiently and leakage currents in the germanium regulating transistors became large enough to cause significant fluctuations in the current supply. It was necessary to have air conditioning installed into the laboratory. Room temperature has been, since then, maintained at about 22 C.

During the period of this research the magnet and its power supply gave little trouble apart from that mentioned above.

C/ The Production of the Pulsed Field Gradient.

The field gradient is produced by passing current through two co-axial coils so that their fields are opposed. The current through the coils is controlled by the pulsed field gradient unit. These are described in the following sections.

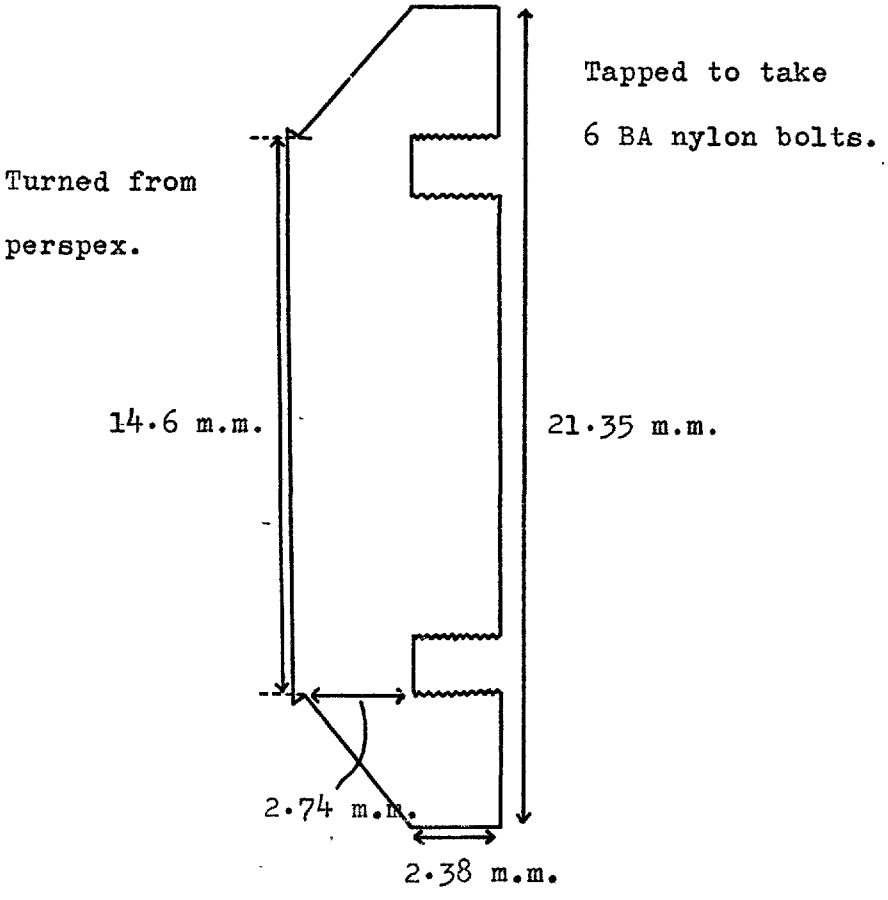
i/ The Gradient Coils.

The field gradient coils used in this work were supplied ready built by Bruker. It was not possible to determine the geometry of the coils since they were sealed in resin. They appeared to be simply a coil of wire rolled like a swiss roll. They were fixed on the outside of the probe.

This type of coil does not have the best geometry for producing a linear field gradient because of the effect of image currents in the pole faces. This has been discussed in detail by Tanner (11,12). It was felt that the replacement of the coils by coils built to Tanner's recommended design would improve the performance of the instrument. A set of such coils was designed and built to fit close to the sample, inside the main body of the probe, within the volume enclosed by the temperature jacket. Details of the coils are given in figure 4-3. These coils have not yet been used because a pulse generator with which they were to be used is still being built.

ii/ The Pulsed Field Gradient Unit.

This unit was supplied by Bruker. Its function is to supply current pulses to the gradient coils. On receipt of a trigger pulse a monostable sets a delay before the start of the first current pulse, a second monostable delays the start of the second pulse from the start of the first. The width of the pulses is controlled by a third monostable. This monostable closes a transistor switch allowing current from a variable current source to flow through the coils.



The coils consist of 14 turns of 36 gauge wire wound in a single layer.

The coils are designed for a pole face separation of 36.5 m.m. with a 12.77 m.m. gap between the gradient coils.

Figure 4-3: DIMENSIONS OF THE FORMERS MADE FOR THE FIELD GRADIENT COILS.

In series with the gradient coils is a known, stable resistance. The size of the gradient pulse is monitored by measuring the voltage developed across this resistance.

This unit caused quite a lot of trouble because, at times, it had a tendency to produce unequal pulses. This was largely due to poor mechanical construction. The effect of unequal gradient pulses is discussed later.

D/ Data Aquisition.

In order to determine the diffusion coefficient it was necessary to measure the following parameters: echo amplitude,size of field gradient pulse, width of field gradient pulse, and the delay between the first and second gradient pulse.

The echo and one of the field gradient pulses were displayed on a Tektronix type 546 Storage Oscilloscope fitted with a type 3A6 dual trace Y amplifier and a type 3B3 time base. One channel of the Y amplifier was fed the output from the receiver and the other measured the voltage across the fixed reisistance in series with the gradient coils. An external unit was used to trigger the the oscilloscope so that the echo and the gradient pulse could both be stored during a pulse sequence. Most of the measurements were made visually from the stored images on the oscilloscope. This procedure was satisfactory for the gradient pulse and also for the spin echo when the signal to noise ratio was good.

When the signal to noise ratio was poor the echo signal was averaged over a number of sweeps on a DL 101

100 point averager made by Data Laboratories Ltd., England. The principle of the averager is that the signal is sampled at 100 points and the voltage at each point stored. The signal is repeated a number of times and each time the voltage at each of the 100 sampling points is added to the previously accumulated voltage. The effect is that any random noise superimposed on the repetitive signal averages out with successive additions and so the signal to noise ratio improves. In general for N sweeps the signal to noise ratio improves $\sqrt{N}$ times. When using the averager one is interested in two parts of the signal - the echo and the base line. An external unit was built which enabled detailed sampling across the spin echo (64 points at 5 points per ms.) followed by a delay of 200 ms. then a final sampling (36 points at 5 points per ms.) of the base line.

The averager has a 1 in 128 resolution over an input range of ± 1 volt. In order that the echo should fill as large a part of this sampling window as possible a preamplifier was built. The amplifier consists of two 741 operational amplifiers connected in inverting configuration each providing a stepped gain of 1, 2·5, 5, and 10 times.

The final averaged signal was viewed visually on an oscillocope built into the spectrometer. The output from the averager was punched onto paper tape by way of an 1132 Data Dynamics punch. The paper tape was processed on Imperial College Computing Centre's CDC 6400 computer to return the

height of the signal across the echo relative to the base line.

Timing intervals (τ, δ, Δ) were measured by counting pulses derived from the master oscillator on a modified SC3-Timer Counter made by Advance Controls Ltd.

4-4 Other Instrumental Methods.

The units of the Bruker spectrometer were made up of descrete components containing a large number of valves. With the advent of cheap monolithic integrated circuits modern instruments tend to be far more compact and to utilise digital techniques to a far greater extent.

In the following sections some of the differences between methods used on the Bruker spectrometer and on other spectrometers are outlined.

A/ Pulse Programmer.

The modern pulse programmer would almost certainly be completely dependent on digital counting techniques rather than on delays set by monostables. With the increasing availability of cheap integrated circuits it has become feasible to build pulse programmers with a far greater variety of possible pulse sequences. Although this is not necessary for simple diffusion measurements, it does enable the spectrometer to be used in more complex pulse experiments and hence provides a more versatile research instrument.

B/ The Transmitter.

Modern transmitters tend to be wide band rather than narrow band as on our instrument. Our instrument has narrow

bandwidth in order that only the 60 MHz signal is transmitted to the probe and other components are filtered out. The resonant frequency in modern instruments is often produced by a synthesizer and no other frequency components are present, hence a wide band transmitter can be used.

The use of a wide band transmitter has several advantages. First of all, pulse distortion is considerably reduced. Secondly, it is far easier to change frequency since the transmitter does not need retuning and the frequency can just be selected on the synthesizer. When investigating different nuclei it is now becoming more common to change frequency in this way rather than to operate at constant frequency and change the field strength.

C/ The Receiver.

As the signal becomes weaker then noise becomes more of a problem. The signal to noise ratio can be improved by averaging techniques, but this takes time and it is best to keep the noise level as low as possible. The noise level of an amplifier is largely dependent on the nature of the first stage. Nowadays this probably uses field effect transistors. In order to reduce attenuation of the signal in the transmission line, modern instruments often have a preamplifier as close to the probe as is physically possible.

Our receiver employs diode detection. The major disadvantage of this method is the non linearity of the transfer function at low signal strengths. It might appear that a phase sensitive detector, which is inherently linear,

would be an improvement. Phase sensitive detection also allows signal averaging to be used to much lower signal strengths (143). However, phase sensitive detection introduces other problems (144) and the tendency is for diode detection to be used in the majority of cases.

The non linearity of the diode detector may be corrected by the use of another non linear network in series with the diode so that the non linearities cancel (145).

D/ Data Collection.

The availability of relatively inéxpensive, small, laboratory computers has made virtually automatic operation of spectrometers possible. Data is transferred to the computer via high speed analog to digital convertors.

Earlier systems often used voltage to frequency convertors to monitor voltage levels.

Signal averaging is now a common procedure. This is carried out by the controlling computer in the most modern systems. A cheaper alternative to the multichannel averager used in these experiments is the boxcar integrator. This is essentially a single channel averager and was quite often used on earlier systems, but it is much slower.

E/ Production of the Field Gradient.

The usual method of producing the field gradient is to use coils producing a gradient in the H_o direction. Another method is to pass current through bundles of wire parallel to the axis of the sample coil (17,91). This produces a gradient perpendicular to H_o. A design based on this method has been recently produced (146).

Chapter 5: EXPERIMENTAL PROCEDURE AND SOURCES OF ERROR.

5-1 Introduction.

In this chapter the general experimental procedure in determining the diffusion coefficients is described. Specific instrument settings are not given here, but are reported with the results for each system studied. Possible sources of error and their treatment are discussed. The effect of unequal gradient pulses is investigated using the equations developed in section 2-9, which describe the evolution of the spin echo signal with time. Finally a brief description of the computing programmes used in this work is given.

5-2 Preparation of Samples.

Binary mixtures were made up either volumetrically or by weighing directly into the n.m.r. tubes. The latter procedure was used for mixtures containing the relatively expensive deuterated compounds and fractionated polypropylene glycol samples. The n.m.r tubes were made of soda glass, were of 6 m.m. diameter, and were filled to a height of about 5 m.m. with the sample under investigation.

Once in the n.m.r. tubes the sample was frozen in liquid nitrogen and the n.m.r. tube sealed in a bunsen flame. No attempt was made to remove dissolved gases from the sample. From an experimental point of view it is an advantage to have small amounts of dissolved oxygen present since this reduces the relaxation time and allows more frequent repetition of

the pulse sequence.

It was found that when sealing the n.m.r. tubes it was best to avoid a narrow drawn out neck. This was because volatile components were liable to condense in this region and a large proportion of liquid could gather in the neck held in position by capillary action. If a well rounded seal was produced then this build up of condensate did not occur.

5-3 Positioning the Probe in the Magnetic Field.

The probe was positioned in a part of the magnetic field so that the observed echo shape corresponded to the expected shape as plotted in figure 2-4. The echo width at half height was typically 4 milliseconds.

5-4 Tuning the Spectrometer.

The spectrometer was brought to resonance with the sample by injecting the 60 MHz signal from the oscillator into the receiver. This heterodyned with the signal from the sample. The magnet field strength was adjusted until the beat frequency came close to zero.

The transmitter was tuned to produce the most powerful r.f. pulse in the following way. The second r.f. pulse was turned off and the length of the first pulse was reduced so that it was shorter than a 90 degree pulse. The free induction decay signal following this pulse was observed and the tuning capacitor on the probe and the tuner on the transmitter adjusted until the signal was a maximum.

The resonance condition was checked before each determination of a diffusion coefficient. The transmitter was tuned in the above fashion about once per week. More detailed tuning of the transmitter and tuning of the receiver were only carried out after maintenance work.

5-5 Adjusting the 90 and 180 Degree Pulses.

After tuning the spectrometer, the length of the first r.f. pulse was gradually increased until the free induction decay signal went through its first maximum. The length of the pulse was then carefully adjusted until the signal was exactly on its maximum. The second r.f. pulse was now turned on and, in a similar fashion, carefully adjusted to produce the maximum echo height.

The time interval, τ, between the r.f. pulses was now selected. Because of spin-spin relaxation a longer interval between the pulses produces a smaller echo, but the interval has to be long enough to allow a reasonable time, Δ, between the field gradient pulses. In practice, τ was set between 28 and 80 milliseconds.

5-6 Positioning the Field Gradient Pulses.

The pulsed field gradient unit takes a while to recover from a gradient pulse before it is ready to produce a second pulse. For this reason at least 28 milliseconds was allowed between the gradient pulses. It was also necessary to allow at least 10 milliseconds between the second gradient pulse

and the spin echo, otherwise the echo became somewhat distorted. In practice the second gradient pulse was positioned shortly after the 180 degree r.f. pulse so that it was well away from the echo. Apart from this, the positioning of the gradient pulses is somewhat arbitrary. In general, when measuring lower diffusion coefficients it is best to have Δ as long as possible so as to get the maximum echo attenuation for a given gradient pulse. However, as mentioned above, this requires a longer interval between the r.f.pulses and so the echo becomes smaller. For samples with low concentration of active nuclei or with short transverse relaxation time this can be a problem.

5-7 Determination of the Diffusion Coefficient.

Before and after each experimental run the probe temperature was checked by inserting a mercury in glass thermometer into the sample space. The sample to be studied was always allowed at least 15 minutes to equilibrate in the probe before any measurements were made.

The diffusion coefficients were determined according to the equation (2-16):

$$\ln \frac{A(2\tau)}{Ao} = -\gamma^2 D\delta^2(\Delta - \frac{\delta}{3})G^2 .$$

The procedure adopted was to keep δ and Δ essentially constant and measure the echo height whilst varying G. G is proportional to the voltage, V, developed across the fixed resistance in series with the gradient coils. V was monitored on the oscilloscope. A least squares fit for a straight line was fitted to a plot of $-\ln A(2\tau)$ against $\delta^2(\Delta - \delta/3)V^2$. The gradient of the line

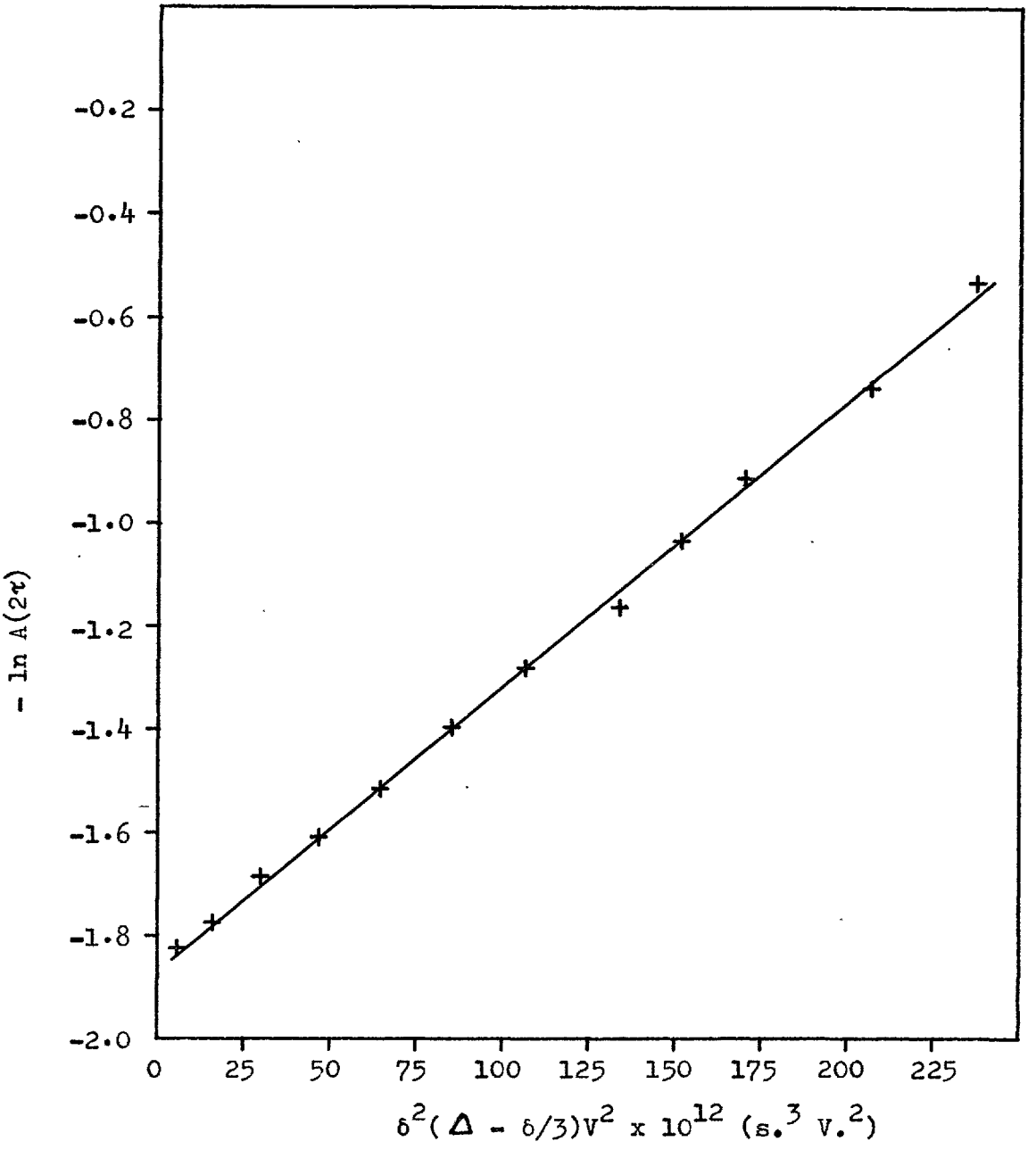


Figure 5-1: A TYPICAL EXPERIMENTAL PLOT PRODUCED IN DETERMINING THE SELF DIFFUSION COEFFICIENT.

was determined together with its 90 per cent confidence limits. The gradient of the line is proportional to the self diffusion coefficient:

$$\text{gradient} = KD.$$

The calibration constant, K, was determined by measuring the gradient for a sample with a known self diffusion coefficient. The choice of calibration standard is discussed in the next section.

A typical experimental plot is shown in figure 5-1.

5-8 Calibration Procedure.

The field gradient coils can be calibrated in three ways. First of all it is possible to determine the magnetic field gradient produced by the coils from a knowledge of the geometry of the coils. When calculating the gradient in this way it is necessary to take into account the image currents in the pole faces of the polarizing magnet.

The gradient can also be determined from the shape of the echo produced for a given sample shape. The most common sample shape is cylindrical with its main axis oriented perpendicular to the field. In the presence of a field gradient, G, the echo shape, as was seen in section 2-9, is given by:

$$\frac{2J_1(\gamma Ga(2\tau - t))}{\gamma Ga(2\tau - t)} \qquad (5\text{-}1)$$

from which it follows that G is given by (49,91):

$$G = 7{\cdot}6634/\gamma at' \text{ gauss cm.}^{-1} \qquad (5\text{-}2)$$

where t' is the separation between the first minima of the echo.

For a sample of square, rather than circular, cross section the echo shape is given by:

$$\frac{\sin(\gamma G(2\tau - t)L/2)}{\gamma G(2\tau - t)L/2} \qquad (5\text{-}3)$$

and G can be determined from (27,66):

$$G = 4\pi/\gamma Lt \qquad (5\text{-}4)$$

where L is the length of the sample side and t is the separation between the first null points of the echo.

The advantage of these methods is that the self diffusion coefficient can be determined absolutely rather than relative to that of another species. However, in practice it seems that errors can easily be introduced. For example, Trappeniers (61) took great care in determining the self diffusion coefficient of water absolutely, but his value of $2{\cdot}51 \times 10^{-9}$ $m.^2s.^{-1}$ would appear to be at least 10 per cent too large.

The third method is to calibrate the instrument against material of known diffusion coefficient. When compiling appendix B it was surprising to note how many workers had calibrated their instruments using water as the standard. The early data of Simpson and Carr (134), $2{\cdot}13 \times 10^{-9}$ $m.^2s.^{-1}$ at 25 C, and that of Trappeniers mentioned above were particularly used. The self diffusion coefficients of water reported in the literature (61,100,135) show a marked variation and so it seems a rather poor choice as standard. In our laboratory we have used benzene at 25 C as the primary standard. The self diffusion coefficient of benzene at this temperature was taken to be $2{\cdot}207 \times 10^{-9}$ $m.^2s.^{-1}$ (100,136). Results by other workers agree very well with this value (137,138). For measurements made at

15 C, 1.860×10^{9} m.^{2}s.$^{-1}$ is taken as the value of the self diffusion coefficient of benzene (136) to be used as the standard. When measuring diffusion coefficients an order of magnitude smaller, n-dodecane was used as a standard, taking the self diffusion coefficient at 25 C to be 8.37×10^{-10} m.^{2}s.$^{-1}$ (139). All the above values were determined using the diaphragm cell technique.

In our experiments it was found necessary to check the calibration constant frequently because there were occasional unaccountable jumps in its value. Normally the calibration was checked before and after measurements on a sample. The mean value was taken as the calibration constant used in determining the self diffusion coefficient of the sample. Such a process was quite tedious and certainly slowed up the rate at which diffusion coefficients could be determined. However, this was the only way to judge the overall stability of the instrument. In general the stability was not good and long periods were often spent servicing parts of the instrument in order to get relatively short periods of stability when worthwhile experimental results could be obtained. So, although the technique is potentially very rapid in determining self diffusion coefficients, much time can be spent in making adjustments so that everything works correctly.

5-9 The Effect of Convection.

Serious errors can be introduced into the measurement of diffusion coefficients if convection is present in the sample. Convection arises from the presence of temperature gradients in

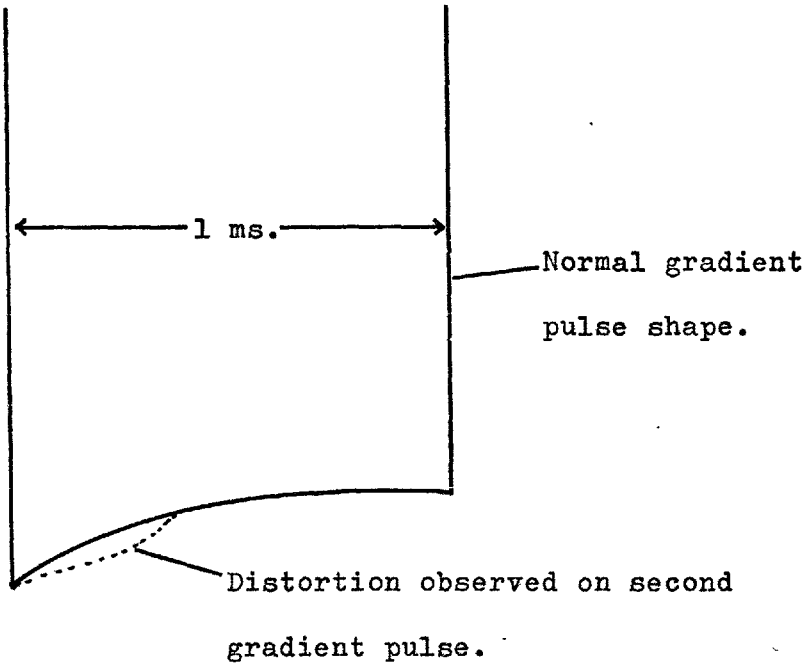
the liquid sample. In order to minimise the presence of temperature gradients samples were always allowed to stand in the thermostatted probe for at least 15 minutes before any measurements were made.

The spin echo method provides a convenient method of detecting the presence of convection. Carr and Purcell (5) have shown that if convection is present then the odd numbered echoes may be much smaller than even numbered echoes in a Carr-Purcell 90-180-180 .... degree pulse sequence. This effect has not been observed on our spectrometer and it was concluded that convection was not present in the samples under study.

5-10 The Effect of Unequal Gradient Pulses.

During this research problems were met with the pulsed field gradient unit. At times severely distorted echoes were produced, the fault being due to unequal field gradient pulses. The type of inequalities and the distortions produced are shown in figure 5-2. The effects of unequal gradient pulses have been discussed previously by Tanner (11), but the equations developed in section 2-9 lend themselves particularly to a demonstration of the effects.

Figures 5-3 to 5-10 show various effects of unequal gradient pulses and should be compared with figure 2-4 which shows the ideal attenuation of the echo due to increasing value of the pulsed field gradient, G. The values of the parameters in equation (2-34) used to generate these figures are given in section 2-9. The values of G, G_x, δ_1, and δ_2 were varied as specified below. The effects shown are primarily



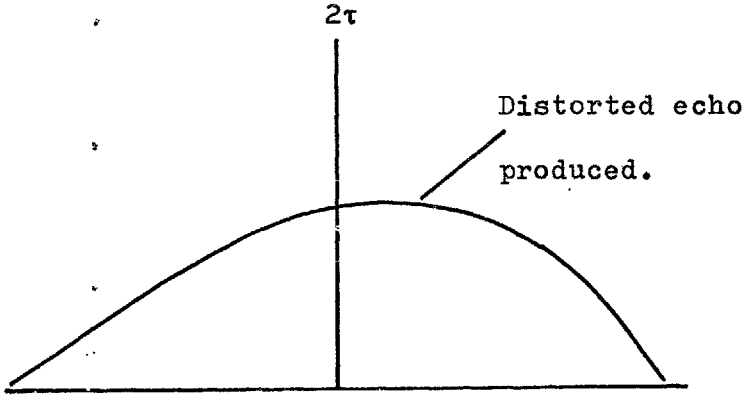


Figure 5-2: OBSERVED INEQUALITIES IN THE FIELD GRADIENT PULSES AND AN EXAMPLE OF THE ECHO DISTORTION PRODUCED.

those due to inequalities in the widths of the gradient pulses. However, similar effects will be seen if the inequalities lie in the amplitudes of the gradient pulses. It can be seen in equation (2-34) that it is the difference in area, $G\delta$, between the pulses that is important.

Figures 5-3 and 5-4 show the case where G_x is zero and G takes values of 0, 20, 40, 60, and 80 gauss cm.$^{-1}$. In figure 5-3 δ_1 equals 1 millisecond and δ_2 equals 1·02 milliseconds, figure 5-4 has the values reversed. In both cases the echo moves progressively further from the 2τ position as G is increased, but the echoes still maintain their symmetry about the maximum. The echoes occur before or after the 2τ position according to whether δ_1 is less than or greater than δ_2. The echo peaks have moved ± 4 milliseconds for each increase in G of 20 gauss cm.$^{-1}$. This is predictable since the echo peak, when G_x is zero, occurs when the term $2J_1(f)/f$ in equation (2-34) has its maximum value of 1. This occurs when f equals 0, that is when:

$$G_o(2\tau - t) = -G(\delta_1 - \delta_2) \qquad (5\text{-}5)$$

and hence when:

$$t = 2\tau + \frac{G}{G_o}(\delta_1 - \delta_2) \quad . \qquad (5\text{-}6)$$

Figures 5-5 to 5-7 show the same conditions as figures 2-4, 5-3, and 5-4 except that G_x has been set to 0·01 gauss cm.$^{-1}$ In figure 5-5 the echoes are slightly smaller than in figure 2-4 due to the small increase in G_x, but apart from this there is no significant difference between the echoes.In figures 5-6 and 5-7 the echoes move in the same direction as when G_x is

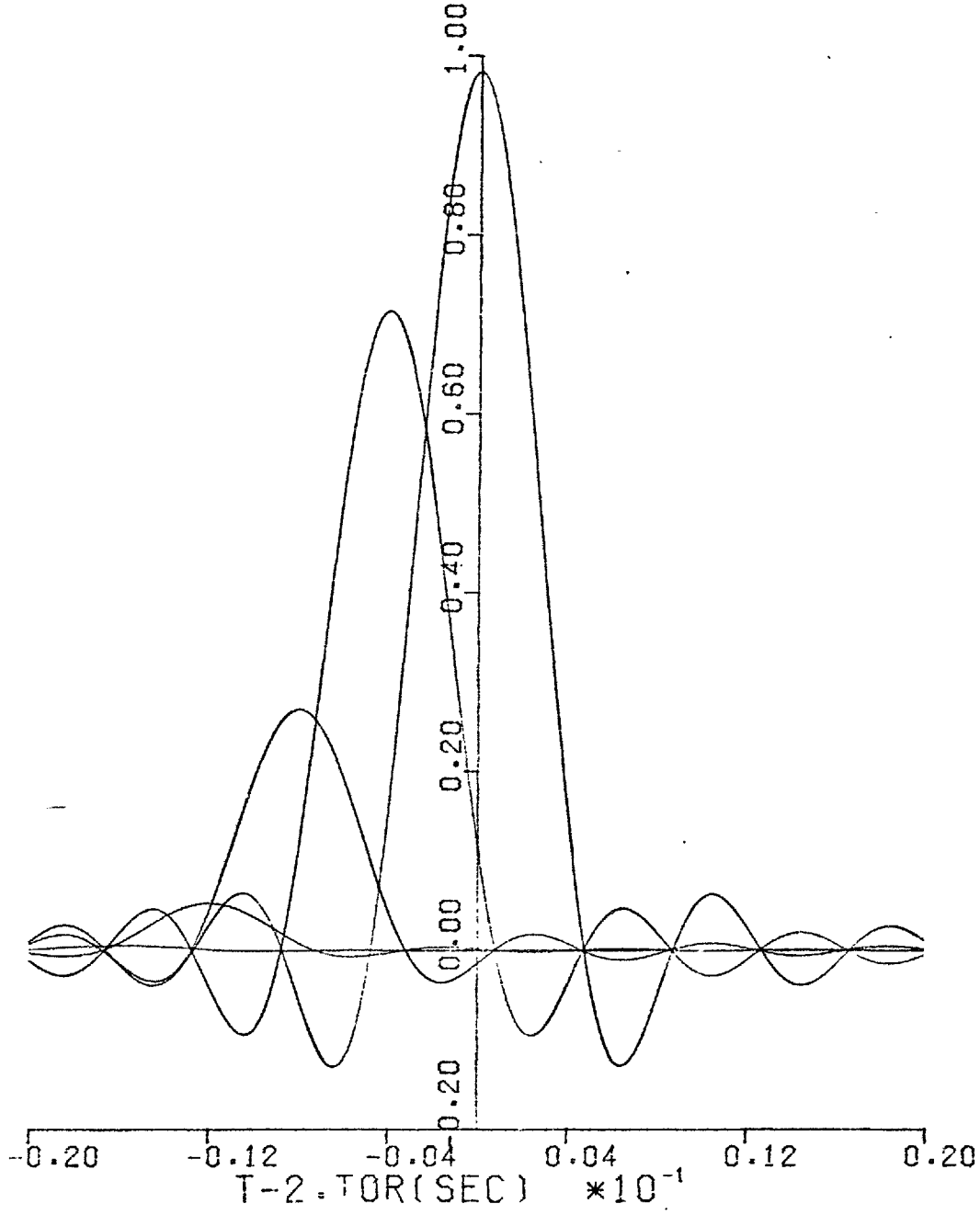


Figure 5-3: THEORETICAL SPIN ECHOES. δ_1 LESS THAN δ_2 AND G_x EQUAL TO ZERO.

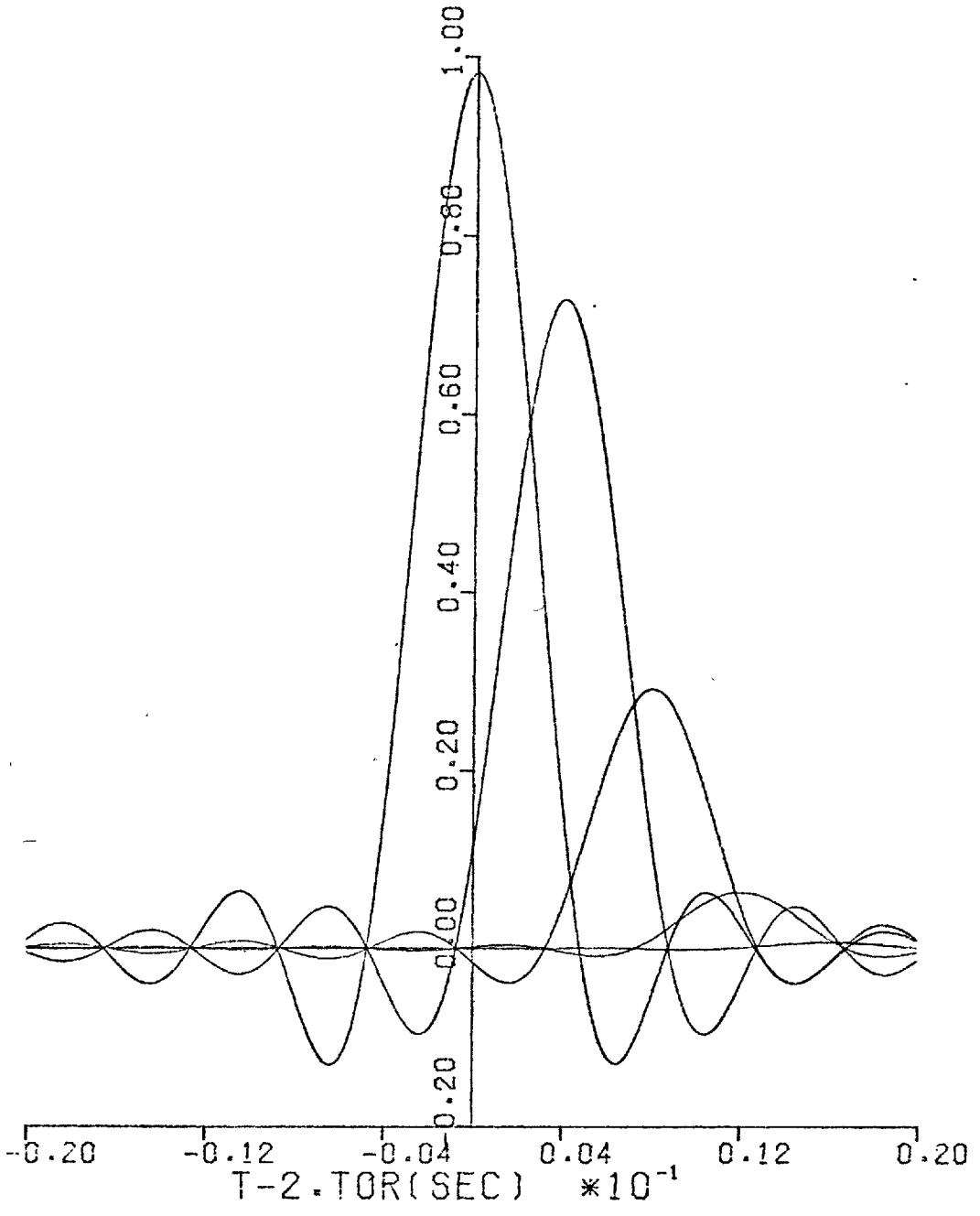


Figure 5-4: THEORETICAL SPIN ECHOES. δ_1 GREATER THAN δ_2 AND G_x EQUAL TO ZERO.

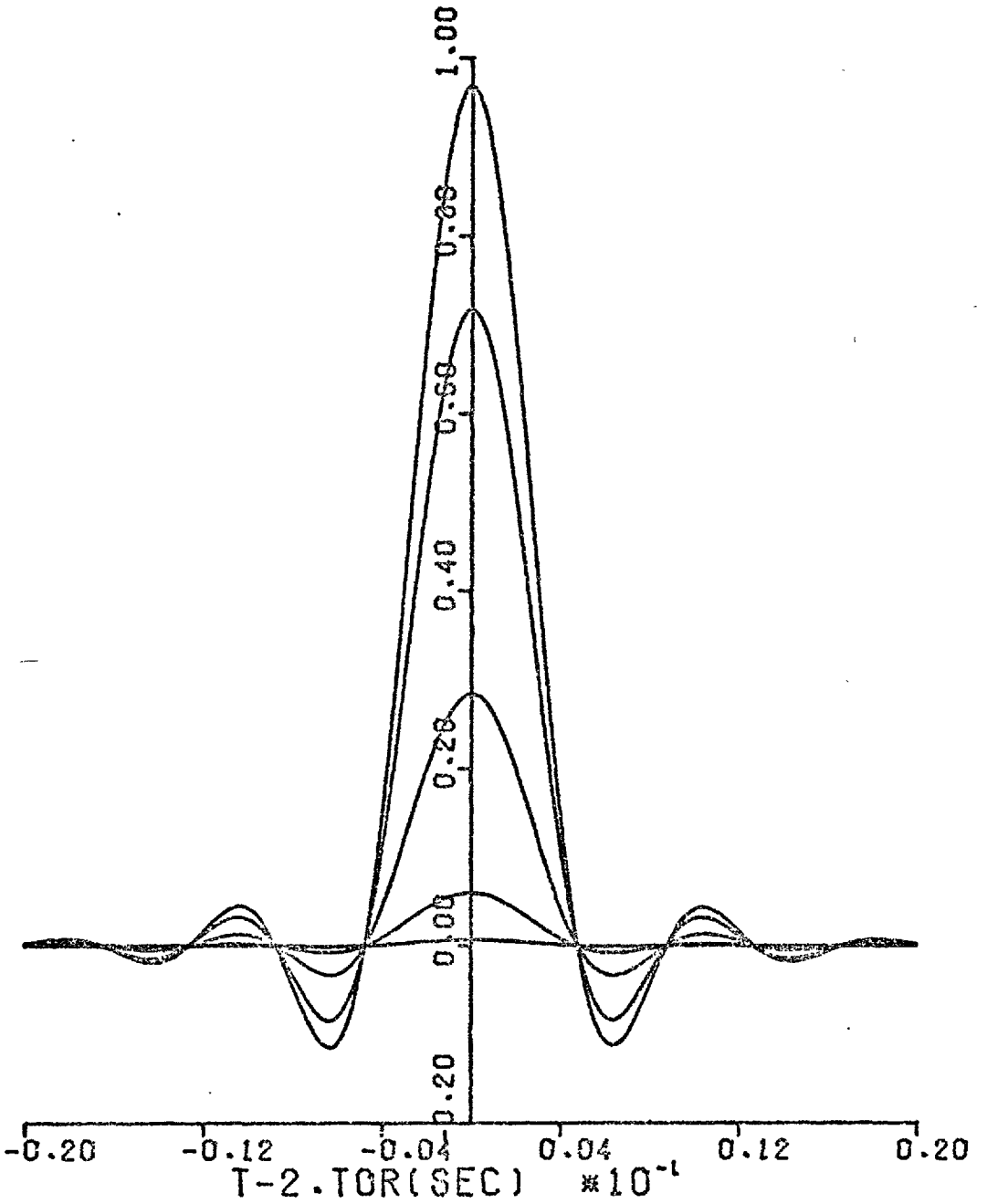


Figure 5-5: THEORETICAL SPIN ECHOES. EQUAL GRADIENT PULSES AND G_x EQUAL TO 0.01 GAUSS CM.$^{-1}$.

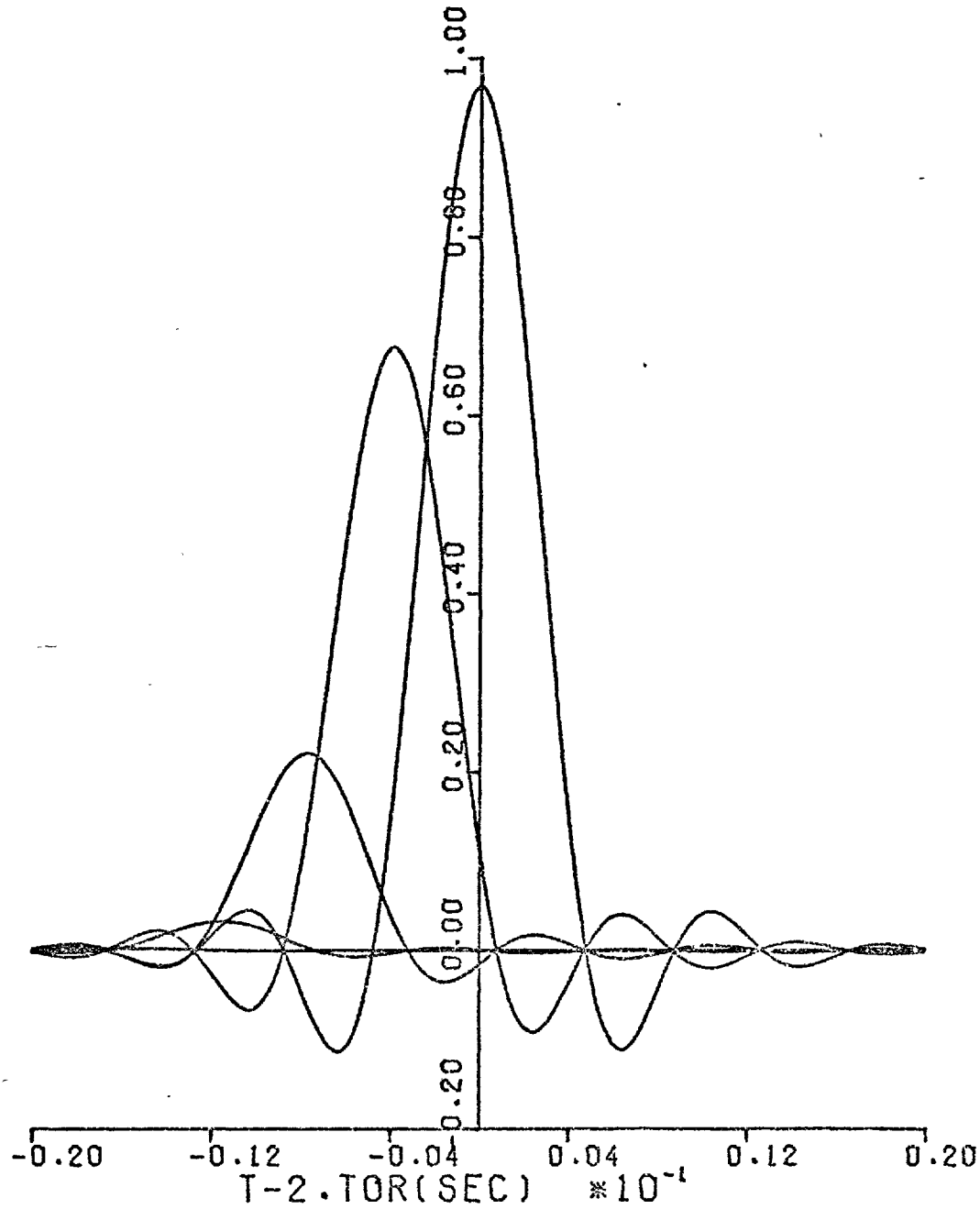


Figure 5-6: THEORETICAL SPIN ECHOES. δ_1 LESS THAN δ_2 AND G_x EQUAL TO 0·01 GAUSS CM.$^{-1}$.

zero, but their peaks are nearer to the 2τ position. The symmetry of the echoes that have been shifted has also been markedly affected. This can be most clearly seen by looking at the first minimum on either side of the echo peak.

Figure 5-8 shows the effect of variations in δ_1 relative to δ_2 with G fixed at 20 gauss $cm.^{-1}$ and G_x set equal to zero. δ_2 is held at 1 millisecond and δ_1 varies from 0.92 milliseconds to 1.08 milliseconds in steps of 0.02 milliseconds. The echoes shift their positions as predicted by equation (5-6). There is a slight increase in the echo amplitude as the echoes occur at later time! This small effect will reverse as T_2 is decreased and the term $\exp(-t/T_2)$ becomes more significant.

Figure 5-9 shows the same sequence but with G_x set equal to 0.01 gauss $cm.^{-1}$ The effect of this relatively small gradient is most marked. The echoes lose their symmetry and decrease in amplitude as the difference between δ_1 and δ_2 increases. The shift away from the 2τ position is not quite as great as when G_x is zero. This damping of the echo as it moves away from the 2τ position is due to the term containing G_x in equation (2-34). Figure 5-10 shows how this term encloses the echoes in figure 5-9.

A test for equal gradient pulses is that the peak of the echo should occur at time 2τ and that it should be symmetric. In our experiments the maximum of the echo was always very close to 2τ, but occasionally the symmetry was not too good. It is likely that any errors so introduced into the experiment would cause a larger attenuation of the echo than expected.

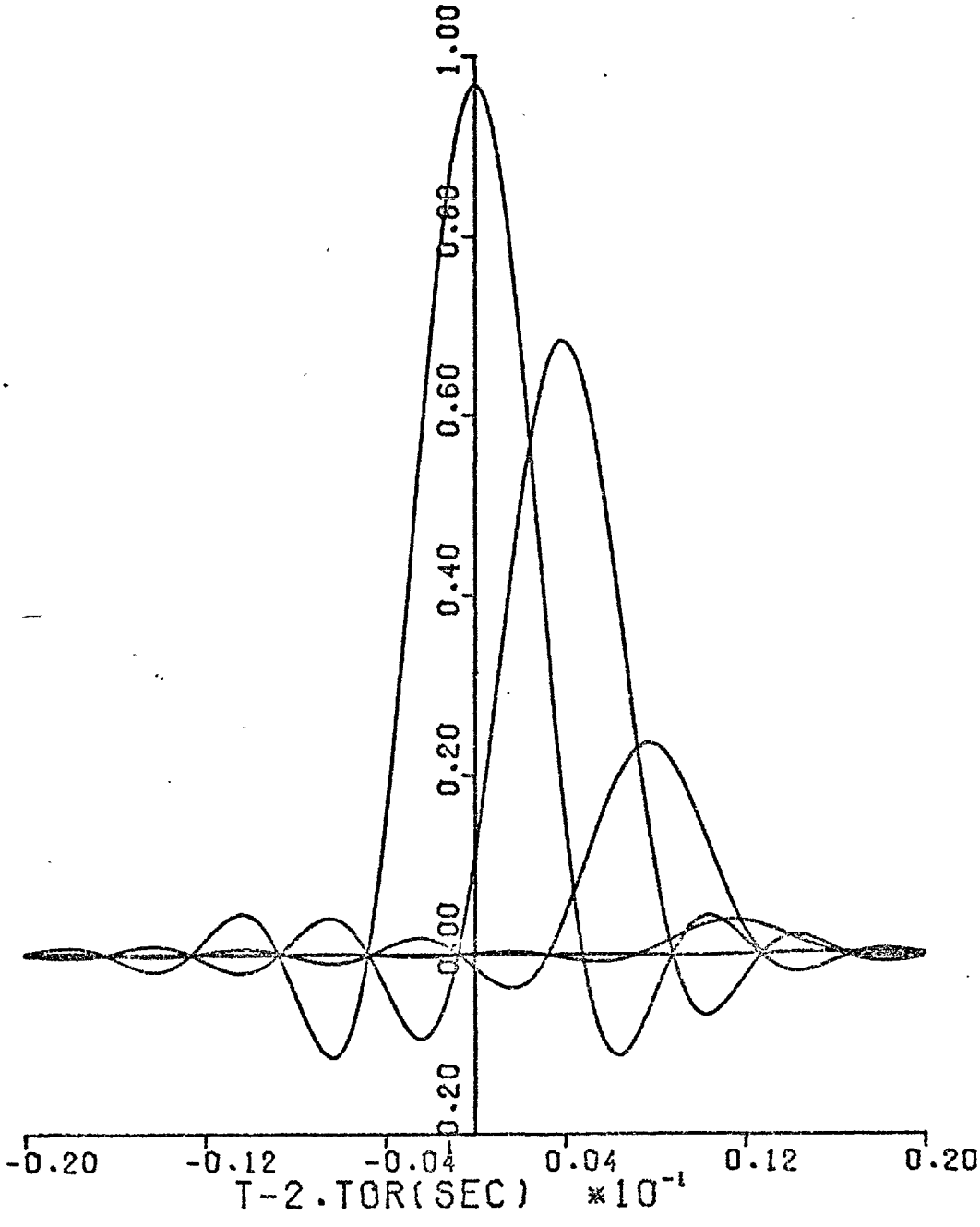


Figure 5-7: THEORETICAL SPIN ECHOES. δ_1 GREATER THAN δ_2 AND G_x EQUAL TO 0.01 GAUSS CM.$^{-1}$.

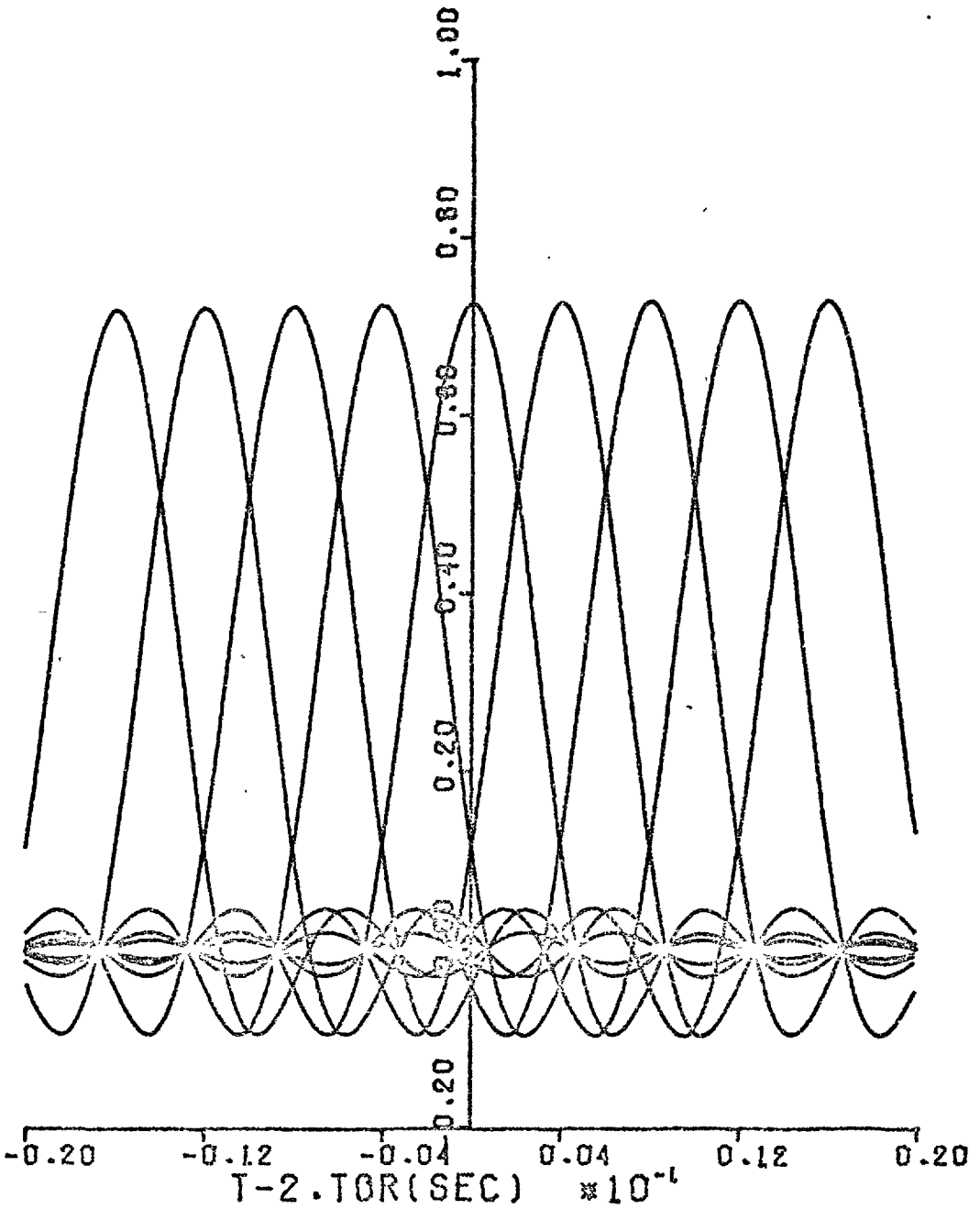


Figure 5-8: THEORETICAL SPIN ECHOES. δ_1 VARYING RELATIVE TO δ_2 AND G_x EQUAL TO ZERO.

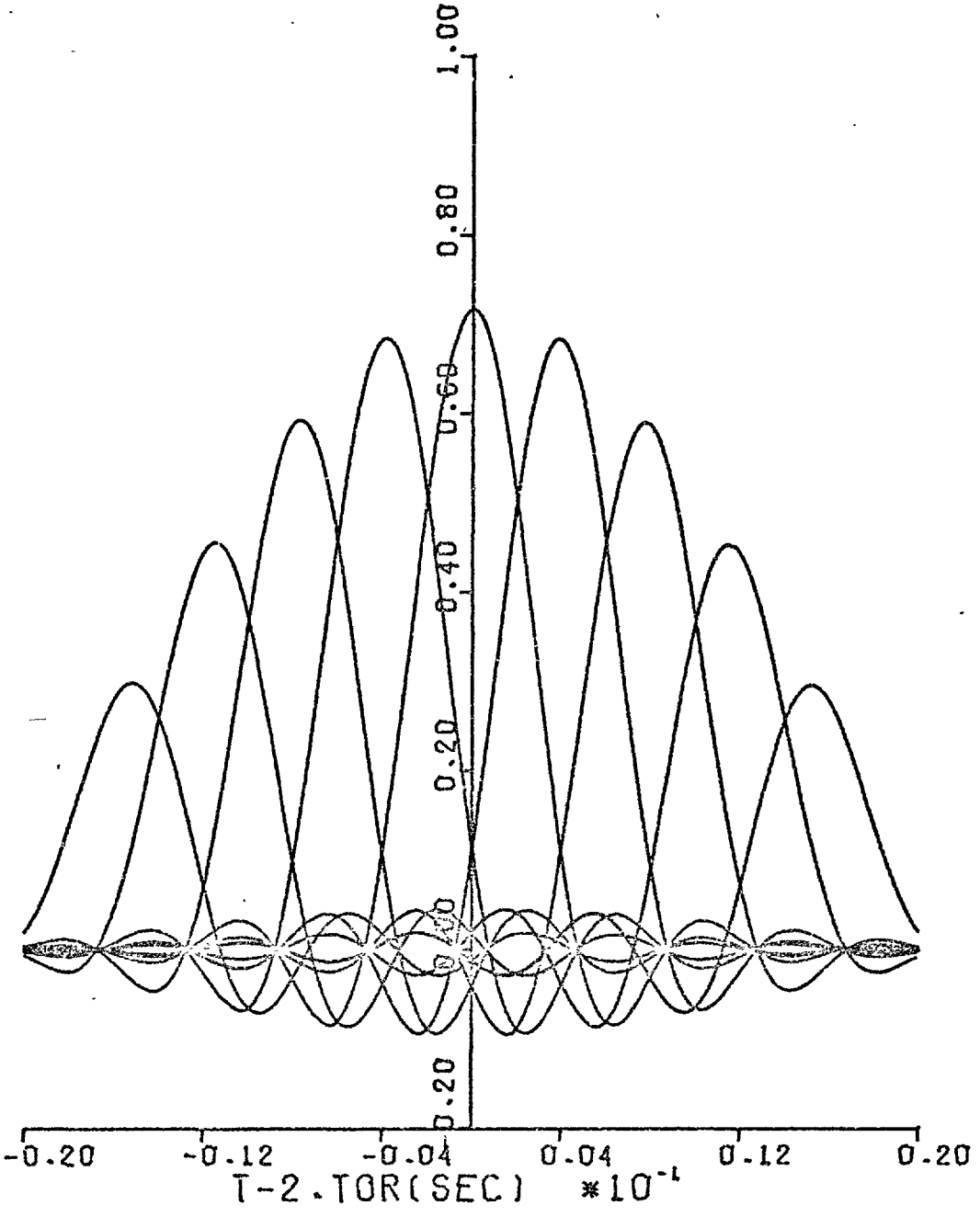


Figure 5-9: THEORETICAL SPIN ECHOES. δ_1 VARYING RELATIVE TO δ_2 AND G_x EQUAL TO 0.01 GAUSS CM.$^{-1}$.

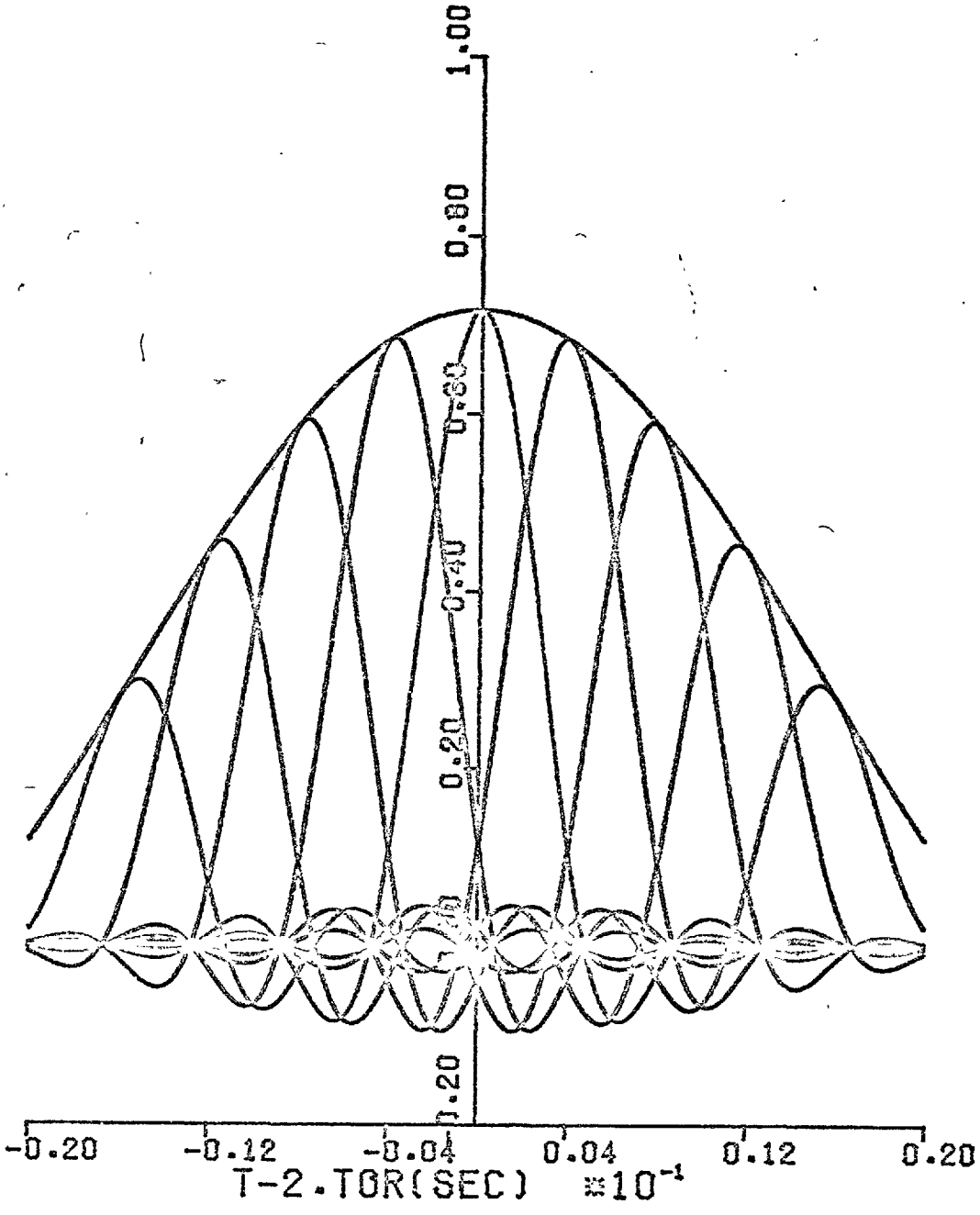


Figure 5-10: THEORETICAL SPIN ECHOES ENVELOPED BY THE TERM CONTAINING G_x IN EQUATION (2-35).

Any consistent error would, however, be essentially the same for the standard and the sample and so not affect the diffusion coefficient determined very much. Random fluctuations would introduce some error.

5-11 Non Linearity of the Diode Detector at Low Signal Strengths.

The transfer characteristic of the diode detector is shown in figure 4-2. It can be seen that this is essentially linear over the range plotted. With the instruments available it was not possible to measure the characteristic at lower signal strengths with any degree of accuracy. However, it is known that the characteristic at lower signal strengths changes slope. A large error could be introduced if the calibration was carried out at normal signal strengths and then the sample was investigated at low signal strengths. It was found that measurements on samples with a signal strength weak enough to lie in the non-linear region produced a much higher diffusion coefficient than might reasonably be expected when measured against a normal calibration standard. It was noticed that plots of $-\ln A(2\tau)$ against $\delta^2(\Delta - \delta/3)V$ for certain samples consisted of two distinct lines of differing slope. This was thought to be due to the signal strength changing from the normal linear region of the characteristic to a second region closely approximated by a second straight line. This was particularly marked in the case of the OMCTS/d-benzene system for the sample of lowest proton concentration. The experimental diffusion coefficient determined from points down to 0·2 volts

at full receiver gain agreed well with the mutual diffusion coefficient at infinite dilution, but the diffusion coefficient indicated by points of lower signal strength was almost 50 per cent larger. This second value provided a correction factor to apply to the slope of lines produced with signals below the 0.2 volt level. In practice the only experimental point corrected in this way was that for the sample of lowest proton concentration in the TPTMCTS/carbon tetrachloride system, all other measurements being made in the linear region plotted in figure 4-2.

5-12 Errors in Measurement.

Time intervals were measured digitally and displayed numerically. There was no significant error in these measurements.

The oscilloscope y amplifiers have a specified accuracy of ± 3 per cent, but any consistent error will be the same for the sample and standard. There will be random errors in the readings taken from the oscilloscope.

The averager has a resolution of 1 in 128 over a 2 volt input range. Repeated measurements on the same sample using the averager normally agreed to within 4 per cent.

The temperature of the probe was measured to within 0.2 C.

Inevitably, even after minimising as far as possible sources of error, there will be random errors in experimental measurements. These were present in both the recorded echo amplitudes and gradient pulse voltage, V. Two lines were fitted to the experimental $-\ln A(2\tau)$ against $\delta^2(\Delta - \delta/3)V$

plots by the method of least squares. In one, x was regressed on y and in the other, y was regressed on x. In percentage terms the 90 per cent confidence limits of the determined gradients were the same for both lines. The difference between y/x for these two lines was seldom more than one per cent. The mean value of y/x was used to calculate the diffusion coefficients. Typically, the 90 per cent confidence limits were ± 2·5 per cent. This error would apply to the measurements on the sample and on the calibration standard. Hence, on this basis, the overall accuracy of the diffusion coefficient would typically be ± 3·5 per cent.

Reproducibility of the results for diffusion coefficients was normally within these limits when the instrument was stable enough to get useful experimental data. Where comparison could be made with data reported in the literature, our results were often in agreement to within a few per cent. Some examples are given in table 5-1.

Sample	T	Expt. D($m.^2s.^{-1}$)	Lit. D($m.^2s.^{-1}$)	Ref.
n-hexane	25 C	4.35×10^{-9}	4.263×10^{-9}	137
chloroform	25 C	2.54×10^{-9}	2.58×10^{-9}	24
n-decane	25 C	1.40×10^{-9}	1.31×10^{-9}	91
chlorobenzene	25 C	1.66×10^{-9}	1.80×10^{-9}	34

Table 5-1: A COMPARISON OF SOME EXPERIMENTALLY DETERMINED DIFFUSION COEFFICIENTS WITH LITERATURE VALUES.

Most of the results reported in this thesis are probably accurate to within ± 4 per cent. A few points measured at low proton

concentration have a poorer accuracy. Estimates of the accuracy of each data set are given with the results.

5-13 Computer Programmes.

Many of the calculations in this work have been carried out on the C.D.C. 6400 computer at the Imperial College Computer Centre (I.C.C.C.). This section describes some of the programmes that have been written. To save space the programmes themselves are not presented, but are available on request to the author. The programmes are written in Fortran IV.

i/ Programme NMR.

Programme NMR together with subroutines ERROR and PLOT was used in the least squares fitting of straight lines to the plot of $-\ln A(2\tau)$ against $\delta^2(\Delta - \delta/3)V^2$. The data read in was echo amplitude, the voltage developed during the field gradient pulse, V, and the time interval Δ. δ was fixed at 1 millisecond. Subroutine ERROR returned the gradients of the lines for y regressed on x and x regressed on y together with its reciprocal. The 90, 95, and 95 per cent confidence limits were also given. Subroutine PLOT produces a quantised plot of the data on the computer output so that any outlying points could be detected visually and if necessary removed.

ii/ Programme AVTO1.

This programme was largely written by my colleague R.N. Sheppard. It converts data from the paper tape output of the averager to the format required by the C.D.C. 6400. Essentially this involves the conversion of the two's complement binary output of the averager to the one's complement binary required

by the C.D.C. 6400. Routines BINBF and BINRD available from the University of London Computer Centre's library were used to facilitate the reading of data records of varying length.

The programme returned the values of the averaged points across the echo together with the base line value. A plot of the echo is also produced on the output which allows one to judge the quality of the echo visually.

Parts of this programme are written in Compass machine code language.

iii/ Programme ABC.

Programme ABC together with subroutines PICT, BOX, DELTA, FITTER, PAPSIZE, and POLYFT was written to facilitate the plotting of figures on the Kingmatic Graph Plotter at Imperial College. The programme together with I.C.C.C. routines START, PLOT, SYMBOL, LINE, and ENPLOT generates magnetic tapes which can be used with the plotter to produce plots of data input and/or draw a line of the polynomial fitted to the data by POLYFT. The programme was quite useful for checking how well a polynomial fitted a particular data set.

POLYFT fits polynomials of order 2 to 6 by the method of least squares. Originally a part of the I.B.M. SHARE library it is available from the I.C.C.C. library.

Many of the figures in this thesis were produced using this programme.

iv/ Programme Echo.

Programme echo was used in conjunction with I.C.C.C. plotting routines to produce plots of the echo shape as predicted by equation (2-35) on the Kingmatic plotter. Values of the

Bessel function were calculated using the CERN library routine C302, BESSEL.

The following programmes have been written for interactive use on the college's terminal network. They are to be found, together with other useful programmes, as records in programme BEN.

v/ Programme DIAM.

This programme was used to fit the molecular diameters for the hard sphere model so that the predicted diffusion coefficients of pure species were close to the experimental values. See table 6-2 for the diameters allocated to various molecules. The programme requests the molecular weight, molar volume, and temperature. It then requests a trial diameter and returns the predicted diffusion coefficient. The programme loops allowing successive trials until the predicted diffusion coefficient is close to the experimental value.

The programme is written using the Percus-Yevick equation to calculate the value of the radial distribution function at contact.

vi/ Programme SPHERE.

Programme SPHERE was used to calculate the predicted diffusion coefficients from the hard sphere model for binary liquid mixtures. The programme also returns the predicted values of the friction coefficients, the radial distribution functions, and the fraction of the total volume occupied by the molecules. The programme loops allowing the user to select the fluid compositions at which calculations are performed.

The programme assumes that the excess volume of mixing of the components is negligible and the Percus-Yevick equation is used to calculate the values of the radial distribution functions.

Small alterations have to be made to programmes DIAM and SPHERE if one uses the Carnahan-Starling equation instead of the Percus-Yevick equation or when the excess volume of mixing is not negligible.

Chapter 6: EXPERIMENTAL RESULTS.

6-1 Introduction.

Results for the following systems are presented in this chapter:

1) benzene/carbon tetrachloride at 25 C,

2) n-hexane/carbon tetrachloride at 25 C,

3) benzene/perdeutero-chloroform at 15 C,

4) chloroform/perdeutero-benzene at 15 C,

5) octamethylcyclotetrasiloxane/perdeutero-benzene at 25 C,

6) tetraphenyltetramethylcyclotetrasiloxane/
carbon tetrachloride at 25 C,

7) polypropylene glycol/carbon tetrachloride at 25 C.

The self diffusion coefficients of the protonated components have been determined at various concentrations. Each value of the diffusion coefficient is the average of three or more measurements. The reproducibility has already been discussed in section 5-12. Where sufficient data are available comparisons have been made between the experimental data and the predictions of equations (3-55) and (3-56) and the hard sphere model using equations (3-79) to (3-81) to calculate the friction coefficients which are substituted into equations (3-42),(3-47), and (3-48) in order to obtain values for the mutual and two self diffusion coefficients.

In section 6-2 details of materials used are given. Section 6-3 discusses the method of approximating the molecules to hard spheres. Results and comparisons are presented in sections 6-4 to 6-9 and a general discussion is given in section 6-10.

6-2 Materials.

The materials used in this work and their sources of origin are given in table 6-1:

benzene	AnalaR Grade	British Drug Houses
carbon tetra-chloride	AnalaR Grade	British Drug Houses
n-hexane	Lab. Reagent Grade	British Drug Houses
chloroform	AnalaR Grade	British Drug Houses
perdeutero-benzene	>99·5 per cent deuterated	Nuclear Magnetic Resonance Limited
perdeutero-chloroform	>99·8 per cent deuterated	Nuclear Magnetic Resonance Limited
OMCTS		Midland Silicones
TPTMCTS		Midland Silicones
poly propylene glycol	Standards 41993 41983	Waters Associates

Table 6-1: MATERIALS USED FOR THE DIFFUSION MEASUREMENTS

The octamethylcyclotetrasiloxane (OMCTS) supplied by Midland Silicones Limited contained a small amount of the pentameric cyclic compound $(Me_2SiO)_5$. This was removed by distillation. The ethanol stabilizer in the chloroform was removed by my colleague B.D.Ludbrooke. Traces of moisture were removed from the samples with type 4A molecular sieve.

Apart from this the materials were used as supplied without further purification.

6-3 Approximating the Molecules to Hard Spheres.

In order to apply the equations of section 3-5 it is necessary to approximate the molecules to hard spheres. The diameter of the equivalent sphere has been treated as a parameter which can be empirically fixed. The diameters have been fixed so that the predicted self diffusion coefficients, as calculated from equations (3-43) and (3-79), for the pure liquids are close to the experimental values. The values allocated are given in table 6-2 together with the predicted self diffusion coefficients obtained with these values.

Molecule	σ(PY) A	D(PY).10^9 $m.^2s.^{-1}$	σ(CS) A	D(CS).10^9 $m.^2s.^{-1}$	σ(ref) A
benzene	5·55	2·205	5·43	2·206	5·270(a)
					5·638(b)
carbon tetra-chloride	5·80	1·31	5·67	1·30	5·881(a)
					5·735(b)
					5·46(c)
n-hexane	5·96	4·27			5·909(a)
					6·545(b)
					6·0(c)
OMCTS	9·2	·385	8·975	·383	

Table 6-2: MOLECULAR DIAMETERS USED IN THE HARD SPHERE MODEL.

a) Lennard-Jones parameter (140)
b) Lennard-Jones parameter (141)
c) Molecular model (142)

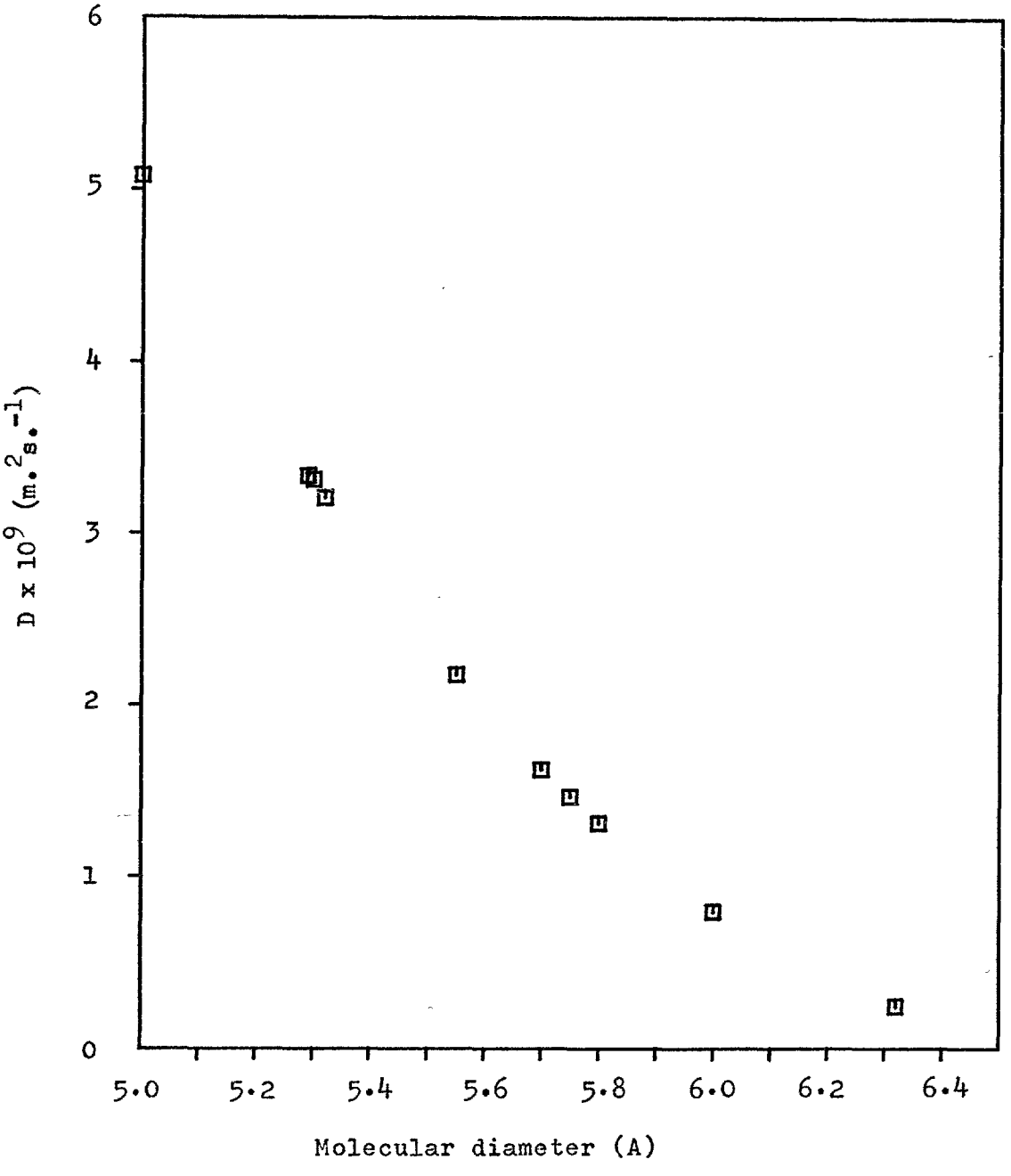


Figure 6-1: DEPENDENCE OF PREDICTED SELF DIFFUSION COEFFICIENT ON MOLECULAR DIAMETER. HARD SPHERE MODEL FOR CARBON TETRACHLORIDE USING THE PERCUS-YEVICK EQUATION.

The values determined depend on the expression used to calculate the value of the radial distribution function at contact. It can be seen that the values for the fitted diameters are larger when using the Percus-Yevick (PY) equation than when using the Carnahan-Starling (CS) equation. Also included in table 6-2 are estimates for the diameters obtained by other methods.

The dependence of the self diffusion coefficient on the molecular diameter is illustrated in figure 6-1. This shows the self diffusion coefficient for pure carbon tetrachloride calculated from equations (3-43) and (3-79) using the Percus-Yevick equation with varying molecular diameters.

6-4 The Benzene-Carbon Tetrachloride System.

The self diffusion coefficient of benzene in the benzene carbon tetrachloride system has been determined across the concentration range at 25 degrees centigrade. The results are shown in table 6-3 and plotted in figure 6-2.

Mole Fraction Benzene	D x 10^9 $m.^2$ $s.^{-1}$
·911	2·12
·812	2·08
·715	1·96
·618	1·97
·545	1·86
·419	1·82
·212	1·62

Table 6-3: EXPERIMENTAL SELF DIFFUSION COEFFICIENTS FOR BENZENE IN CARBON TETRACHLORIDE.

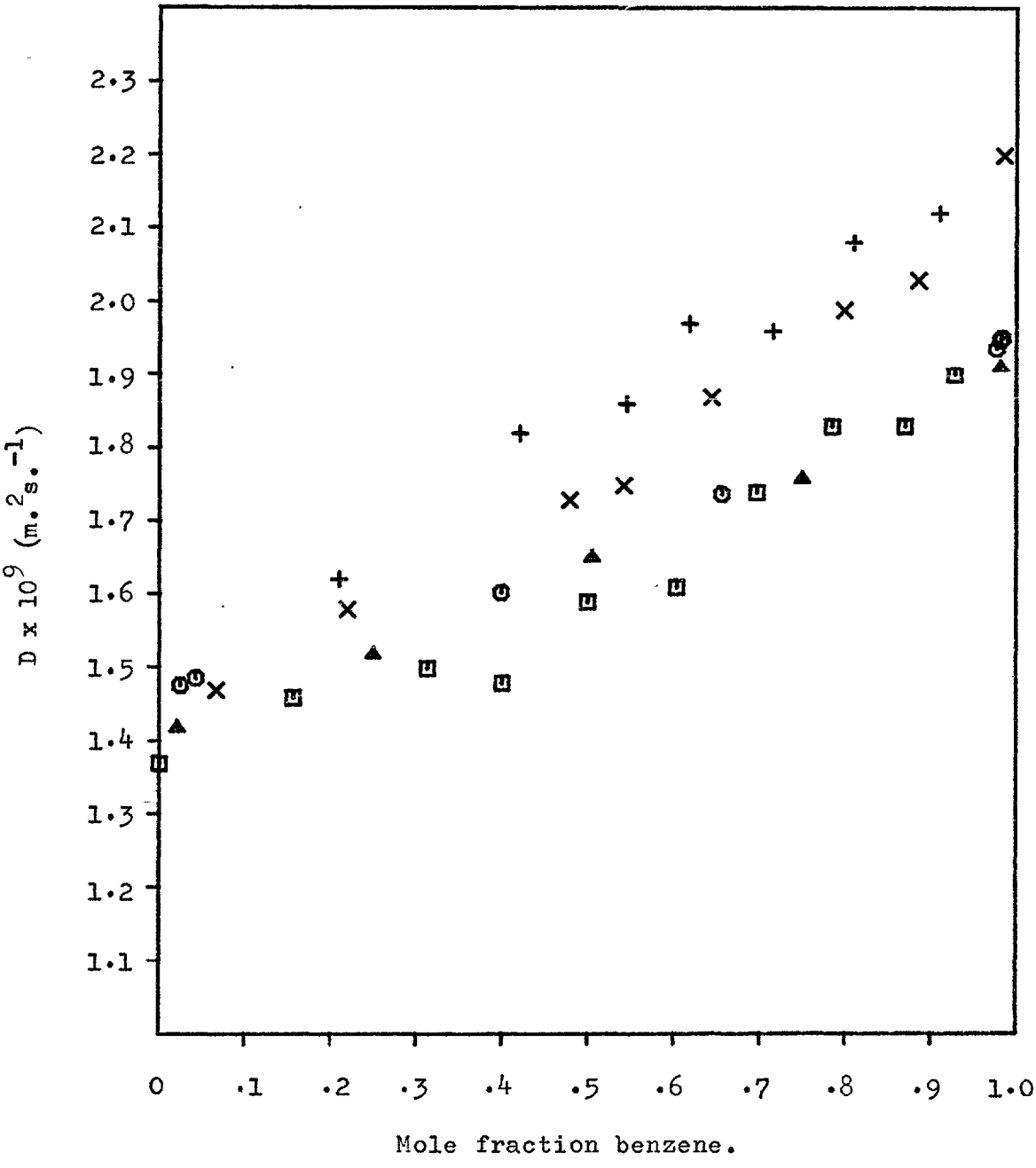


Figure 6-2: EXPERIMENTAL DIFFUSION COEFFICIENTS FOR THE BENZENE-CARBON TETRACHLORIDE SYSTEM.

\+ Self diffusion coefficient benzene (this work)

× Self diffusion coefficient benzene (147) ±5 p.c.

△ Mutual diffusion data (149) ±1 p.c.

⊙ Mutual diffusion data (150) ±0·1 p.c.

⊡ Self diffusion coefficient CCl_4 (148) ±5 p.c.

The experimental points were calibrated against the self diffusion coefficient of pure benzene at 25 C being 2.207×10^{-9} m.^{2}s.$^{-1}$ (136). Measurements were conducted with δ = 1 ms., τ = 31.90 ms., and Δ about 35 ms. They are estimated to be accurate to within 4 per cent.

Also shown in figure 6-2 are the self diffusion coefficients of benzene determined by Johnson and Babb (147), the self diffusion coefficients of carbon tetrachloride determined by Hardt and co-workers (148), and the mutual diffusion data of Caldwell and Babb (149) and Staker and Dunlop (150). The self diffusion coefficients were determined using a capillary cell and the mutual data by use of a Mach-Zehnder interferometer (149) and a Gouy diffusiometer (150). The reported accuracy of these points is indicated on figure 6-2. It should be mentioned that the data of Caldwell and Babb were obtained at slightly above 25 C. The self diffusion coefficient of pure carbon tetrachloride as determined by Hardt and co-workers does not agree well with that determined by Mills (136), 1.296×10^{-9} m.^{2}s.$^{-1}$

The agreement between our data and that of Johnson and Babb is quite reasonable, but our values seem to be consistently a little higher.

Activity data for the system were obtained by correcting the data of Christian et alia (151) at 20 C to 25 C (152).

Equations (3-55) and (3-56) were tested by calculating the self diffusion coefficients for each component from the mutual diffusion data of Staker and Dunlop. The excess volume of mixing for this system is very small and additivity of volumes was assumed. The data are presented in table 6-4 and

plotted in figure 6-3.

Mole Fraction Benzene(1)	$D_{12} \times 10^9$ $m.^2 s.^{-1}$	Q	$D_{11} \times 10^9$ $m.^2 s.^{-1}$	$D_{22} \times 10^9$ $m.^2 s.^{-1}$
·0240	1·476	·9936	1·49	1·37
·0420	1·485	·9889	1·51	1·39
·3982	1·602	·9340	1·77	1·63
·6558	1·737	·9379	1·95	1·80
·97735	1·937	·9939	2·11	1·94
·98153	1·948	·9950	2·12	1·95
·98353	1·952	·9955	2·13	1·96

Table 6-4: DATA AND PREDICTED SELF DIFFUSION COEFFICIENTS FOR A TEST OF EQUATIONS (3-55) AND (3-56).

The molar volume of benzene was taken as 89·47 ml. and that of carbon tetrachloride as 97·11 ml.

It can be seen that the diffusion coefficients predicted by equations (3-55) and (3-56) agree very well with our experimental values. At high benzene concentrations the agreement is not quite so good. The benzene-carbon tetrachloride sytem is a good approximation to the regular solution which Bearman (117) showed would obey equation (3-68) and hence equations (3-55) and (3-56). There are no strong molecular interactions, the excess volume of mixing is small, and the molecules are of similar size and shape. Bearman's theories also predicted that the $D\eta$ product should be a constant for regular solutions. The predicted consistency is tested in table 6-5. The viscosity of the mixture has been reported across the composition range (153)

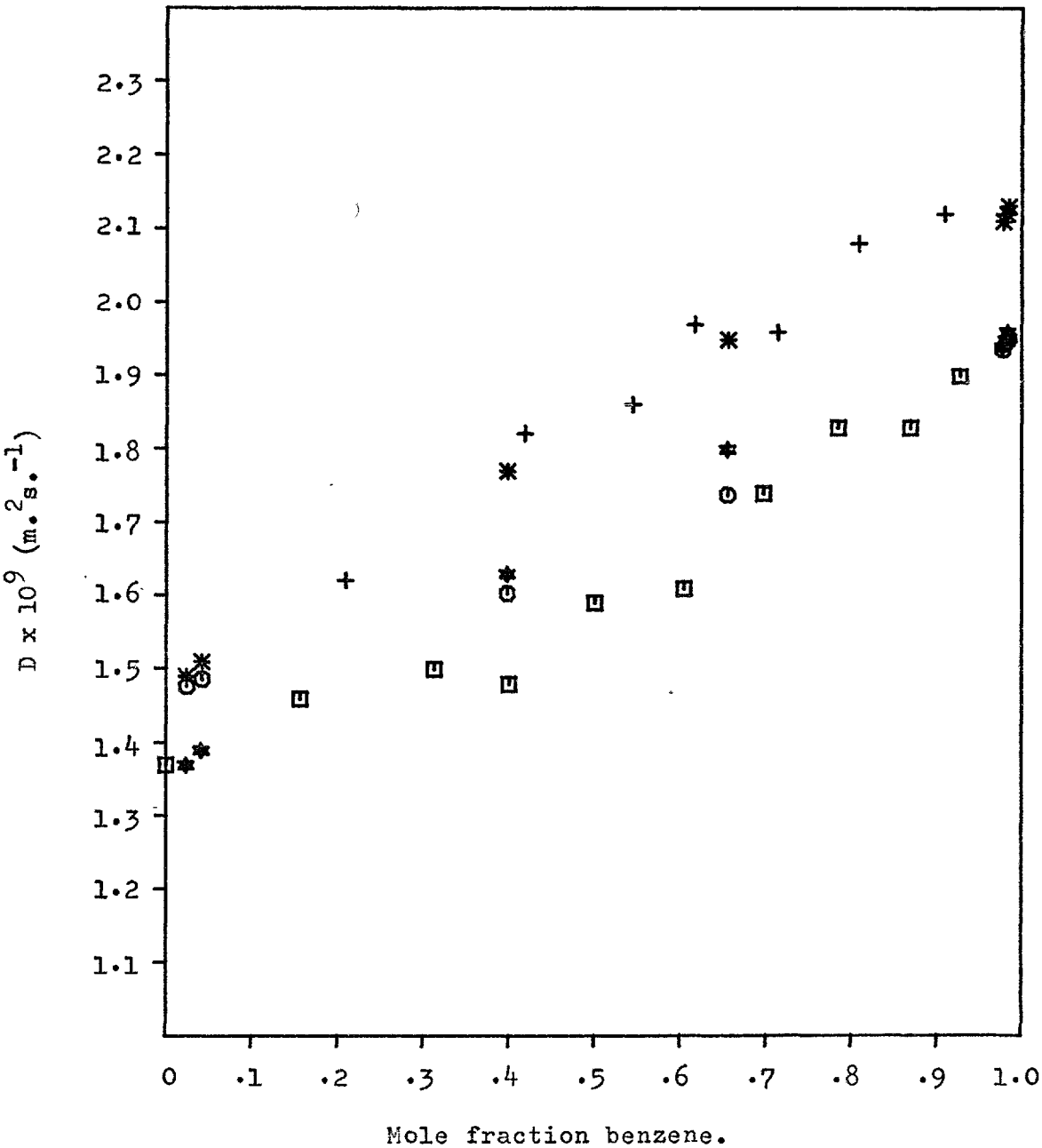


Figure 6-3: COMPARISON OF THE PREDICTIONS OF EQUATIONS (3-55) AND (3-56) WITH EXPERIMENTAL DATA.

✱ Predicted self diffusion coefficients of benzene.

✱ Predicted self diffusion coefficients of carbon tetrachloride.

Other symbols as defined in figure 6-2.

and the values given in table 6-5 have been interpolated from these data.

Mole Fraction Benzene	$D_{11} \times 10^9$ $m.^2 s.^{-1}$	η cp.	$D_{11}\eta \times 10^7$ dynes
0.0	1.466[a]	.898	1.32
.212	1.62	.819	1.33
.419	1.75	.755	1.37
.546	1.86	.727	1.35
.619	1.91	.696	1.37
.812	2.04	.641	1.33
.911	2.09	.612	1.30
1.0	2.207[b]	.599	1.32

Table 6-5: TEST OF THE CONSISTENCY OF THE $D\eta$ PRODUCT FOR THE SELF DIFFUSION OF BENZENE IN CARBON TETRACHLORIDE.

a) Estimated from the data of Staker and Dunlop (150)

b) Value used as calibration standard (136)

It can be seen that within experimental error the $D\eta$ product is constant.

The hard sphere model has been used to predict the concentration dependence of the diffusion coefficients using both the Percus-Yevick and the Carnahan-Starling equations to predict the value of the radial distribution function at contact. Additivity of volume was assumed when determining the mean molar volume. The results are presented in tables 6-6 and 6-7.

Mole Fraction Benzene	$D_{11} \times 10^9$ $m.^2 s.^{-1}$	$D_{22} \times 10^9$ $m.^2 s.^{-1}$	$D'_{12} \times 10^9$ $m.^2 s.^{-1}$	Q	$D_{12} \times 10^9$ $m.^2 s.^{-1}$
0.0	1.696	1.311	1.696	1.0	1.696
.1	1.738	1.350	1.706	.9752	1.664
.2	1.781	1.390	1.716	.9560	1.640
.3	1.827	1.433	1.727	.9422	1.626
.4	1.874	1.477	1.737	.9339	1.622
.5	1.923	1.525	1.748	.9312	1.628
.6	1.975	1.574	1.759	.9339	1.641
.7	2.028	1.627	1.770	.9422	1.667
.8	2.084	1.682	1.781	.9560	1.702
.9	2.143	1.741	1.792	.9752	1.748
1.0	2.205	1.803	1.803	1.0	1.803

Table 6-6: PREDICTED DIFFUSION COEFFICIENTS FOR THE BENZENE CARBON TETRACHLORIDE SYSTEM. HARD SPHERE MODEL USING PERCUS-YEVICK EQUATION.

There are only small differences between the predicted diffusion coefficients when using the Percus-Yevick or Carnahan-Starling equations. This is because the effect of the smaller diameter is balanced by larger values for the radial distribution function.

The predicted diffusion coefficients given in table 6-6 have been fitted to sixth order polynomials. These lines are plotted in figure 6-4 together with the experimental points.

It can be seen that the general shape of the diffusion coefficients' dependence on composition is predicted correctly. The maximum deviation from the experimental points is about

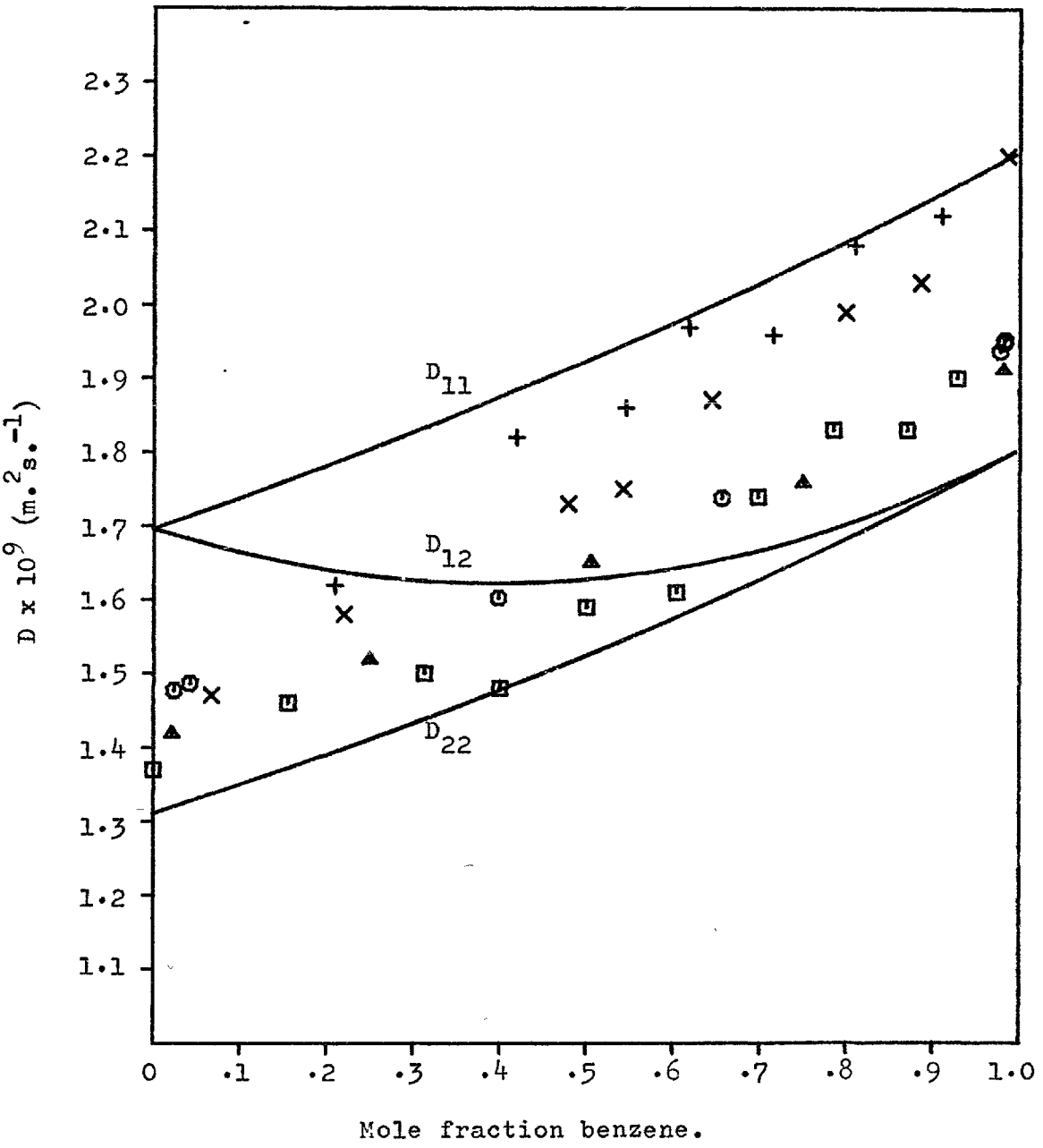


Figure 6-4: COMPARISON OF THE PREDICTIONS OF THE HARD SPHERE MODEL WITH EXPERIMENTAL DATA.

—— Lines fitted to predicted values.

Symbols as defined in figure 6-2.

Mole Fraction Benzene	$D_{11} \times 10^9$ $m.^2 s.^{-1}$	$D_{22} \times 10^9$ $m.^2 s.^{-1}$	$D'_{12} \times 10^9$ $m.^2 s.^{-1}$	Q	$D_{12} \times 10^9$ $m.^2 s.^{-1}$
0.0	1.690	1.299	1.690	1.0	1.690
.1	1.732	1.337	1.700	.9752	1.658
.2	1.776	1.378	1.710	.9560	1.635
.3	1.822	1.421	1.720	.9422	1.621
.4	1.870	1.465	1.730	.9339	1.616
.5	1.920	1.513	1.741	.9312	1.621
.6	1.972	1.563	1.751	.9339	1.635
.7	2.027	1.616	1.762	.9442	1.660
.8	2.084	1.672	1.772	.9560	1.694
.9	2.143	1.731	1.783	.9752	1.739
1.0	2.206	1.794	1.794	1.0	1.794

Table 6-7: PREDICTED DIFFUSION COEFFICIENTS FOR THE BENZENE CARBON TETRACHLORIDE SYSTEM. HARD SPHERE MODEL USING CARNAHAN-STARLING EQUATION.

15 per cent. The agreement is not as good as that obtained from equations (3-55) and (3-56).

6-5 The n-Hexane-Carbon Tetrachloride System.

The hexane-carbon tetrachloride system has not received a great deal of attention. Bidlack and Anderson (152) have reported measurements of the mutual diffusion coefficient across the composition range together with viscosity and density data. The excess volume of mixing is small (161) and additivity of volumes has been assumed. Activity data were available from the same source as for the benzene-carbon tetrachloride system (151) and were corrected to 25 C in the same manner (152).

The self diffusion coefficient of n-hexane has been measured at six points across the composition range. As far as is known, this is the first time that the self diffusion of n-hexane in carbon tetrachloride has been investigated at 25 C. It has, however, been studied at 20 C by means of the steady gradient n.m.r. spin echo method (38). The results are presented in table 6-8 and plotted, together with the data of Bidlack and Anderson (152), in figure 6-5.

Mole Fraction Carbon Tetrachloride	$D_{22} \times 10^9$ $m.^2 s.^{-1}$
0.0	4.35
.2133	3.73
.4041	3.21
.5755	2.71
.7305	2.36
.8714	1.99

Table 6-8: EXPERIMENTAL SELF DIFFUSION COEFFICIENTS FOR n-HEXANE IN CARBON TETRACHLORIDE.

These points were determined using benzene at 25 C as the calibration standard, δ = 1 ms., τ = 30.90 ms., and about 35 ms. The estimated accuracy was ± 4 per cent.

As can be seen in table 5-1 the value for the self diffusion coefficient for pure n-hexane is in good agreement with other determinations.

Equations (3-55) and (3-56) have been tested in the same manner as with the benzene-carbon tetrachloride system.

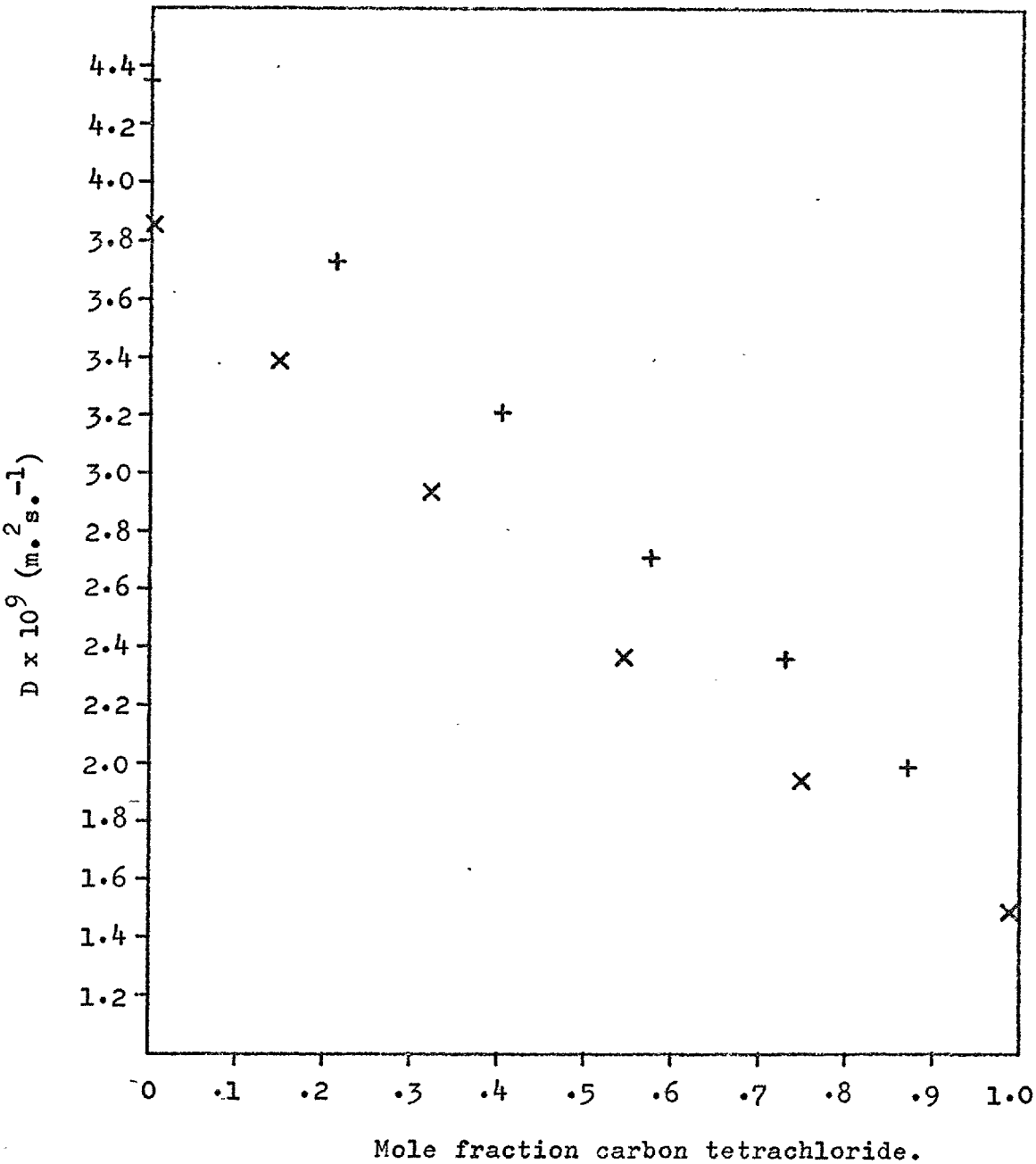


Figure 6-5: EXPERIMENTAL DIFFUSION COEFFICIENTS FOR THE n-HEXANE-CARBON TETRACHLORIDE SYSTEM.

\+ Self diffusion coefficient n-hexane (this work).

× Mutual diffusion data (152) ±1 p.c.

The mutual diffusion data have been used to calculate the self diffusion coefficients of each component. The mutual diffusion data have been interpolated from that of Bidlack and Anderson (152). The results are presented in table 6-9 and plotted in figure 6-6.

Mole Fraction Carbon Tetrachloride	$D_{12} \times 10^9$ $m.^2 s.^{-1}$	Q	$D_{11} \times 10^9$ $m.^2 s.^{-1}$	$D_{22} \times 10^9$ $m.^2 s.^{-1}$
0·0	$3·86_9$	1·0	3·87	2·86
·1729	$3·33_0$	·9494	3·67	2·71
·3869	$2·76_0$	·9160	3·35	2·47
·5869	$2·28_8$	·9142	2·96	2·18
·7906	$1·85_3$	·9414	2·48	1·83
1·0	$1·47_1$	1·0	1·99	1·47

Table 6-9: DATA AND PREDICTED SELF DIFFUSION COEFFICIENTS FOR A TEST OF EQUATIONS (3-55) AND (3-56) IN THE n-HEXANE-CARBON TETRACHLORIDE SYSTEM.

It can be seen that the predicted values for the self diffusion coefficients of n-hexane are very different from the experimental values. Unfortunately there have been no measurements on the self diffusion of carbon tetrachloride in n-hexane with which to make comparison.

The viscosity data of Bidlack and Anderson (152) have been interpolated to allow calculation of the $D\eta$ product for the experimentally determined self diffusion coefficients. The results are presented in table 6-10.

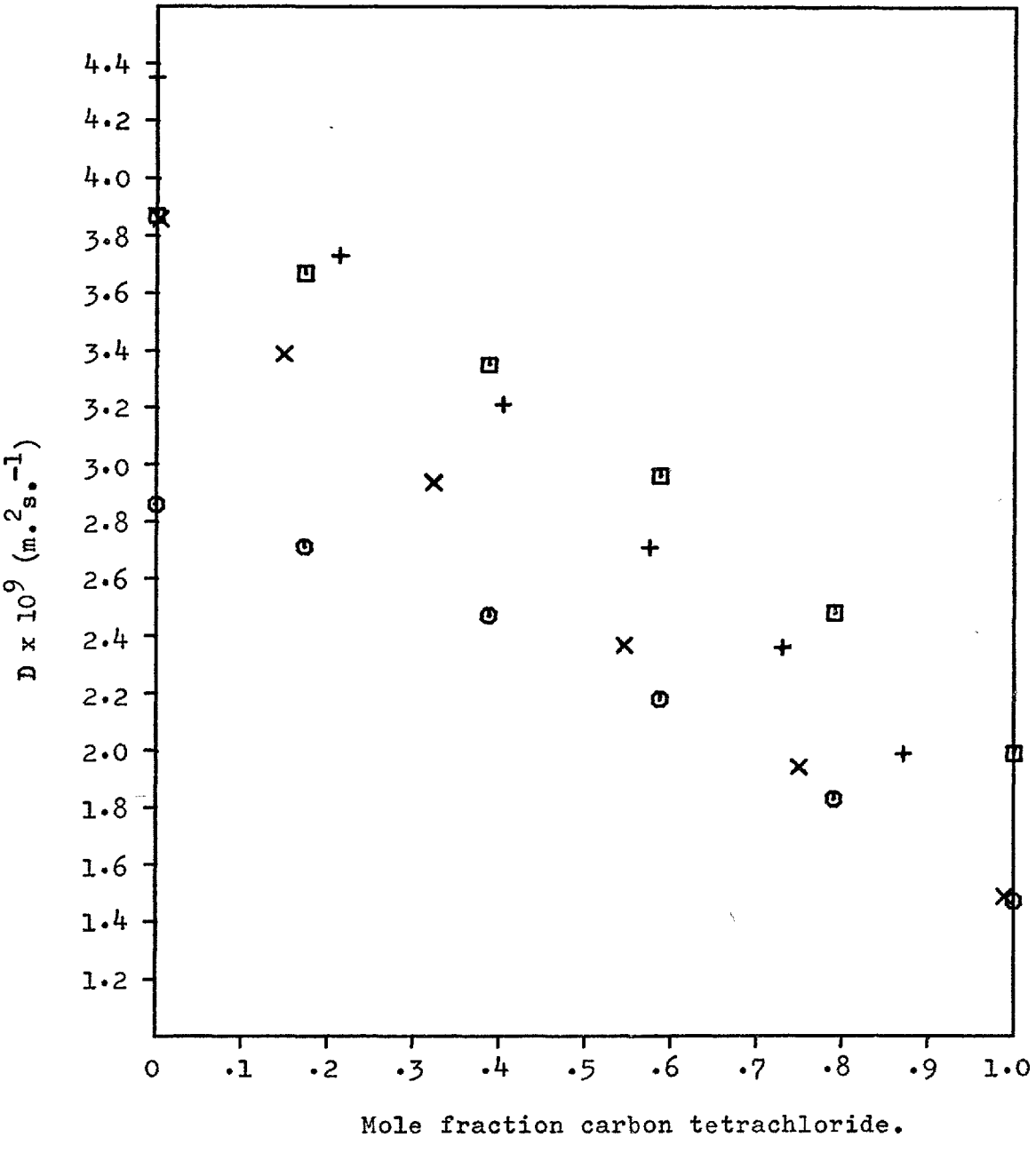


Figure 6-6: COMPARISON OF THE PREDICTIONS OF EQUATIONS (3-55) AND (3-56) WITH EXPERIMENTAL DATA.

⊙ Predicted self diffusion coefficients of n-hexane.

⊡ Predicted self diffusion coefficients of carbon tetrachloride.

Other symbols as defined in figure 6-5.

Mole Fraction Carbon Tetrachloride	$D_{22} \times 10^9$ $m.^2 s.^{-1}$	η cp.	$D_{22}\eta \times 10^7$ dynes
0.0	4.26[a]	.296	1.26
0.0	4.35	.296	1.29
.2133	3.73	.353	1.32
.4041	3.21	.420	1.35
.5755	2.71	.498	1.35
.7305	2.36	.597	1.41
.8714	1.99	.723	1.45
1.0	1.58[b]	.896	1.42

Table 6-10: TEST OF THE CONSISTENCY OF THE $D\eta$ PRODUCT FOR THE SELF DIFFUSION OF n-HEXANE IN CARBON TETRACHLORIDE.

a) Value determined by Harris et al. (137)

b) Extrapolation of mutual data (152)

The $D\eta$ product is not a constant.

As with the benzene-carbon tetrachloride system there are no strong molecular interactions and the assumption of additivity of volume is reasonable, but, in this case, the molecules are of different shape. It is likely that it is this difference in shape that is primarily responsible for the failure of equation (3-56) to predict the behaviour of the self diffusion coefficient of n-hexane across the composition range and for the variation in the $D\eta$ product. The difference in shape results in the radial distribution functions being dependent on the composition of the mixture.

In view of the fact that the molecular shape of the n-hexane molecule is probably not very well represented by a sphere, it might be thought that the predictions of the hard sphere model would also be rather poor. In fact the agreement with experiment is reasonably good and better than that for the benzene-carbon tetrachloride system. The results for the model are shown in table 6-11 and figure 6-7.

Mole Fraction Carbon Tetrachloride	$D_{11} \times 10^9$ $m.^2 s.^{-1}$	$D_{22} \times 10^9$ $m.^2 s.^{-1}$	$D'_{12} \times 10^9$ $m.^2 s.^{-1}$	Q	$D_{12} \times 10^9$ $m.^2 s^{-1}$
0.0	3.909	4.270	3.909	1.0	3.909
.1729	3.348	3.687	3.428	.9494	3.255
.3869	2.738	3.042	2.884	.9160	2.642
.5869	2.219	2.485	2.398	.9142	2.192
.7906	1.751	1.975	1.941	.9414	1.827
1.0	1.311	1.490	1.490	1.0	1.490

Table 6-11: PREDICTED DIFFUSION COEFFICIENTS FOR THE n-HEXANE CARBON TETRACHLORIDE SYSTEM. HARD SPHERE MODEL USING PERCUS-YEVICK EQUATION.

The hard sphere model has only been fitted using the diameters and values of the radial distribution function at contact appropriate to the Percus-Yevick equation.

A feature of the results is the very close agreement between the experimental and predicted mutual diffusion coefficients at either end of the concentration range. The maximum deviation of the predicted points from the experimental

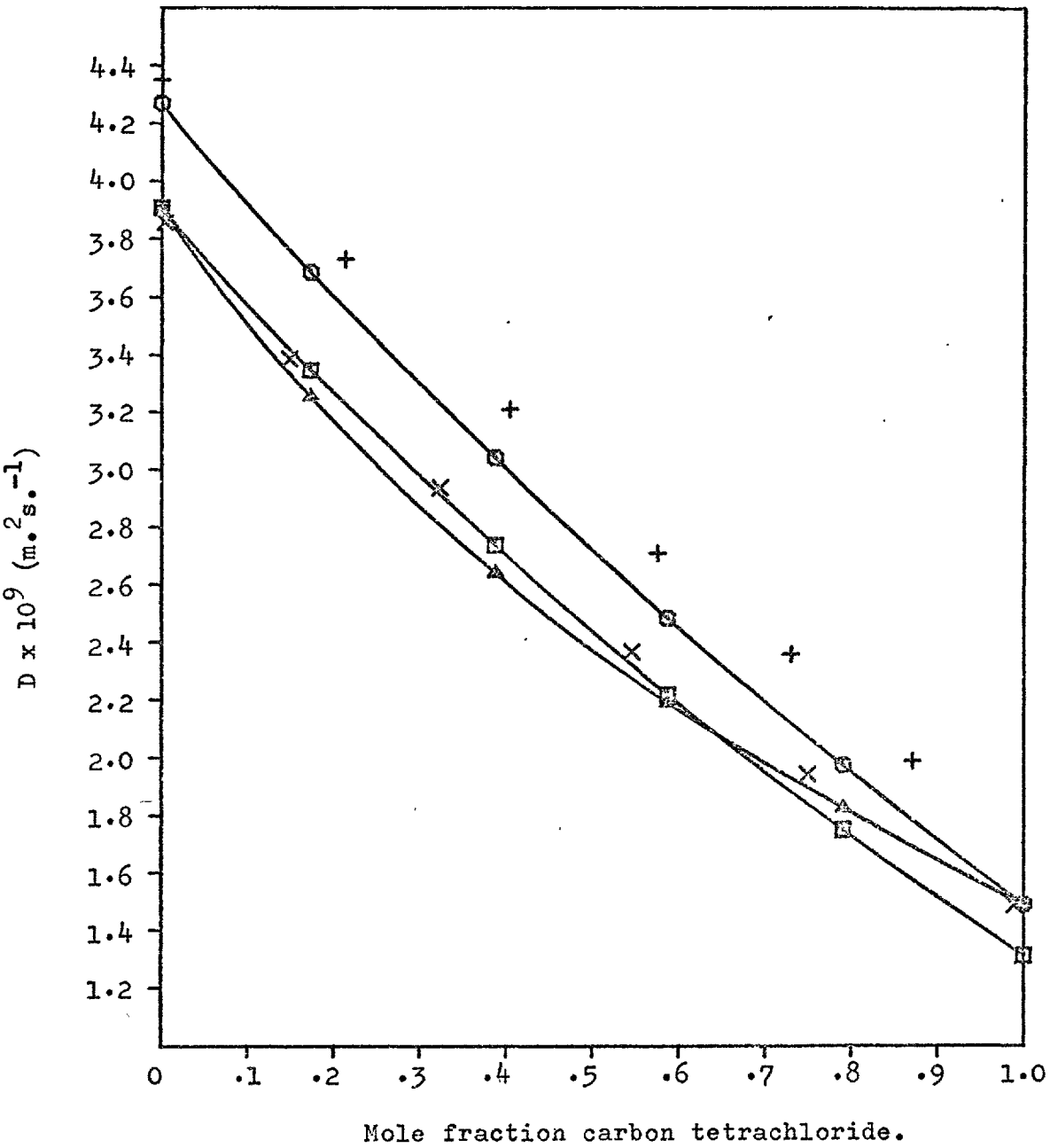


Figure 6-7: COMPARISON OF THE PREDICTIONS OF THE HARD SPHERE MODEL WITH EXPERIMENTAL DATA.

- ⊙ Predicted self diffusion coefficients of n-hexane.
- ⊡ Predicted self diffusion coefficients of carbon tetrachloride.
- ⊿ Predicted mutual diffusion coefficients.

Other symbols as defined in figure 6-5.

points is about 10 per cent.

6-6 The Benzene-Chloroform System.

The benzene-chloroform system has been approximated by measuring the self diffusion coefficient of benzene in deuterated chloroform and of chloroform in deuterated benzene across the concentration range. Measurements were made at 15 C. The results are given in table 6-12 and plotted in figure 6-8.

Mole Fraction benzene	$D_{11} \times 10^9$ $m.^2 s.^{-1}$	Mole Fraction d-benzene	$D_{22} \times 10^9$ $m.^2 s.^{-1}$
1·0	1·86[a]	0·0	2·08
·820	1·88	·154	2·14
·644	1·92	·313	2·11
·475	1·99	·477	2·12
·312	2·04	·646	2·22
·156	2·20	·910	2·41

Table 6-12: EXPERIMENTAL SELF DIFFUSION COEFFICIENTS IN THE BENZENE-CHLOROFORM SYSTEM

a) Calibration standard (136)

Instrument settings for these measurements were δ = 1 ms., τ = 30·90 ms., and Δ was about 30·6 ms. The results were estimated to be accurate to ± 4 per cent except for the point at ·910 mole fraction deutero-benzene. The signal from this sample was weak and measurements were made by averaging over 64 sweeps at a 20 second repetition rate. This point is estimated to be accurate to within 6 per cent.

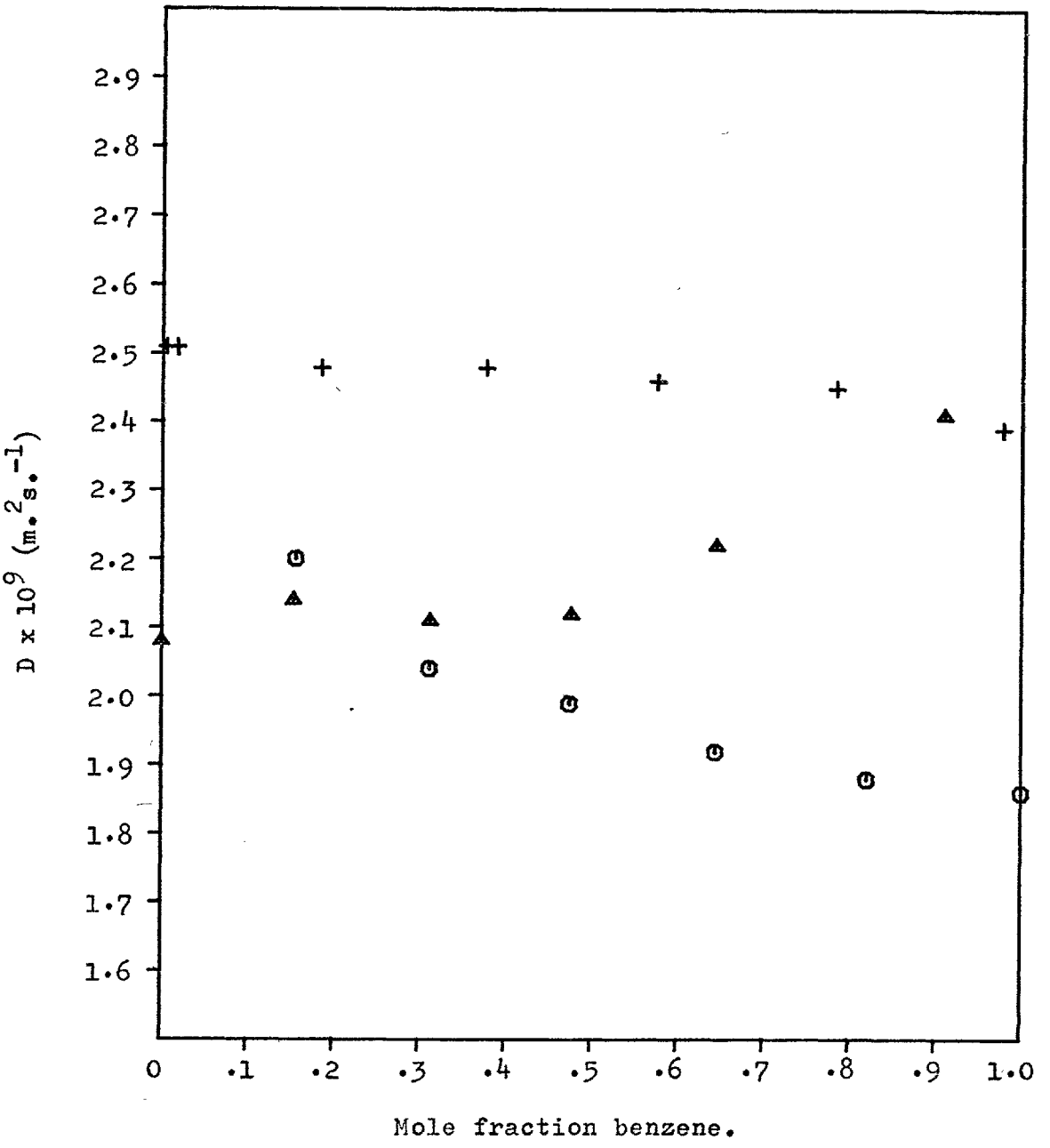


Figure 6-8: EXPERIMENTAL DIFFUSION COEFFICIENTS FOR THE BENZENE-CHLOROFORM SYSTEM.

⊙ Self diffusion coefficient benzene (this work).

▲ Self diffusion coefficient chloroform (this work).

\+ Mutual diffusion data (154) ±4 p.c.

Also plotted in figure 6-8 are the mutual diffusion data of Lemonde (154) for the benzene-chloroform system at 15 C. This set of data is reported to be accurate to ± 4 per cent, but it is rather old and the accuracy may not be that good (155). However, our results, within experimental error, can be extrapolated so that the self and mutual diffusion coefficients coincide at infinite dilution.

Because data concerning the excess volume of mixing were not available the results are considered in relation to equation (3-53), i.e.:

$$D_{12} = (x_1 D_{22} + x_2 D_{11})\, Q \,.$$

A problem was how to determine the thermodynamic factor, Q. The excess free energy of mixing has been reported (156) at 25.5 C, calculated from vapour pressure data. It appears that the free energies given are the result of fitting the experimental data to the form $G^E = Ax_1x_2$. (This is essentially the method used for the benzene-carbon tetrachloride and n-hexane-carbon tetrachloride systems.) The agreement is only approximate for this system and so the Q terms derived can only be regarded as giving a rough indication of the thermodynamic term. The data set was corrected to 15 C by assuming a linear relationship between A and the absolute temperature. The Q terms were calculated from the 2 suffix Margules equation via the term:

$$(\partial \ln a_1 / \partial \ln x_1) = 1 + \frac{8.44.8}{RT}\, x_1 x_2$$

The predicted mutual diffusion coefficients given by equation (3-53) are shown in table 6-13.

It can be seen that if equation (3-53) is to fit the

Mole Fraction Benzene	$D_{11} \times 10^9$ $m.^2 s.^{-1}$	$D_{22} \times 10^9$ $m.^2 s.^{-1}$	$(x_1 D_{22} + x_2 D_{11}) \times 10^9$ $m.^2 s.^{-1}$	Q	$D_{12} \times 10^9$ $m.^2 s.^{-1}$
1.0	1.86[a]	2.37[c]	2.37	1.0	2.37
.645	1.92	2.22	2.11	1.14	2.41
.476	1.99	2.12	2.05	1.16	2.38
.312	2.04	2.11	2.06	1.14	2.35
.155	2.20	2.14	2.19	1.08	2.37
0.0	2.51[b]	2.08	2.51	1.0	2.51

Table 6-13: TEST OF EQUATION (3-53) FOR THE BENZENE CHLOROFORM SYSTEM.

a) Calibration standard (136)

b) Extrapolated from mutual data (154)

c) Extrapolated from mutual data (154)

data, then Q must be greater than 1. That is, the system must show negative deviations from Raoult's law. This is the case and there is a considerable negative excess volume of mixing. Negative deviations from Raoult's law are indicative of strong attractive forces between the molecules. In the benzene-chloroform system it is known that hydrogen bonding occurs between the the hydrogen on the chloroform molecule and the π electrons of the benzene ring.

The fact that the self-diffusion coefficients of benzene and chloroform are the same at about 0.25 mole fraction benzene leads one to wonder if there might be formation of a single diffusing species made up of 3 chloroform and one benzene molecule held together by hydrogen bonding. The phase diagram for the system (156) shows no indication of compound formation

although it is interesting to note that a eutectic is formed at 26·5 mole per cent benzene.

Lemonde (154) has also measured the viscosity coefficients for the system. Using interpolated values the $D\eta$ products are given in table 6-14.

Mole Fraction Benzene	D_{11} x 10^9 $m.^2s.^{-1}$	D_{22} x 10^9 $m.^2s.^{-1}$	η cp.	$D_{11}\eta$ x10^7 dynes	$D_{22}\eta$ x 10^7 dynes
1·0	1·86[a]	2·37[c]	·700	1·30	1·66
·910	-	2·41	·676	-	1·63
·820	1·88	-	·658	1·24	-
·645	1·92	2·22	·636	1·22	1·41
·476	1·99	2·12	·623	1·24	1·32
·313	2·04	2·11	·615	1·25	1·30
·155	2·20	2·14	·607	1·34	1·30
0·0	2·51[b]	2·08	·595	1·49	1·24

Table 6-14: $D\eta$ PRODUCTS FOR THE BENZENE-CHLOROFORM SYSTEM.

a) Calibration constant (136)

b) Extrapolated from mutual data (154)

c) Extrapolated from mutual data (154)

The hard sphere model has not been applied to this system due to a lack of sufficient data. It is unlikely that the agreement with systems in which there are strong attracive forces would be good.

6-7 The Octamethylcyclotetrasiloxane-Benzene System.

This system is a good example of the diffusion of large globular molecules in the presence of smaller molecules. The mutual diffusion coefficients across the composition range at 25 C have been determined by Marsh (157) and the self diffusion coefficients of labelled benzene in OMCTS have been determined by Mills (106). Activity and viscosity data are also available (106,157) and the excess volume of mixing is small (158). Additivity of volumes is assumed in the calculations made for this system. In order to complete the set of diffusion coefficients for the system it is necessary to measure the self diffusion coefficients of OMCTS in benzene. This has been approximated to by measuring the self diffusion coefficients of OMCTS in deuterated benzene at 25 C across the composition range. The results obtained are presented in table 6-15 and figure 6-9. Also shown in figure 6-9 are the data of Mills and a polynomial fitted to Marsh's mutual data.

Measurements were made with n-dodecane as the calibration standard, taking its self diffusion coefficient at 25 C to be 8.37×10^{-10} m.^{2}s.$^{-1}$(139). Measurements were taken with δ = 1 ms., τ = 75.90 ms., and Δ about 63.5 ms. The results are estimated to be accurate to within ± 4 per cent. The two points at 0.049 and 0.018 mole fraction OMCTS were determined with signal averaging. Typically 64 sweeps at a 10 second repetition rate were taken, although some measurements were made with up to 1,024 sweeps.

This system is a very suitable one for study by means of the spin echo technique since there is a large variation in the

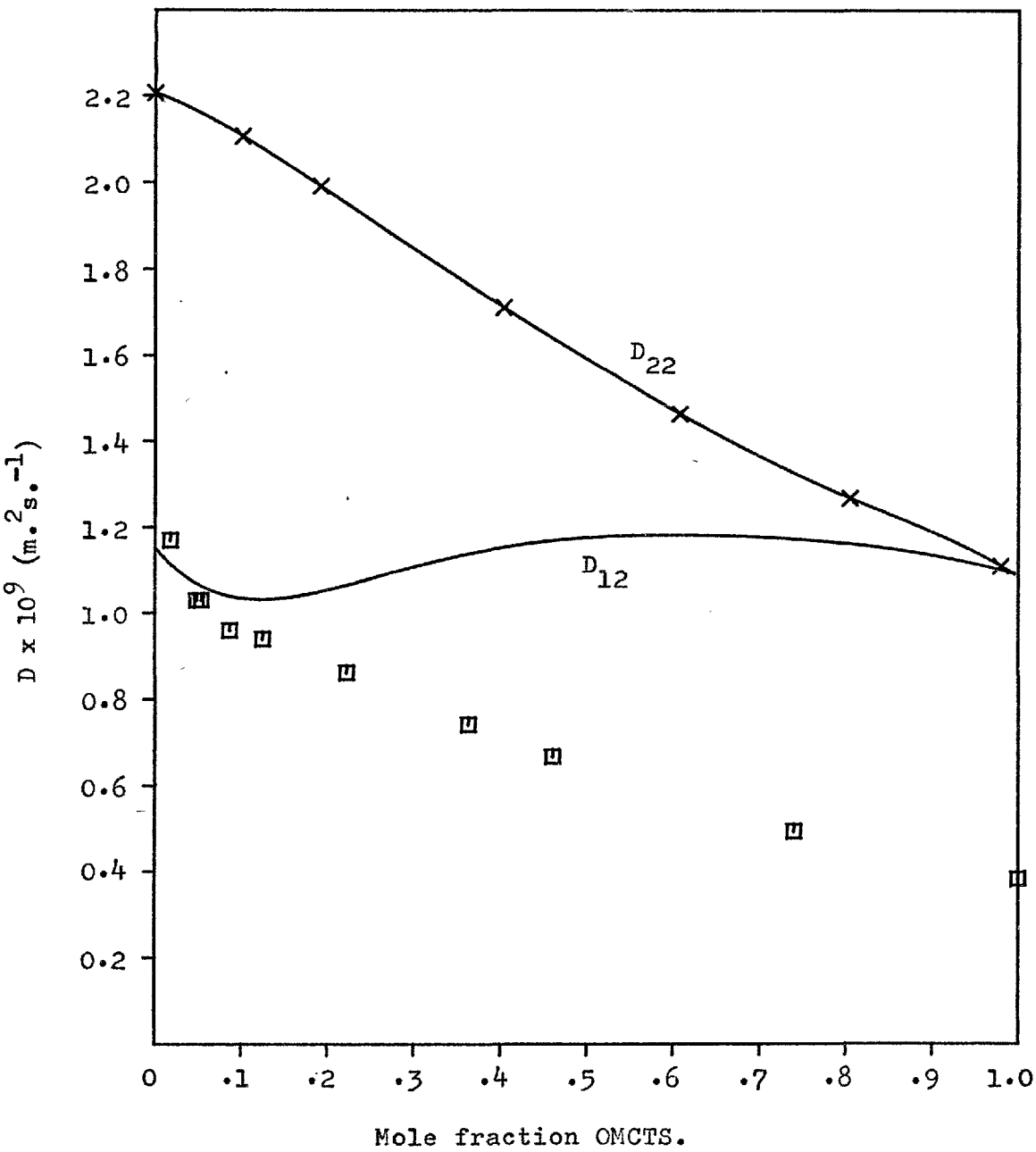


Figure 6-9: EXPERIMENTAL DIFFUSION COEFFICIENTS FOR THE OMCTS-BENZENE SYSTEM.

⊡ Self diffusion coefficient OMCTS (this work)

× Self diffusion coefficient benzene (106) ±0·1 p.c.

—— Line fitted to mutual data (157) ±0·2 p.c.

Mole Fraction OMCTS	$D_{11} \times 10^{10}$ $m.^2 s.^{-1}$
1.0	3.83
.740	4.94
.461	6.69
.363	7.43
.222	8.62
.125	9.40
.087	9.60
.054	10.3
.049	10.3
.018	11.7

Table 6-15: EXPERIMENTAL SELF DIFFUSION COEFFICIENTS FOR OMCTS IN d-BENZENE.

values of the diffusion coefficient with changes in composition and because of the large number of protons on the OMCTS molecule it is possible to make measurements at quite low OMCTS concentrations. This allows a close approach to measurements at infinite dilution where the self and mutual diffusion coefficients should coincide. It can be seen from figure 6-9 that there is good agreement with this condition.

Equations (3-55) and (3-56) have been tested by calculating the predicted self diffusion coefficients for the two components from the mutual data. The results are shown in table 6-16. Figure 6-10 shows a plot of the polynomials fitted to these predictions together with the experimental data. The predicted self diffusion coefficients for OMCTS agree to within 16 per cent

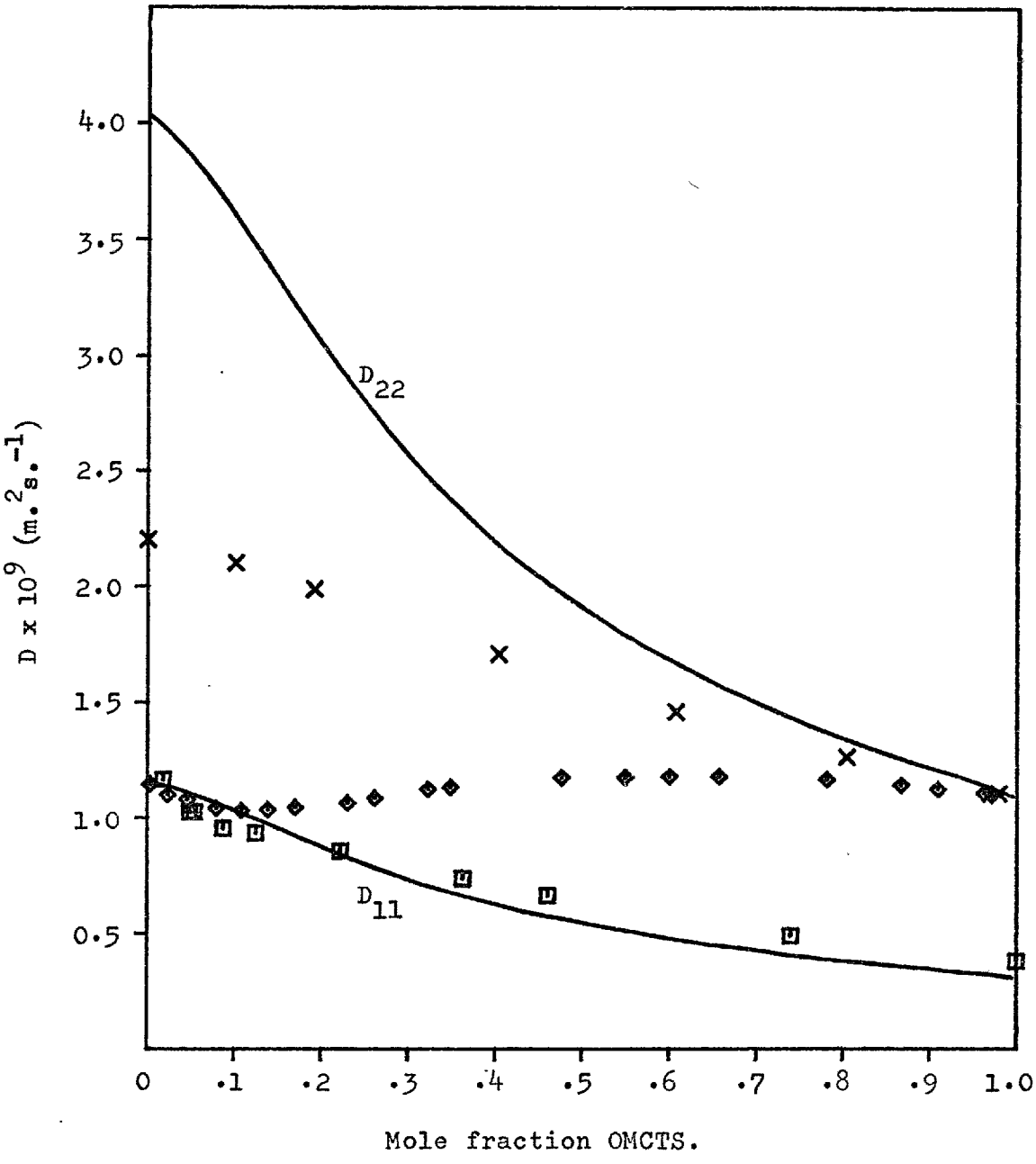


Figure 6-10: COMPARISON OF THE PREDICTIONS OF EQUATIONS (3-55) AND (3-56) WITH EXPERIMENTAL DATA.

—— Lines fitted to predicted values.

◈ Mutual data (157).

Other symbols as defined in figure 6-9.

Mole Fraction OMCTS	$D_{12} \times 10^9$ $m.^2 s.^{-1}$	Q^a	$D_{11} \times 10^{10}$ $m.^2 s.^{-1}$	$D_{22} \times 10^9$ $m.^2 s.^{-1}$
·0031	1·145	·9847	11·5	4·03
·0033	1·147	·9840	11·6	4·03
·0237	1·101	·9203	11·3	3·94
·0460	1·080	·8684	11·2	3·89
·0795	1·042	·8187	10·6	3·71
·1085	1·033	·7967	10·2	3·56
·1388	1·036	·7890	9·76	3·40
·1706	1·046	·7927	9·26	3·23
·2304	1·066	·8189	8·27	2·89
·2617	1·087	·8374	7·86	2·74
·3227	1·126	·8746	7·14	2·49
·3489	1·134	·8896	6·82	2·38
·4767	1·176	·9471	5·68	1·98
·5494	1·177	·9691	5·13	1·79
·6006	1·181	·9814	4·82	1·68
·6578	1·182	·9927	4·52	1·58
·7814	1·169	1·007	3·94	1·38
·8672	1·146	1·006	3·61	1·26
·9098	1·129	1·003	3·45	1·20
·9630	1·111	1·002	3·26	1·14
·9714	1·104	1·000	3·23	1·13

Table 6-16: DATA AND PREDICTED SELF DIFFUSION COEFFICIENTS FOR A TEST OF EQUATIONS (3-55) AND (3-56) IN THE OMCTS-BENZENE SYSTEM.

a) Interpolated from values in reference (106).

with the experimental points. The discrepancy between the experimental and predicted self diffusion coefficients of benzene is up to 82 per cent.

The viscosity data of Marsh have been interpolated to allow calculation of the $D\eta$ product for the experimentally determined self diffusion coefficients. The results are presented in table 6-17.

Mole Fraction OMCTS	D_{11} x 10^{10} $m.^2 s.^{-1}$	η cp.	$D\eta$ x 10^8 dynes
1.0	3.83	2.190	8.39
.740	4.94	1.586	7.83
.461	6.69	1.102	7.37
.363	7.43	0.964	7.16
.222	8.62	0.792	6.83
.125	9.40	0.695	6.53
.087	9.60	0.662	6.36
.054	10.3	0.637	6.56
.049	10.3	0.633	6.52
.018	11.7	0.613	7.17
0.0	11.5[a]	0.602	6.92

Table 6-17: THE $D\eta$ PRODUCT FOR THE SELF DIFFUSION OF OMCTS IN BENZENE.

a) Extrapolated from mutual diffusion data (157).

The $D\eta$ product is not constant and has a minimum at about the same point as the minimum in the mutual diffusion data.

The hard sphere model has been fitted using both the

Mole Fraction OMCTS	D_{11} x 10^{10} $m.^2 s.^{-1}$	D_{22} x 10^9 $m.^2 s.^{-1}$	D'_{12} x 10^9 $m.^2 s.^{-1}$	Q	D_{12} x 10^9 $m.^2 s^{-1}$
0.0	8.467	2.205	0.8467	1.000	0.8467
.1	7.233	1.954	0.8685	.803	0.6974
.2	6.378	1.771	0.8951	.807	0.7223
.3	5.755	1.632	0.9249	.859	0.7945
.4	5.282	1.523	0.9571	.913	0.8738
.5	4.913	1.436	0.9910	.956	0.9474
.6	4.616	1.365	1.026	.984	1.009
.7	4.373	1.305	1.062	.999	1.061
.8	4.171	1.255	1.099	1.005	1.104
.9	4.001	1.212	1.137	1.004	1.141
1.0	3.855	1.175	1.175	1.000	1.175

Table 6-17: PREDICTED DIFFUSION COEFFICIENTS FOR THE OMCTS BENZENE SYSTEM. HARD SPHERE MODEL USING PERCUS YEVICK EQUATION.

Percus-Yevick and Carnahan-Starling equations to give the value of the radial distribution function at contact. The results are presented in tables 6-17 and 6-18. In figure 6-11 are plotted polynomials fitted to the predictions of the hard sphere model using the Percus-Yevick equation together with the experimental points. It can be seen that the agreement between the experimental and predicted points is somewhat better than the agreement found when using equations (3-55) and (3-56). The behaviour of the diffusion coefficients is qualitatively predicted. The maximum discrepancy between the predicted and experimental values is 27 per cent.

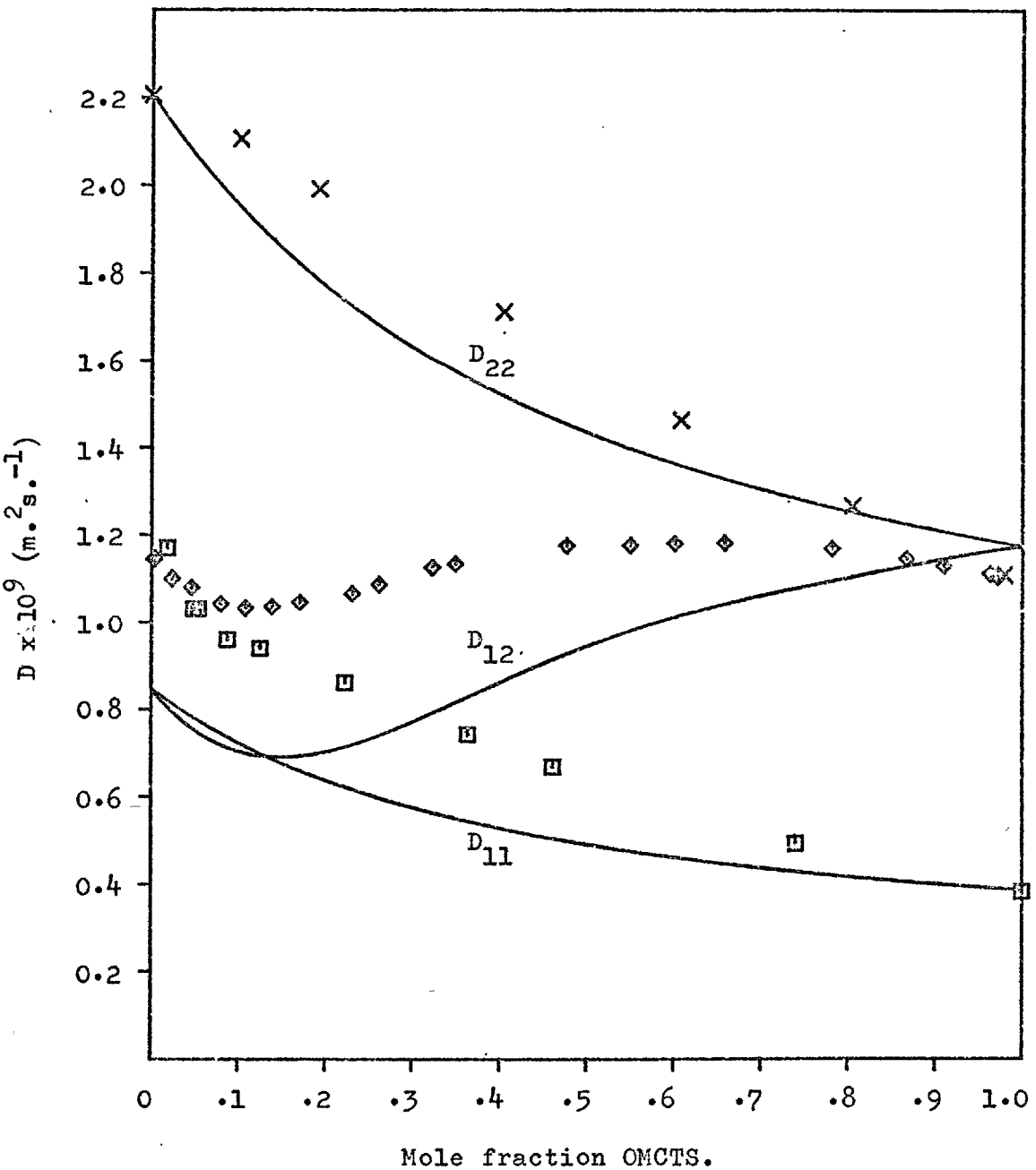


Figure 6-11: COMPARISON OF THE PREDICTIONS OF THE HARD SPHERE MODEL WITH EXPERIMENTAL DATA.

—— Lines fitted to predicted values.

Symbols as defined in figures 6-9 and 6-10.

Mole Fraction OMCTS	$D_{11} \times 10^{10}$ $m.^2 s.^{-1}$	$D_{22} \times 10^{9}$ $m.^2 s.^{-1}$	$D'_{12} \times 10^{9}$ $m.^2 s.^{-1}$	Q	$D_{12} \times 10^{9}$ $m.^2 s.^{-1}$
0.0	7.973	2.206	0.7973	1.000	0.7973
.1	6.822	1.987	0.8415	.803	0.6757
.2	6.044	1.828	0.8888	.807	0.7173
.3	5.486	1.707	0.9382	.859	0.8059
.4	5.068	1.612	0.9890	.913	0.9030
.5	4.744	1.537	1.041	.956	0.9952
.6	4.486	1.475	1.094	.984	1.076
.7	4.276	1.423	1.147	.999	1.146
.8	4.102	1.379	1.201	1.005	1.207
.9	3.955	1.342	1.255	1.004	1.260
1.0	3.830	1.310	1.310	1.000	1.310

Table 6-18: PREDICTED DIFFUSION COEFFICIENTS FOR THE OMCTS BENZENE SYSTEM. HARD SPHERE MODEL USING CARNAHAN STARLING EQUATION.

It can be seen that there are differences of up to about 10 per cent between the predictions of the hard sphere model when using the Percus-Yevick and Carnahan-Starling equations.

6-8 The Tetraphenyltetramethylcyclotetrasiloxane-Carbon Tetrachloride System.

Tetraphenyltetramethylcyclotetrasiloxane (TPTMCTS) is a white solid. Its self diffusion coefficient when dissolved in carbon tetrachloride has been measured up to 0.1 mole fraction at 25 C. The results are given in table 6-19 and plotted in figure 6-12.

Mole Fraction TPTMCTS	$D_{11} \times 10^{10}$ $m.^2 s.^{-1}$
·010	4·68
·027	4·61
·048	3·48
·072	2·95
·083	2·59

Table 6-19: EXPERIMENTAL SELF DIFFUSION COEFFICIENTS FOR TPTMCTS IN CARBON TETRACHLORIDE.

Measurements were calibrated relative to the self diffusion coefficient of n-dodecane (139). The point at ·01 mole fraction had to be corrected for non-linearity in the diode detector as described in section 5-11. Instrument settings were δ = 1 ms., τ = 75·90 ms., and Δ was about 65 ms. All measurements were made with the use of signal averaging. Typically 64 sweeps at a 10 second repetition rate were averaged. The results are estimated to be accurate to ± 6 per cent except for the 0·01 mole fraction result which is estimated to be accurate to ± 8 per cent.

It is interesting to compare the extrapolated self diffusion coefficient at infinite dilution with that for OMCTS in carbon tetrachloride at infinite dilution. This is known accurately from mutual diffusion measurements made by Marsh (157). The value for the self diffusion coefficient of OMCTS at infinite dilution in carbon tetrachloride was taken to be $7{\cdot}22 \times 10^{-10}$ $m.^2 s.^{-1}$.

As a simple approximation the two large molecules might

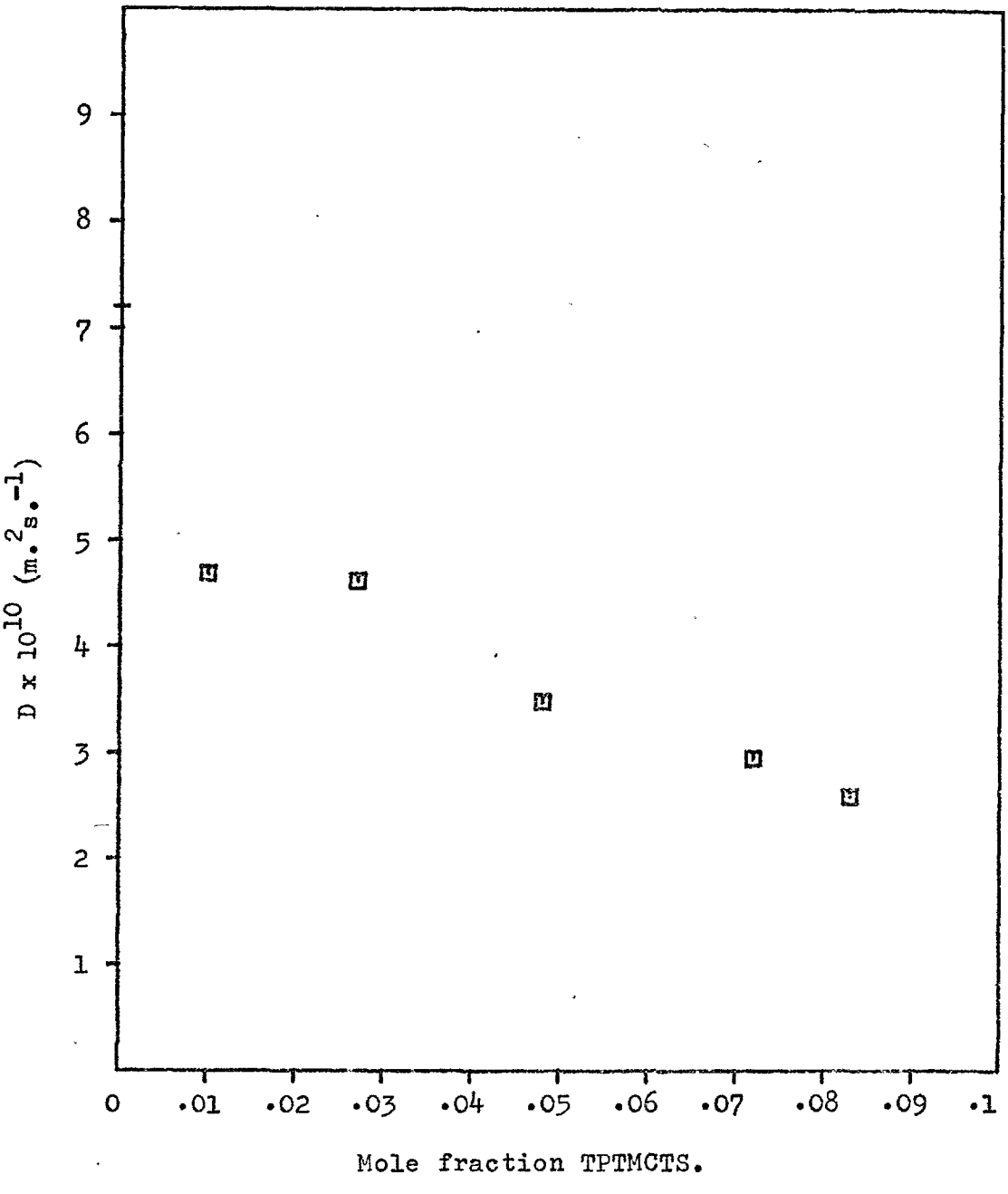


Figure 6-12: EXPERIMENTAL DIFFUSION COEFFICIENTS FOR THE TPTMCTS-CARBON TETRACHLORIDE SYSTEM.

□ Self diffusion coefficient TPTMCTS (this work).

\+ Self diffusion coefficient OMCTS (mutual data at infinite dilution (157)).

be considered as having the same interaction with the solvent molecules and as having the same size and shape. The difference in the self diffusion coefficients at infinite dilution is then due to the difference in molecular mass. The phenomenological theory indicates that the ratio of the diffusion coefficients at infinite dilution is equal to the inverse ratio of the friction coefficients. That is:

$$D_{22}^{\infty}/D_{33}^{\infty} = R_{13}/R_{12} \qquad (6\text{-}1)$$

where the subscripts 1, 2, 3 denote carbon tetrachloride, TPTMCTS, and OMCTS respectively. If the friction coefficients are given by equation (3-80) then, since we have assumed $\sigma_{22} = \sigma_{33}$:

$$D_{22}^{\infty}/D_{33}^{\infty} = (\mu_{13}/\mu_{12})^{1/2} \qquad (6\text{-}2)$$

where μ represents the reduced mass.

This approach predicts a value of 6.32×10^{-10} m.^{2}s.$^{-1}$ for the self diffusion coefficient of TPTMCTS in carbon tetrachloride at infinite dilution. This appears to be too high a value to be consistent with the experimental results. It may well be that the assumption of equality in the sizes of the TPTMCTS and OMCTS molecules is poor. TPTMCTS is a larger molecule and this would reduce the value of the self diffusion coefficient.

As far as the simple model is concerned, one gets better agreement with experiment if the ratio of the diffusion coefficients is taken equal to the square root of the inverse ratio of the molecular masses:

$$D_{22}^{\infty}/D_{33}^{\infty} = (m_3/m_2)^{1/2} \quad . \qquad (6\text{-}3)$$

This predicts a value of 5.33×10^{-10} m.^{2}s.$^{-1}$ for the self diffusion coefficient of TMTPCTS at infinite dilution in

carbon tetrachloride. This value is not inconsistent with the experimental results.

6-9 The Polypropylene Glycol-Carbon Tetrachloride System.

Relatively few measurements have been made of the self diffusion coefficients of polymers in solution by the n.m.r. spin echo method. The availability of well characterized, narow molecular weight distribution polymers makes possible studies of the dependence of the diffusion coefficient on concentration and molecular weight.

A suitable system for such a study is polypropylene glycol in carbon tetrachloride. The polymer is available as narrow molecular weight distribution G.P.C. fractions with molecular weights 790, 1220, 2020, 3900. The low molecular weight of the polymers also means that the diffusion coefficients should not be very low and so their measurement should be relatively easy.

Initial studies have been made on 790 and 3900 molecular weight fractions. Unfortunately the reproducibility of the results was extremely poor. The results obtained are plotted in figure 6-13.

The reason for the poor reproducibility has not been resolved. It was thought that perhaps the polymer was in some way degrading in solution. In order to check this out a solution was made up and left to stand for several months. A G.P.C. analysis was then carried out on this sample together with a reference solution of freshly dissolved polymer. There was no significant difference between the results obtained and the

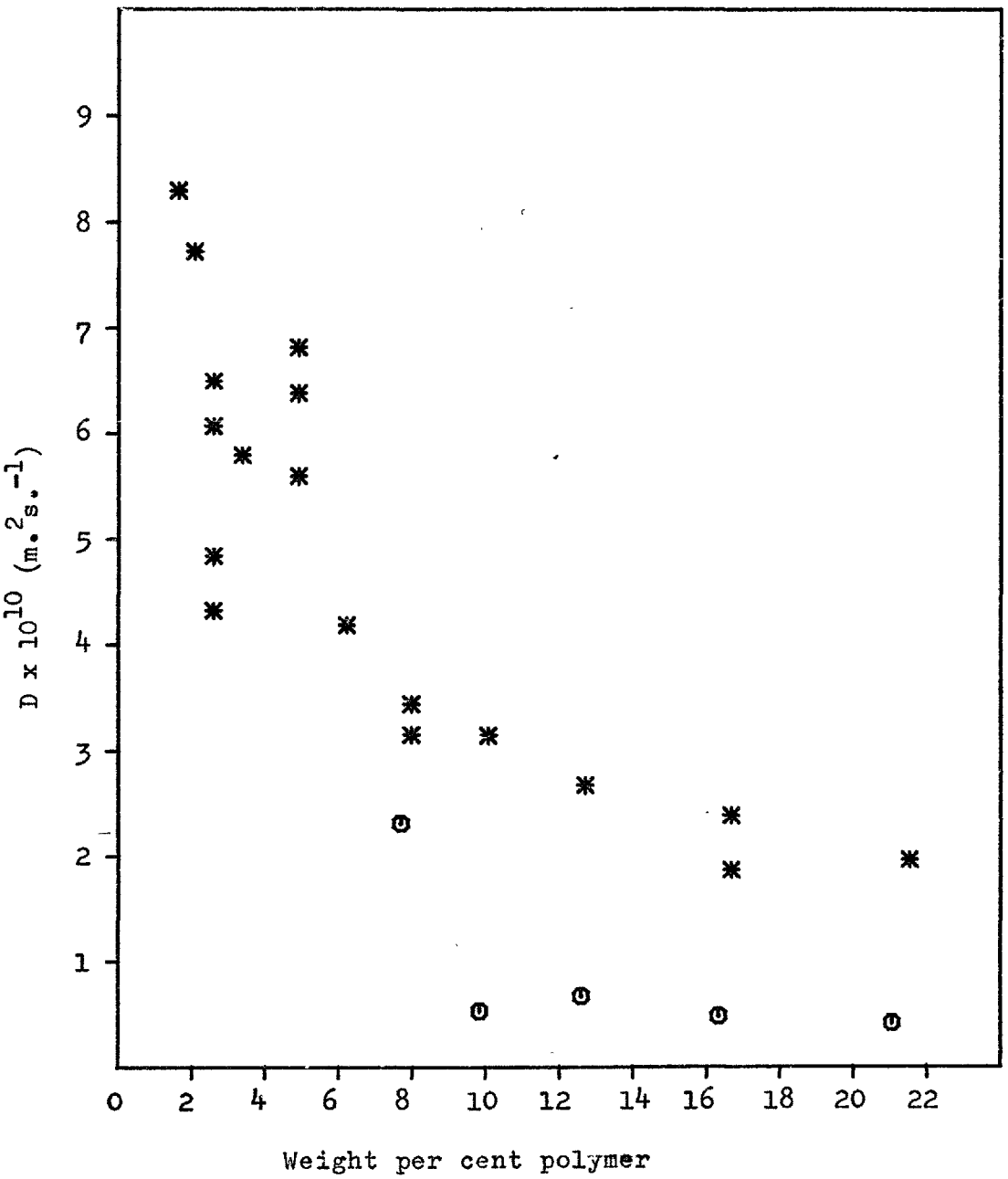


Figure 6-13: EXPERIMENTAL SELF DIFFUSION COEFFICIENTS OF POLYPROPYLENE GLYCOL IN CARBON TETRACHLORIDE.

* Molecular weight 790

⊙ Molecular weight 3900

specified molecular weight and distribution.

All measurements have been made using the signal averager. A 10 second repetition rate was used to average the signal between 32 and 512 times. Instrumental settings were δ = 1 ms., τ = 75·90 ms., and Δ was in the region of 64 ms. The calibration standard was n-dodecane.

In terms of polymer solution theory the solutions studied are relatively concentrated. It has been suggested (51) that in certain polymer solutions the concentration dependence of the diffusion coefficient is exponential:

$$D = D_o \exp(-bc).$$

Our results are not inconsistent with a relationship of this kind, but they are not considered good enough to merit further comparison.

6-10 Discussion.

The three systems benzene/carbon tetrachloride, n-hexane/carbon tetrachloride, and OMCTS/perdeutero-benzene provide an interesting comparison between experiment, the predictions of the hard sphere model, and the predictions of equations (3-55) and (3-56).

When both equations (3-55) and (3-56) hold then equation (3-53) also holds. Bearman (117) has shown that equation (3-53) would hold for solutions where the radial distribution function is independent of composition and where the excess volume of mixing is zero. Bearman points out that this might be expected to hold for systems where the molecules have similar size, shape,

and interaction potentials. It has been seen that the experimental results for the benzene/carbon tetrachloride system are predicted quite well by equations (3-55) and (3-56), and indeed this is the type of system that fits the required conditions. However, the agreement between experiment and the predictions from equations (3-55) and (3-56) is rather poor for the n-hexane/carbon tetrachloride and OMCTS/benzene systems. This could well be due to the differences in shape and size between the components. In the former system the molecules are of similar size but different shape and in the latter system they are of different size but have the same basic shape.

The predictions of the hard sphere model do not appear to be as sensitive to differences in molecular size or actual shape, indeed the best agreement with experimental data is obtained for the n-hexane/carbon tetrachloride system. The predictions of the hard sphere model are, on the whole, closer to the experimental values for the n-hexane/carbon tetrachloride and OMCTS/benzene systems than those from equations (3-55) and (3-56). The hard sphere model also has the advantage that less data is required for its application. Apart from thermodynamic and volume data the hard sphere model only requires a knowledge of the self diffusion coefficients of the pure components, in order to calculate appropriate molecular diameters, and the dependences of both self and the mutual diffusion coefficients are predicted as functions of composition. Equations (3-55) and (3-56) require mutual diffusion data across the composition range in order to calculate the variation in the self diffusion coefficients.

The radial distribution functions have been evaluated at contact by use of the Percus-Yevick and Carnahan-Starling equations. For the systems studied the use of the Percus-Yevick equation leads to better agreement, on the whole, with experimental results. However, this is probably fortuitous since the Carnahan-Starling equation predicts values in better agreement with the results of molecular dynamics studies (159). It should be noted that for the systems studied the number density is high enough for both the Carnahan-Starling and the Percus-Yevick equations to deviate from the machine results.

Implicit in many of the results presented is the assumption that deuteration of one of the components of a binary mixture does not appreciably affect the diffusion of the molecules. Any errors inherent in this assumption will be most marked at those compositions with a high concentration of the deuterated component. Measurements made in our laboratory have indicated that the viscosity of deuterated benzene may be up to 5 per cent higher than that of protonated benzene. Relationships such as the Stokes-Einstein equation would then predict that the self-diffusion coefficient of a component at infinite dilution in protonated benzene would be about 5 per cent higher than that in deuterated benzene. However, the close agreement between the measured self diffusion coefficient of OMCTS in deutero-benzene and Marsh's mutual data (157) at low OMCTS concentrations indicates that any error is not that great.

It is hoped that the work presented in this thesis has provided further diffusion data which will be of use to others and that the comparisons with the hard sphere model will encourage

others to make similar comparisons. The hard sphere model seems to present us with alternatives to the Darken and related equations with which to compare experimental results. Better agreement can hoped for between the diffusion data for group O elements and the hard sphere model, but even for the relatively complex systems investigated here the agreement is semi-quantitative. Before definite conclusions can be drawn as to the applicability of the hard sphere model to real liquids more systems need to be analysed in a similar manner to that presented here.

APPENDICES.

Appendix A: THE EVALUATION OF $\langle \varphi'^2 \rangle$.

$$\varphi' = \gamma G_o \left\{ \int_0^{t_1} Z(t)\,dt + \int_{t_1+\delta_1}^{\tau} Z(t)\,dt - \int_{\tau}^{t_2} Z(t)\,dt - \int_{t_2+\delta_2}^{t} Z(t)\,dt \right\}$$
$$+\gamma G_x \left\{ \int_0^{\tau} X(t)\,dt - \int_{\tau}^{t} X(t)\,dt \right\}$$
$$+\gamma (G_o + G) \left\{ \int_{t_1}^{t_1+\delta_1} Z(t)\,dt - \int_{t_2}^{t_2+\delta_2} Z(t)\,dt \right\}$$

and so:

$$\langle \varphi'^2 \rangle = \Bigg\langle \Bigg[\gamma G_o \left\{ \int_0^{t_1} Z(t)\,dt + \int_{t_1+\delta_1}^{\tau} Z(t)\,dt - \int_{\tau}^{t_2} Z(t)\,dt - \int_{t_2+\delta_2}^{t} Z(t)\,dt \right\}$$
$$+\gamma G_x \left\{ \int_0^{\tau} X(t)\,dt - \int_{\tau}^{t} X(t)\,dt \right\}$$
$$+\gamma (G_o + G) \left\{ \int_{t_1}^{t_1+\delta_1} Z(t)\,dt - \int_{t_2}^{t_2+\delta_2} Z(t)\,dt \right\} \Bigg]^2 \Bigg\rangle$$

$$= \gamma^2 G_o^2 \Bigg\{ \int_0^{t_1}\int_0^{t_1} \langle Z(t).Z(s) \rangle \,dt\,ds$$
$$+ \int_{t_1+\delta_1}^{\tau}\int_{t_1+\delta_1}^{\tau} \langle Z(t).Z(s) \rangle \,dt\,ds$$
$$+ \int_{\tau}^{t_2}\int_{\tau}^{t_2} \langle Z(t).Z(s) \rangle \,dt\,ds$$
$$+ \int_{t_2+\delta_2}^{t}\int_{t_2+\delta_2}^{t} \langle Z(t).Z(s) \rangle \,dt\,ds$$
$$+ 2 \int_0^{t_1}\int_{t_1+\delta_1}^{\tau} \langle Z(t).Z(s) \rangle \,dt\,ds$$
$$+ 2 \int_{\tau}^{t_2}\int_{t_2+\delta_2}^{t} \langle Z(t).Z(s) \rangle \,dt\,ds$$
$$- 2 \int_0^{t_1}\int_{\tau}^{t_2} \langle Z(t).Z(s) \rangle \,dt\,ds$$
$$- 2 \int_0^{t_1}\int_{t_2+\delta_2}^{t} \langle Z(t).Z(s) \rangle \,dt\,ds$$
$$- 2 \int_{t_1+\delta_1}^{\tau}\int_{\tau}^{t_2} \langle Z(t).Z(s) \rangle \,dt\,ds$$
$$- 2 \int_{t_1+\delta_1}^{\tau}\int_{t_2+\delta_2}^{t} \langle Z(t).Z(s) \rangle \,dt\,ds \Bigg\}$$

$$
\begin{aligned}
&+ 2\gamma^2(G_o G + G_o^2)\Bigg\{ \int_0^{t_1}\int_{t_1}^{t_1+\delta_1} \langle Z(t).Z(s)\rangle \, dt\, ds \\
&\quad + \int_{t_1+\delta_1}^{\tau}\int_{t_1}^{t_1+\delta_1} \langle Z(t).Z(s)\rangle \, dt\, ds \\
&\quad + \int_{\tau}^{t_2}\int_{t_2}^{t_2+\delta_2} \langle Z(t).Z(s)\rangle \, dt\, ds \\
&\quad + \int_{t_2+\delta_2}^{t}\int_{t_2}^{t_2+\delta_2} \langle Z(t).Z(s)\rangle \, dt\, ds \\
&\quad - \int_{\tau}^{t_2}\int_{t_1}^{t_1+\delta_1} \langle Z(t).Z(s)\rangle \, dt\, ds \\
&\quad - \int_{t_2+\delta_2}^{t}\int_{t_1}^{t_1+\delta_1} \langle Z(t).Z(s)\rangle \, dt\, ds \\
&\quad - \int_{0}^{t_1}\int_{t_2}^{t_2+\delta_2} \langle Z(t).Z(s)\rangle \, dt\, ds \\
&\quad - \int_{t_1+\delta_1}^{\tau}\int_{t_2}^{t_2+\delta_2} \langle Z(t).Z(s)\rangle \, dt\, ds \Bigg\} \\
&+ \gamma^2(G_o + G)^2 \Bigg\{ \int_{t_1}^{t_1+\delta_1}\int_{t_1}^{t_1+\delta_1} \langle Z(t).Z(s)\rangle \, dt\, ds \\
&\quad + \int_{t_2}^{t_2+\delta_2}\int_{t_2}^{t_2+\delta_2} \langle Z(t).Z(s)\rangle \, dt\, ds \\
&\quad - 2\int_{t_1}^{t_1+\delta_1}\int_{t_2}^{t_2+\delta_2} \langle Z(t).Z(s)\rangle \, dt\, ds \Bigg\} \\
&+ \gamma^2 G_x^2 \Bigg\{ \int_0^{\tau}\int_0^{\tau} \langle X(t).X(s)\rangle \, dt\, ds \\
&\quad + \int_{\tau}^{t}\int_{\tau}^{t} \langle X(t).X(s)\rangle \, dt\, ds \\
&\quad - 2\int_0^{\tau}\int_{\tau}^{t} \langle X(t).X(s)\rangle \, dt\, ds \Bigg\}
\end{aligned}
$$

Cross terms involving G_x with G_o and G are zero since these gradients are orthogonal.

The following conditions also hold:

$$\langle Z(t).Z(s)\rangle = \langle Z^2(t)\rangle \quad \text{if } t < s$$
$$= \langle Z^2(s)\rangle \quad \text{if } s < t$$

and $$\langle Z^2(t)\rangle = 2Dt$$

where D represents the self diffusion coefficient.

Evaluation of the above integrals leads, after considerable algebra, to equation (2-36).

As examples two of the integrals are evaluated below:

A) $$\int_0^{t_1}\int_0^{t_1} \langle Z(t).Z(s)\rangle \; dt\, ds$$

$$= 2\int_0^{t_1}\int_0^{t=s} 2Dt \; dt\, ds$$

$$= 4\, Dt_1^{\,3}/6$$

B) $$\int_0^{t_1}\int_{t_1+\delta_1}^{\tau} \langle Z(t).Z(s)\rangle \; dt\, ds$$

In the region t greater than s:

$$= \int_0^{t_1} ds \int_{t_1+\delta_1}^{\tau} 2Ds \; dt$$

$$= \int_0^{t_1} 2Ds(\tau - (t_1 + \delta_1))\, ds$$

$$= Dt_1^{\,2}(\tau - (t_1 + \delta_1))$$

Appendix B: DIFFUSION MEASUREMENTS IN NON-ELECTROLYTE LIQUID SYSTEMS BY MEANS OF THE N.M.R. SPIN ECHO METHOD

This appendix summarises the non-electrolyte liquid systems in which free diffusion has been studied since about 1963. Systems studied prior to then have been summarized elsewhere (91).

The appendix is divided into three sections:

B-1: Pure non-electrolyte liquids.

B-2: Non-electrolyte binary liquid mixtures.

B-3: Polymer solutions.

Diffusion coefficients have units of $cm.^2 s.^{-1}$ and are written in E format. Thus 2·2E-5 is to be read as 2.2×10^{-5} $cm.^2 s.^{-1}$ Graphical data is indicated by the word GRAPH. The following abreviations are used for the methods:

S.G. - Steady field gradient.

P.G. - Pulsed field gradient.

S.E. - Stimulated echo.

A.P.G. - Alternating pulsed field gradient.

sin.F.G.- Sinusoidal field gradient.

Appendix B-1:

In this summary the activation data is given where available. Most is presented as appropriate to the equation:

$$D = Do \exp(-E/RT).$$

The units of the activation energy, E, are kilocalories per mole. The temperature range over which the equation is valid is also indicated.

Reference (19) also reports the volume of activation and reference (72) gives data appropriate to an equation of the form:

$$D = Do \exp(-\beta Vo/Vf) \exp(-E/RT).$$

COMPOUND	T	D	ERROR	OTHER DATA	METHOD	REF.
ACETONE	60.0C	7.0E-5	10pc	Do = 1.75E-3	S.G.	30
	25.0C	4.3E-5		E = 2.1		
	-9.4C	3.1E-5		for:		
	-35.3C	2.1E-5		$3.0 < \frac{10^3}{T} < 5.4$		
	-53.8C	1.32E-5				
	-70.2C	9.2E-6				
	-87.1C	5.3E-6				
		GRAPH				
ACETONE	298K	4.0E-5		Do = (1.21±.1) E-3	S.G.	34
				E = 2.0± .1		
				for:		
				180K to 300K		
ACETIC ACID	84.0C	3.0E-5	10pc	Do = 6.1E-3	S.G.	30
	50.0C	1.83E-5		E = 3.7		
	30.0C	1.27E-5		for:		
	17.0C	8.9E-6		$3.0 < \frac{10^3}{T} < 4.4$		
		GRAPH				
ANILINE	20C	2.7E-6	10pc		S.G	85
	30C	4.5E-6				
	40C	5.9E-6				
	50C	8.2E-6				
	60C	1.1E-5				
	70C	1.3E-5				
	80C	1.7E-5				
BENZENE	20C to 360C	GRAPH	10pc	Do = 2.6E-3 E = 2.0 β = 1 Vo = 0.67	S.G.	72
BENZENE	0C	1.21E-5		Do = 3.5E-3	P.G.	31
	5C	1.36E-5		E = 3.1		
	10C	1.53E-5				
	20C	1.86E-5				
	25C	1.97E-5				
	30C	2.20E-5				
	40C	2.46E-5				
	50C	2.89E-5				
	60C	3.39E-5				
	70C	3.90E-5				
	80C	4.60E-5				
	90C	4.96E-5				
	100C	5.66E-5				
		GRAPH				

COMPOUND	T	D	ERROR	OTHER DATA	METHOD	REF.
BENZENE	293·2K	1·91E-5			S.G.	27
	313·2K	2·58E-5				
	333·2K	3·40E-5				
	353·2K	4·37E-5				
	373·2K	5·50E-5				
	393·2K	6·92E-5				
	413·2K	8·65E-5				
	433·2K	1·08E-4				
	453·2K	1·36E-4				
	473·2K	1·775E-4				
	493·2K	2·25E-4				
	503·2K	2·54E-4				
	513·2K	2·931E-4				
	523·2K	3·44E-4				
BENZENE	15C	1·90E-5	5pc	E = 3·1	S.G.	98
	25C	2.27E-5				
	35C	2·68E-5				
	45C	3·15E-5				
	55C	3·63E-5				
		(SMOOTHED) GRAPH				
BENZENE	300K to 380K	GRAPH	5pc	E = 3·5	S.G.	21
BENZENE	25C	2·07E-5	3pc		P.G.	49
	25C	2·10E-5	±·05		A.P.G.	
tert BUTYL ALCOHOL	295K to 355K	GRAPH		Do = 9·71E-1 E = 7·51	S.G.	22
tert BUTYL BROMIDE	260K to 330K	GRAPH		Do = 1·82E-3 E = 2·87	S.G.	22
tert BUTYL CHLORIDE	250K to 315K	GRAPH		Do = 1·45E-3 E = 2·49	S.G.	22
tert BUTYL CYANIDE	215K to 330K	GRAPH		Do = 1·97E-3 E = 2·58	S.G.	22
tert BUTYL IODIDE	240K to 345K	GRAPH		Do = 2·03E-3 E = 3·13	S.G.	22

COMPOUND	T	D	ERROR	OTHER DATA	METHOD	REF.
CHLORO-BENZENE	300K to 380K	GRAPH	5pc	E = 3.7	S.G.	21
CHLORO-BENZENE	298K 220K to 400K	1.80E-5		Do = (3.6±.3) E-3 E = 3.12±.15	S.G.	34
CHLORO-FORM	200K 300K	5E-6 3.3E-5		E = 2.2	S.G.	26
CYCLO-HEXANE	290K to 360K			Do = (3.7±1.2) E-3 E = 3.33±.3	S.G.	35
CYCLO-HEXANE	293.2K 313.2K 333.2K 353.2K 373.2K 393.2K 413.2K 433.2K 453.2K 473.2K 493.2K 513.2K 523.2K	1.23E-5 1.75E-5 2.34E-5 3.14E-5 4.10E-5 5.32E-5 6.70E-5 8.60E-5 1.10E-4 1.50E-4 1.87E-4 2.50E-4 3.00E-4			S.G.	27
		GRAPH				
CYCLO-HEXANOL	350K to 440K			Do = (3.5±1.9) E-4 E = 7.8±.6	S.G.	35
CYCLO-HEXANONE	260K to 440K			Do = (6.6±1.1) E-3 E = 4.12±.2	S.G.	35
DECANE	300K to 518K	GRAPH			S.G.	87
DIBROMO-METHANE	25C 0C to 80C	1.55E-5 GRAPH		E = 2.42±.03	S.G.	59

COMPOUND	T	D	ERROR	OTHER DATA	METHOD	REF.
1,2 DICHLORO-ETHANE	25C	1.32E-5	±.03E-5		S.G.	88
DICHLORO-METHANE	25C 0C to 60C	3.85E-5 GRAPH		E = 2.12±.04	S.G.	59
DIETHYL ETHER	14.2C -6.3C -33.5C -62.0C -84.0C -106.0C	6.3E-5 5.2E-5 3.3E-5 1.74E-5 9.6E-6 4.3E-6 GRAPH	10pc	Do = 2.6E-3 E = 2.1	S.G.	30
DIGLYCOL-DIMETHYL-ETHER	60.0C 22.0C -14.7C -20.0C -39.5C -50.0C -59.0C -68.8C -74.7C -78.6C -83.2C -84.6C -89.4C -91.6C -93.9C -97.0C	2.3E-5 1.26E-5 6.0E-6 5.2E-6 2.5E-6 1.42E-6 1.00E-6 4.5E-7 2.9E-7 1.93E-7 1.20E-7 8.5E-8 5.3E-8 2.6E-8 2.9E-8 2.2E-8 GRAPH	10pc 20pc 20pc	Do = 2.4E-3 E = 3.1	S.G. P.G. S.E.	30
DIIODO-METHANE	25C 0C to 80C	5.6E-6 GRAPH		E = 3.29±.06	S.G.	59
1,2 DIMETHOXY ETHANE	90.0C 60.0C 19.7C 2.0C -24.7C -42.8C -57.8C -75.8C -91.0C	7.5E-5 5.3E-5 3.0E-5 2.4E-5 1.48E-5 9.9E-6 6.7E-6 3.7E-6 1.86E-6 GRAPH	10pc	Do = 2.5E-3 E = 2.5 for: $2.75 < \frac{10^3}{T} < 4.9$	S.G.	30

COMPOUND	T	D	ERROR	OTHER DATA	METHOD	REF.
DIETHOXY METHANE	60.0C	5.3E-5	10pc	Do = 2.2E-3	S.G.	30
	21.5C	3.2E-5		E = 2.5		
	-12.0C	2.1E-5				
	-34.8C	1.4E-5				
	-50.2C	8.7E-6				
	-65.0C	5.7E-6				
	-84.6C	3.0E-6				
		GRAPH				
DIMETHYL ANILINE	300K to 380K	GRAPH	5pc	E = 6.3	S.G.	21
DIPHENYL AMINE	50C	2.3E-6	5pc		S.G.	85
	60C	3.6E-6				
	70C	4.9E-6				
	80C	6.15E-6				
ETHANE	c280K to 340K	GRAPH	5pc		S.G.	81
ETHANE	89.9K to 305.4K	GRAPH		E = 0.5 at 100K E = 3.5 at 300K	S.G.	48
ETHANE	155K to 298K	GRAPH			S.G.	79
ETHYL ALCOHOL	60.0C	2.6E-5	10pc	Do = 7.3E-3	S.G.	30
	23.3C	1.37E-5	20pc	E = 3.7	P.G.	
	22.7C	1.26E-5	10pc		S.G.	
	-14.0C	4.8E-6				
	-34.2C	2.7E-6				
	-51.4C	1.47E-6				
	-68.2C	7.2E-7				
	-84.6C	3.8E-7	20pc		P.G.	
	-100.8C	1.45E-7				
	-114.5C	5.0E-8				
		GRAPH				
ETHYLENE	-10C to 7C	GRAPH	5pc		S.G.	56
ETHYLENE GLYCOL	0C to 60C	GRAPH	5pc		S.G.	25

COMPOUND	T	D	ERROR	OTHER DATA	METHOD	REF.
GLYCEROL	10C	5·8E-9	3pc	E = 13·6	P.G.	49
	15C	9·18E-9				
	20C	1·18E-8				
	30C	2·60E-8				
	40C	5·87E-8				
	50C	1·16E-7				
	60C	2·16E-7				
	70C	3·60E-7				
	80C	6·03E-7				
	90C	8·56E-7				
	100C	1·20E-6				
		GRAPH				
GLYCEROL	293·2K	1·37E-8	12pc at		P.G.	93
	313·2K	6·60E-8	low T			
	333·2K	2·19E-7				
	353·2K	5·70E-7				
	373·2K	1·21E-6				
	393·2K	2·23E-6				
	413·2K	3·65E-6				
	433·2K	5·51E-6				
		GRAPH				
GLYCEROL	26C	2·5E-8	±.2E-8		P.G.	10
HELIUM	0·5K to 4·2K	GRAPH	2pc		S.G.	69
HELIUM	0·35K to 3·0K	GRAPH	40pc		S.G.	99
HEPTANE	25C	3·20E-5	±.08E-5		S.G.	88
HEPTANE	292K to 517K	GRAPH			S.G.	87
HEXANE	25C	4·12E-5	±.10E-5		S.G.	88
HEXANE	290K to 500K	GRAPH			S.G.	86
HEXANE	292K to 505K	GRAPH			S.G.	87

COMPOUND	T	D	ERROR	OTHER DATA	METHOD	REF.
HYDROGEN	14K to 20K	GRAPH	6pc	Do = 10E-4 E = .088	S.G.	7
HYDROGEN CHLORIDE	250K 150K	1.2E-4 2.4E-5 GRAPH		E = 1.2	S.G.	26 62
HYDROGEN FLUORIDE	298K	1.00E-4	±.15E-4	Do = (10.1±1.6) E-3 E = 2.63±.1	S.G.	26 63
ISOPENTANE	c300K to c500K	GRAPH			S.G.	86
LITHIUM (6+7)	188C 1190C	RATIO OF ISOTOPE Ds			P.G.	58
LITHIUM (7)	187C 211C 245C	7.1E-5 8.2E-5 9.2E-5 GRAPH	±.6E-5	Do =(9±4) E-3 E = 2.3±.3	P.G.	54
LITHIUM (6+7)	184C to 257C	GRAPH			P.G.	57
METHANE	90.7K to 111.7K	GRAPH		Do = 8.05E-4 E = .67±.09	S.G.	29
METHANE	90.92K 95.94K 100.00K 105.26K 111.11K 117.65K 125.00K 133.33K 142.86K 153.85K 166.67K 173.91K 181.82K 186.05K 190.48K	2.52E-5 3.01E-5 3.61E-5 4.35E-5 5.23E-5 6.34E-5 7.76E-5 9.56E-5 1.18E-4 1.53E-4 2.12E-4 2.49E-4 3.03E-4 3.58E-4 5.85E-4	2pc		S.G.	60

COMPOUND	T	D	ERROR	OTHER DATA	METHOD	REF.
METHYL ALCOHOL	0C to 50C	GRAPH	5pc		S.G.	25
METHYL-CYCLO-HEXANE	293.2K 313.2K 333.2K 353.2K 373.2K 393.2K 413.2K 433.2K 453.2K 473.2K 493.2K 513.2K 523.2K	1.70E-5 2.42E-5 3.28E-5 4.35E-5 5.60E-5 7.30E-5 9.20E-5 1.16E-4 1.45E-4 1.87E-4 2.40E-4 3.20E-4 3.80E-4			S.G.	27
METHYL-CYCLO-HEXANE	25C	1.84E-5	±.04		S.G.	88
METHYL IODIDE	21.0C -3.0C -23.0C -40.0C -60.0C	2.5E-5 1.86E-5 1.38E-5 1.02E-5 6.9E-6 GRAPH	10pc	Do = 7.4E-4 E = 2.0 for: $3.0 \quad \frac{10^3}{T} \quad 4.7$	S.G.	30
NEO-PENTANE	25C 260K to 305K	4.03E-5 GRAPH		Do = 3.85E-3 E = 2.69	S.G.	22
NEO-PENTANE	25C 308K to 256K	4.5E-5 GRAPH		E = 3.5 Va = 31	S.G.	19
NITRO-BENZENE	300K to 380K	GRAPH	5pc	E = 1.9	S.G.	21
NITRO-BENZENE	270K to 435K			Do = (6.7±.7) E-3 E = 4.05±.15	S.G.	34
NITRO-METHANE	298K 220K to 370K	2.10E-5		Do =(1.60±.15) E-3 E = 2.53±.15	S.G.	34

COMPOUND	T	D	ERROR	OTHER DATA	METHOD	REF.
NONANE		GRAPH			S.G.	87
OCTANE	25C	2·06E-5	±·03E-5		S.G.	88
OCTANE		GRAPH			S.G.	87
PIPER-IDINE	300K to 380K	GRAPH	5pc	E = 1·6	S.G.	21
PIPER-IDINE	20C 30C 40C 50C 60C 70C 80C	8·5E-6 1·09E-5 1·41E-5 1·61E-5 1·90E-5 2·3E-5 2·6E-5	5pc		S.G.	85
PYRIDINE	300K to 380K	GRAPH	5pc	E = 2·1	S.G.	21
PYRIDINE	20C 30C 40C 50C 60C 70C 80C	1·34E-5 1·63E-5 1·98E-5 2·30E-5 2·64E-5 3·10E-5 3·55E-5	5pc		S.G.	85
SODIUM	106C 107C 134C 135C 180C	3·97E-5 4·00E-5 4·75E-5 4·93E-5 6·58E-5 (corrected for bounded media effects)		Do =(9·5±1·1) E-4 E = 2·38±·10	P.G.	53
SULPHUR HEXA-FLUORIDE	223K 228K 233K 243K 248K 253K 263K 268K 273K	2·11E-5 2·41E-5 2·64E-5 2·82E-5 3·28E-5 3·90E-5 4·21E-5 4·71E-5 4·84E-5	10pc		S.G.	89

COMPOUND	T	D	ERROR	OTHER DATA	METHOD	REF.
SULPHUR HEXA-FLUORIDE (cont.)	278K	5.48E-5				
	283K	5.83E-5				
	288K	6.42E-5				
	293K	6.42E-5				
	297K	8.61E-5				
	303K	8.95E-5				
	306K	1.11E-4				
	309K	1.12E-4				
	312K	1.26E-4				
	315K	1.49E-4				
		GRAPH				
SULPHUR HEXA-FLUORIDE	240K	3.35E-5	6pc		S.G.	83
	250K	3.94E-5				
	260K	4.66E-5				
	270K	5.59E-5				
	280K	6.71E-5				
	290K	8.29E-5				
	300K	1.05E-4				
	310K	1.44E-4				
	314K	1.70E-4				
	316K	1.92E-4				
	317K	2.08E-4				
	318K	2.31E-4				
	318.7K	2.92E-4				
TETRA-FLUORO-METHANE	88K	3.02E-6	8.1pc	Do = 6.79E-4 E = 0.96 for: $88 < T < 143K$	S.G.	90
	90.5K	3.39E-6				
	93K	3.33E-6				
	95.5K	4.50E-6				
	98K	4.84E-6				
	103K	6.23E-6				
	108K	7.59E-6				
	113K	9.20E-6				
	118K	1.12E-5				
	123K	1.28E-5				
	128K	1.59E-5				
	133K	1.79E-5				
	138K	2.11E-5				
	143K	2.40E-5				
		GRAPH				
TETRA-HYDRO-FURAN	60.0C	5.5E-5	20pc	Do = 8.0E-4 E = 1.8 for: $3.0 < \frac{10^3}{T} < 4.8$	P.G.	30
	20.0C	3.0E-5				
	-11.7C	2.3E-5				
	-36.6C	1.45E-5				
	-57.2C	1.16E-5				
	-66.0C	9.0E-6				
	-79.3C	6.0E-6				
	-92.6C	4.0E-6				
	-98.8C	3.0E-6				
	-111.2C	1.96E-6				
		GRAPH				

COMPOUND	T	D	ERROR	OTHER DATA	METHOD	REF.
TETRA-METHOXY GERMANE	290K to 380K	GRAPH		Do = 6.96E-4 E = 2.47	S.G.	22
TETRA-METHOXY SILANE	275K to 370k	GRAPH		Do = 1.16E-3 E = 2.62	S.G.	22
TETRA-METHYL GERMANE	220K to 310K	GRAPH		Do = 9.31E-4 E = 2.02	S.G.	22
TETRA-METHYL LEAD	250K to 325K	GRAPH		Do = 4.27E-4 E = 1.96	S.G.	22
TETRA-METHYL SILANE	210K to 300K	GRAPH		Do = 1.58E-3 E = 2.19	S.G.	22
TETRA-METHYL SILANE	25C 192K to 303K	3.6E-5 GRAPH		E = 1.16 Va = 22	S.G.	19
TETRA-METHYL TIN	240K to 330K	GRAPH		Do = 5.87E-4 E = 1.90	S.G.	22
THIOPHENE	300K to 380K	GRAPH	5pc	E = 2.7	S.G.	21
TOLUENE	55.6C	3.3E-5	10pc	Do = 1.5E-3 E = 2.5 for: $3.0 < \frac{10^3}{T} < 4.5$	S.G.	30
	21.0C	2.1E-5				
	-8.3C	1.16E-5				
	-35.6C	7.8E-6				
	-49.8C	5.5E-6				
	-62.8C	3.6E-6				
	-71.0C	2.9E-6				
	-82.6C	1.46E-6				
	-83.9C	1.34E-6	20pc		S.E.	
	-85.2C	1.34E-6	10pc		S.G.	
	-98.8C	5.7E-7				
	-106.0C	2.7E-7				
	-113.2C	1.27E-7	20pc		P.G.	
	-114.4C	1.39E-7	10pc		S.G.	
	-120.1C	5.8E-8	20pc		P.G.	
	-123.6C	1.9E-8	20pc		S.E.	
	-125.2C	1.3E-8				
	-126.5C	1.5E-8	20pc		P.G.	
	-127.6C	7.7E-9	20pc		S.E.	
		GRAPH				

COMPOUND	T	D	ERROR	OTHER DATA	METHOD	REF.
TOLUENE	293.2K	2.32E-5			S.G.	27
	313.2K	2.95E-5				
	333.2K	3.66E-5				
	353.2K	4.58E-5				
	373.2K	5.60E-5				
	393.2K	6.93E-5				
	413.2K	8.40E-5				
	433.2K	1.00E-4				
	453.2K	1.25E-4				
	473.2K	1.531E-4				
	493.2K	1.90E-4				
	503.2K	2.17E-4				
	513.2K	2.45E-4				
	523.2K	2.85E-4				
TRI-ETHYL-AMINE	20C	2.8E-5	5pc		S.G.	85
	30C	3.15E-5				
	40C	3.50E-5				
	50C	4.0E-5				
	60C	4.5E-5				
	70C	5.1E-5				
	80C	5.7E-5				
TRI-FLUORO-BENZENE (1,3,5)	84.0C	6.5E-5		Do = 4.2E-3	S.G.	30
	49.2C	4.5E-5		E = 3.0		
	21.6C	2.5E-5		for:		
	1.7C	1.76E-5		$3.0 < \frac{10^3}{T} < 3.8$		
	-10.8C	1.44E-5				
		GRAPH				
TRI-METHYL-BROMO-SILANE	230K to 330K	GRAPH		Do = 9.79E-4 E = 2.40	S.G.	22
TRI-METHYL-CHLORO-SILANE	220K to 315K	GRAPH		Do = 1.47E-3 E = 2.39	S.G.	22
TRI-METHYL-FLUORO-SILANE	200K to 295K	GRAPH		Do = 1.35E-3 E = 2.05	S.G.	22
TRI-METHYL PHOSPHITE	3.8C	1.68E-5	20pc	Do = 4.5E-3	P.G.	30
	-17.0C	1.13E-5		E = 3.0		
	-20.0C	1.02E-5		for:		
	-26.5C	8.1E-6		$3.6 < \frac{10^3}{T} < 4.7$		
	-44.0C	5.6E-6				
	-60.0C	3.1E-6				
		GRAPH				

COMPOUND	T	D	ERROR	OTHER DATA	METHOD	REF.
WATER	20C to 380C	GRAPH	10pc		S.G.	72
WATER	25C	2·37E-5	±·07E-5		S.G.	88
WATER	25C	2·51E-5	±·01E-5		S.G.	61
WATER	25C	2·23E-5	±·06E-5		S.G.	34
WATER	20C 25C	1·99E-5 2·24E-5	1pc		S.G.	40
WATER	-5C to 120C	GRAPH		E = 4.6 for:0 to 30C E = 3·5 for:80 to 120C	P.G.	43
WATER	17·9C 18.4C 19·0C	1·89E-5 1·96E-5 1·936E-5	7pc		S.G. P.G.	53
WATER (D_2O)	21·1C 22·0C 22·0C	1·685E-5 1·68E-5 1·70E-5	7pc		S.G. P.G.	53
WATER	298·2K 285·3K 273·5K 263·5K 261·5K 258·7K 255·8K 254·0K 251·8K 250·0K 248·2K 246·3K 244·4K 242·5K	2·23E-5 1·58E-5 1·05E-5 7·00E-6 6·33E-6 5·53E-6 4·77E-6 4·38E-6 3·95E-6 3·41E-6 3·21E-6 2·63E-6 2·19E-6 1·87E-6	5pc	E = 11 at -31C	S.G.	92
XENON	177K to 281K	GRAPH	5pc		P.G.	80
σ-XYLENE	300K to 380K	GRAPH	5pc	E = 3·2	S.G.	21

COMPOUND	T	D	ERROR	OTHER DATA	METHOD	REF.
m-XYLENE	300K to 380K	GRAPH	5pc	E = 3·2	S.G.	21
p-XYLENE	300K to 380K	GRAPH	5pc	E = 3·3	S.G.	21

Appendix B-2.

The binary systems are arranged alphabetically according to component A. Component A always comes before component B alphabetically.

Xa represents the mole fraction of component A unless indicated otherwise:

M - moles of solute / 55.5 moles of water,

V - volume per cent.

AX represents data across the composition range.

A	B	T	Xa	Da	Db	ERROR	METHOD	REF.
ACETONE	BENZENE	25C	0.0	2.75E-5	2.28E-5	5pc	S.G.	24
			0.1	2.81E-5	2.38E-5	to		
			0.2	2.97E-5	2.67E-5	10pc		
			0.3	3.19E-5	2.86E-5			
			0.4	3.39E-5	3.01E-5			
			0.5	3.59E-5	3.16E-5			
			0.6	3.79E-5	3.35E-5			
			0.7	3.99E-5	3.54E-5			
			0.8	4.18E-5	3.74E-5			
			0.9	4.46E-5	3.93E-5			
			1.0	4.86E-5	4.12E-5			
				GRAPH	GRAPH			
ACETONE	CHLORO-FORM	25C	0.0	2.35E-5	2.58E-5	5pc	S.G.	24
			0.1	2.41E-5	2.67E-5	to		
			0.2	2.54E-5	2.83E-5	10pc		
			0.3	2.72E-5	2.89E-5			
			0.4	2.86E-5	2.91E-5			
			0.5	3.02E-5	3.05E-5			
			0.6	3.23E-5	3.21E-5			
			0.7	3.49E-5	3.42E-5			
			0.8	3.80E-5	3.60E-5			
			0.9	4.20E-5	3.62E-5			
			1.0	4.90E-5	3.62E-5			
				GRAPH	GRAPH			
ACETONE	WATER	25C	0.0	1.28E-5	2.45E-5	5pc	S.G.	24
			0.1	0.97E-5	1.74E-5	to		
			0.2	1.08E-5	1.51E-5	10pc		
			0.3	1.36E-5	1.64E-5			
			0.4	1.70E-5	1.91E-5			
			0.5	2.14E-5	2.20E-5			
			0.6	2.65E-5	2.44E-5			
			0.7	3.13E-5	2.74E-5			
			0.8	3.50E-5	3.23E-5			
			0.9	3.99E-5	4.24E-5			
			1.0	4.94E-5	c5.5E-5			
				GRAPH	GRAPH			
ACETONE	WATER	0C 20C 25C 30C 40C 60C 80C 100C 120C	0 to .46		GRAPH		P.G.	43
ACETONE	WATER	20C	AX	GRAPH OF PROTON DIFFUSION COEFF.			S.G.	33
ACETONE	WATER	20C	AX	GRAPH OF PROTON DIFFUSION COEFF.		7pc	S.G.	40

A	B	T	Xa	Da	Db	ERROR	METHOD	REF.
ACETONE	WATER	25C	0 to 16M	GRAPH	GRAPH	10pc	S.G.	20
ACETONE	WATER	32C 37C 72.5C	0 to .37	GRAPH OF PROTON DIFFUSION COEFF.			S.G.	41
ANILINE	CYCLO-HEXANE	32C 42C	AX	GRAPH	GRAPH		sin. F.G.	13
ARGON	METHANE	91K 93K 95K 97K 99K 101K 103K 105K 107K 109K 77K 77.5K 79K 81K 83K 85K 87K 89K 91K 93K 95K 97K 99K 101K 103K 105K 107K 109K	0 0.9 atm of A to 0.1 atm B		2.23E-5 2.41E-5 2.63E-5 2.77E-5 3.03E-5 3.18E-5 3.48E-5 3.73E-5 3.94E-5 4.04E-5 0.92E-5 1.00E-5 1.10E-5 1.32E-5 1.53E-5 1.68E-5 1.96E-5 2.09E-5 2.24E-5 2.41E-5 2.55E-5 2.74E-5 2.94E-5 3.23E-5 3.39E-5 3.53E-5 3.87E-5 4.06E-5	8.1pc	S.G.	90
ARGON	TETRA-FLUORO-METHANE	88K 90.5K 93K 95.5K 98K 103K 108K 113K 118K 123K 128K 133K 138K 143K	0 0.9 atm of A to 0.1 atm		3.02E-6 3.39E-6 3.33E-6 4.50E-6 4.84E-6 6.23E-6 7.59E-6 9.20E-6 1.12E-5 1.28E-5 1.59E-5 1.79E-5 2.11E-5 2.40E-5	8.1pc	S.G.	90

A	B	T	Xa	Da	Db	ERROR	METHOD	REF.
ARGON	TETRA-FLUORO-METHANE (cont.)	70K	0.9 atm of A to 0.1 atm B		1.37E-6			
		72K			3.30E-6			
		75K			5.99E-6			
		77K			6.94E-6			
		81K			9.13E-6			
		85K			1.09E-5			
		87K			1.15E-5			
		89K			1.42E-5			
		91K			1.38E-5			
		93K			1.60E-5			
		97K			1.72E-5			
		101K			1.87E-5			
		101.5K			1.88E-5			
		105.5K			1.88E-5			
		109K			1.84E-5			
		109.5K			1.95E-5			
		111K			1.70E-5			
		113K			1.21E-5			
		117K			1.46E-5			
		121K			1.51E-5			
		125K			1.68E-5			
		130K			1.74E-5			
		133K			1.84E-5			
BENZENE	CARBON TETRA-CHLORIDE	21C	AX	GRAPH		5pc to 15pc	S.G.	36
BENZENE	CARBON DI-SULPHIDE	21C	AX	GRAPH		5pc to 15pc	S.G.	36
BENZENE	CHLORO-FORM	17C	AX	GRAPH OF PROTON DIFFUSION COEFF.		7pc	S.G.	40
BENZENE	CYCLO-HEXANE	25C	0.0	1.88E-5	1.42E-5	5pc to 10pc	S.G.	23 24
			0.1	2.11E-5	1.58E-5			
			0.2	2.26E-5	1.76E-5			
			0.3	2.34E-5	1.87E-5			
			0.4	2.41E-5	1.97E-5			
			0.5	2.44E-5	2.03E-5			
			0.6	2.44E-5	2.09E-5			
			0.7	2.42E-5	2.15E-5			
			0.8	2.38E-5	2.21E-5			
			0.9	2.31E-5	2.14E-5			
			1.0	2.25E-5	2.09E-5			
				GRAPH	GRAPH			

A	B	T	Xa	Da	Db	ERROR	METHOD	REF.
BENZENE	HEXA-FLUORO-BENZENE	25C 60C	AX	GRAPH	GRAPH	5pc to 15pc	S.G.	36
n-BUTYL ALCOHOL	CARBON TETRA-CHLORIDE	20C	.1 to 1.0	GRAPH			S.G.	39
tert BUTYL ALCOHOL	CARBON TETRA-CHLORIDE	21C	AX	GRAPH		5pc to 15pc	S.G.	36
tert BUTYL ALCOHOL	CARBON DI-SULPHIDE	21C	AX	GRAPH		5pc to 15pc	S.G.	36
tert BUTYL ALCOHOL	WATER	0C	1 to 14M	GRAPH	GRAPH	10pc	S.G.	20
CARBON TETRA-CHLORIDE	ETHYL ALCOHOL	20C	.1 to 1.0		GRAPH		S.G.	39
CARBON TETRA-CHLORIDE	DECANE	20C	AX		GRAPH		S.G.	38
CARBON TETRA-CHLORIDE	DODECANE	20C	AX		GRAPH		S.G.	38
CARBON TETRA-CHLORIDE	HEXANE	20C	AX		GRAPH		S.G.	38
CARBON TETRA-CHLORIDE	METHYL ALCOHOL	20C	.1 to 1.0		GRAPH		S.G.	39
CARBON TETRA-CHLORIDE	METHYL CYANIDE	21C	AX		GRAPH	5pc to 15pc	S.G.	36
CARBON TETRA-CHLORIDE	OCTANE	20C	AX		GRAPH		S.G.	38

A	B	T	Xa	Da	Db	ERROR	METHOD	REF.
CARBON TETRA-CHLORIDE	PROPYL ALCOHOL	20C	.1 to 1.0		GRAPH		S.G.	39
CARBON TETRA-CHLORIDE	TETRA-DECANE	20C	AX		GRAPH		S.G.	38
CARBON TETRA-CHLORIDE	TETRA-METHOXY SILANE	21C	AX		GRAPH	5pc to 15pc	S.G.	36
CARBON TETRA-CHLORIDE	TETRA-METHYL SILANE	21C	AX		GRAPH	5pc to 15pc	S.G.	36
CARBON TETRA-CHLORIDE	TETRA-METHYL TIN	21C	AX		GRAPH	5pc to 15pc	S.G.	36
CARBON TETRA-CHLORIDE	TRI-METHYL-IODO-METHANE	21C	AX		GRAPH	5pc to 15pc	S.G.	36
CARBON DISULPHIDE	METHYL ALCOHOL	36C to c50C	.21 .36 .57		GRAPH	2pc	S.G.	37 65
CARBON DI-SULPHIDE	TETRA-METHOXY SILANE	21C	AX		GRAPH	5pc to 10pc	S.G.	36
CARBON DI-SULPHIDE	TETRA-METHYL SILANE	21C	AX		GRAPH	5pc to 10pc	S.G.	36
CARBON DI-SULPHIDE	TETRA-METHYL TIN	21C	AX		GRAPH	5pc to 10pc	S.G.	36
CARBON DI-SULPHIDE	TRI-METHYL-IODO-METHANE	21C	AX		GRAPH	5pc to 10pc	S.G.	36

A	B	T	Xa	Da	Db	ERROR	METHOD	REF.
CHLOROFORM	TRI-ETHYL-AMINE	17C	AX	GRAPH OF PROTON DIFFUSION COEFF.		7pc	S.G.	40
CYCLO-HEXANE	HEXA-FLUORO-BENZENE	25C 60C	AX	GRAPH	GRAPH	5pc to 10pc	S.G.	36
DI-METHYL-SULPHOXIDE	WATER	15C 26C 35C	AX	GRAPH	GRAPH	5pc	P.G.	67 68
DIOXAN	WATER	20C	AX	GRAPH OF PROTON DIFFUSION COEFF.			S.G.	33
DIOXAN	WATER	54C 34C 10C 54C 34C 10C	AX 0 to .6 0 to .6	GRAPH GRAPH	 GRAPH		S.G.	77
DIOXAN	WATER	25C 46C 59C 	100V 75 50 33 9.1 100V 75 50 33 9.1 100V 75 50 33 9.1	1.24E-5 7.16E-6 6.00E-6 6.56E-6 8.5E-6 1.90E-5 1.29E-5 1.07E-5 1.02E-5 1.7E-5 2.42E-5 1.81E-5 1.45E-5 1.72E-5 1.80E-5		5pc to 10pc	S.G.	78
ETHYL ALCOHOL	WATER	25C	1 to 16M	GRAPH	GRAPH	10pc	S.G.	20
ETHYL ALCOHOL	WATER	20C	AX	GRAPH OF PROTON DIFFUSION COEFF.			S.G.	66

A	B	T	Xa	Da	Db	ERROR	METHOD	REF.
ETHYLENE	SULPHUR HEXA-FLUORIDE	6.2C to 25.5C	.8	GRAPH	GRAPH	3pc	S.G.	94 55
		17.5C to 39C	.51	GRAPH	GRAPH			
		38C to 58C	.18		GRAPH			
ETHYLENE GLYCOL	METHYL ALCOHOL	0C to 60C	AX	GRAPH	GRAPH	5pc	S.G.	25
FORMAMIDE	WATER	32C 37C 72.5C	0 to .37	GRAPH OF PROTON DIFFUSION COEFF.			S.G.	41
HEPTANE	PER-FLUORO-METHYL-CYCLO-HEXANE	26C to c67C	.31 .59 .73	GRAPH		2pc	S.G.	37 65
HEXA-FLUORO-BENZENE	TETRA-METHYL-SILANE	-5C 25C	AX	GRAPH	GRAPH	5pc to 15pc	S.G.	36
HEXA-METHYLENE-TETRAMINE	WATER	0C	0 to .09	GRAPH			P.G.	68
METHYL ALCOHOL	WATER	20C	AX	GRAPH OF PROTON DIFFUSION COEFF.			S.G.	66
1-METHYL PYRIDINE	WATER	20C	AX	GRAPH OF PROTON DIFFUSION COEFF.			S.G.	33
iso-PROPYL ALCOHOL	WATER	20C	AX	GRAPH OF PROTON DIFFUSION COEFF.			S.G.	66
n-PROPYL ALCOHOL	WATER	20C	AX	GRAPH OF PROTON DIFFUSION COEFF.			S.G.	66

A	B	T	Xa	Da	Db	ERROR	METHOD	REF.
PYRIDINE	WATER	27C	100V	1·89E-5		5pc	S.G.	78
			75	7·17E-6		to		
			50	6·84E-6		10pc		
			25	7·80E-6				
			12·5	1·1E-5				
		51C	100V	2·62E-5				
			75	1·44E-5				
			50	1·41E-5				
			25	1·59E-5				
			12·5	1·7E-5				
		74C	100V	3·57E-5				
			75	2·44E-5				
			50	2·27E-5				
			25	2·34E-5				
			12·5	2·3E-5				
TRI-ETHYL-AMINE	WATER	17C	AX	GRAPH OF PROTON DIFFUSION COEFF.		7pc	S.G.	40 95
UREA	WATER	32C	0	GRAPH OF PROTON			S.G.	41
		37C	to	DIFFUSION COEFF.				
		72·5C	·37					

Appendix B-3.

The systems are arranged alphabetically according to the polymeric component. The molecular weight is given when reported. D.P. stands for degree of polymerization.

X_p indicates the weight per cent of polymer.

POLYMER	SOLVENT	T	X_P	D_P	D_S	ERROR	METHOD	REF.
POLY ETHYLENE OXIDE M.Wt. 590 7300 28K 120K 870K 3M	DEUTERO-CHLORO-FORM.	33±2 C	0.5 to 100 p.c.	GRAPH			P.G. and S.E.	32
	CARBON TETRA-CHLORIDE			GRAPH				
	DEUTERATED WATER			GRAPH				
POLY DIMETHYL SILOXANE M.Wt. 746 4.6K 40K 100K 800K	DEUTERO-CHLORO-FORM.	33±2 C	0.5 to 100 p.c.	GRAPH			P.G. and S.E.	32
	CARBON TETRA-CHLORIDE			GRAPH				
	DEUTERATED WATER			GRAPH				
POLY-L-GLUTAMIC ACID D.P. 530	DEUTERATED WATER	25 C	Dil.	GRAPH vs. pH.		10 p.c.	P.G.	76
POLY-ISO-BUTYLENE M.Wt. c.l.5M	BENZENE	70.4 C	0		5.40E-5		P.G.	50
			2.3	2.2±.2E-7	4.59E-5			
			3.8		4.35E-5			
			6.9		4.25E-5			
			10.4	2.7±1E-9	3.81E-5			
			20.2		3.04E-5			
			30.9		2.39E-5			
			38.7		1.87E-5			
			40.6		1.97E-5			
			51.2		1.37E-5			
			59.1		1.02E-5			
			69.5 p.c.		6.85E-6 GRAPH			
POLY-ISO-BUTYLENE	CARBON TETRA-CHLORIDE	300 to 400K	100 p.c.	GRAPH			S.G.	51
		50 C and 30 C	7 to 46 p.c.	GRAPH				
	CARBON DI-SULPHIDE	30 C	7 to 52 p.c.	GRAPH				
	CYCLO-HEXANE	50 C AND 30 C	0 to 59 p.c.		GRAPH			

POLYMER	SOLVENT	T	X_P	D_P	D_S	ERROR	METHOD	REF.
DEUTERATED POLY METHYL METH-ACRYLATE	BENZENE	24±1C	0 10 20 30 p.c.		2.50E-5 1.80E-5 1.17E-5 8.8E-6	± 5p.c.		52
POLY DI-METHYL SILOXANE		322 K to 435 K (M.Wt.= 15K)	100 p.c.	GRAPH			S.G.	91
		296 K to 417 K (M.Wt.= 32K)	100 p.c.	GRAPH				
POLY-STYRENE	BENZENE	25 C	16 p.c.	6.0E-8	1.45E-5		P.G.	49

BIBLIOGRAPHY.

(1) E.M.Purcell, H.C.Torrey, R.V.Pound. Phys.Rev., 69, 37, (1946).

(2) F.Bloch, ibid, 70, 460, (1946).

F.Bloch, W.W.Hansen, M.Packard. ibid, 70, 474, (1946).

(3) E.L.Hahn. ibid, 80, 580, (1950).

(4) E.L.Hahn. Physics Today, Nov., 4, (1953).

(5) H.Y.Carr, E.M.Purcell. Phys.Rev., 94, 630, (1954).

(6) L.J.Burnett,J.F.Harmon. J.Chem.Phys., 57, 1293, (1972).

(7) W.P.A.Hass, G.Seidel, N.J.Poulis. Physica, 26, 834, (1960).

(8) S.K.Gosh, S.K.Sinha. Indian J.Phys., 34, 339, (1960).

(9) H.C.Torrey. Phys.Rev.,104, 563, (1956).

(10) E.O.Stejskal, J.E.Tanner J.Chem.Phys., 42, 288, (1965).

(11) J.E.Tanner. Ph.D. Thesis, The University of Wisconsin, (1966).

(12) T.P.Das, A.K.Saha. Phys.Rev., 93, 749, (1954).

(13) J.E.Anderson, W.H.Geritz. J.Chem.Phys., 53, 2584, (1970).

(14) D.E.Woessner. ibid, 34, 2057, (1960).

(15) J.E.Tanner. ibid, 52, 2523, (1970).

(16) J.E.Tanner. Rev.Sci.Instr., 36, 1086, (1965).

(17) D.C.Douglass, D.W.McCall. J.Phys.Chem., 62, 1102, (1958).

(18) A.G.Anderson, R.I.Garwin, E.L.Hahn, J.W.Horton,
G.L.Tucker, R.M.Walker. J.Appl.Phys., 26, 1324, (1955).

(19) D.C.Douglass, D.W.McCall, E.W.Anderson.
J.Chem.Phys., 34, 152, (1960).

(20) E.V.Goldammer, H.G.Hertz. J.Phys.Chem., 74, 3734, (1970).

(21) A.Kitchlew, B.D. Nageswara Rao. Mol.Phys., 21, 1145, (1971).

(22) D.Kessler, A.Weiss, H.Witte. Ber.Bunsenges.Phys.Chem.,
71, 3, (1967).

(23) D.W.McCall, E.W.Anderson. J.Phys.Chem., 70, 601, (1966).

BIBLIOGRAPHY (continued).

(24) D.W.McCall, D.C.Douglass. J.Phys.Chem., 71, 987, (1967).

(25) K.H.Nothnagel, A.Weiss. Ber.Bunsenges.Phys.Chem., 73, 1033,(1969).

(26) D.E.O'Reilly. J.Chem.Phys., 49, 5416, (1968).

(27) G.M.Panchenkov, V.V.Erchenkov, E.E.Borucenko. Sovrem.Probl.Fiz.Khim., 14, 316, (1970).

(28) D.E.Woessner. J.Phys.Chem., 67, 1365, (1963).

(29) J.V.Gaven, J.S.Waugh, W.H.Stockmayer. J.Chem.Phys.,38,287,(1963).

(30) G.J.Krüger, R.Weiss. Z.Naturforsch., 25a, 777, (1970).

(31) W.Dietrich, B.Gross, R.Kosfeld. ibid, 25a, 40, (1970).

(32) J.E.Tanner, K.J.Liu, J.E.Anderson. Macromolecules, 4, 586,(1971).

(33) M.I.Emel'yanov, I.N.Nikolaev, F.M.Samigullin. Zhurnal.Strukt.Khim., 12, 161, (1971).

(34) D.E.O'Reilly, E.M.Peterson. J.Chem.Phys., 55, 2155, (1971).

(35) D.E.O'Reilly, E.M.Peterson, D.L.Hogenboom. J. Chem. Phys., 57, 3969, (1972).

(36) D.Kessler, H.Witte, A.Weiss. Ber.Bunsenges.Phys.Chem.,73, 368, (1969).

(37) H.Hamann, C.Hoheisel, H.Richtering. Ber.Bunsenges.Phys.Chem., 76, 249, (1972).

(38) A.N.Agishev, M.I.Emel'yanov. Zhurnal Strukt.Khim.,5,377,(1964).

(39) K.A.Valiev, M.I.Emel'yanov. ibid, 5, 814, (1964).

(40) Yu.I.Neronov, G.M.Drabkin. ibid, 7, 662, (1966).

(41) I.V.Matyash, A.I.Toryanik, V.V.Kisel'nik. ibid, 8, 418, (1967).

(42) K.A.Valiev, M.I.Emel'yanov, F.M.Samigullin. ibid, 5, 371, (1964).

(43) R.Kosfeld, J.Schlegel. Adv.Mol.Relaxation Processes, 3, 159, (1972).

(44) B.Boddenberg, R.Haul, G.Oppermann, ibid, 3, 61, (1972).

BIBLIOGRAPHY (continued).

(45) E.O.Stejskal. Adv.Mol.Relaxation Processes, 3, 27, (1972).

(46) K.J.Packer, C.Rees. ibid, 3, 206, (1972).

(47) A.Weiss, K.H.Nothnagel. Ber.Bunsenges.Phys.Chem., 75, 216,(1971).

(48) J.V.Gaven, W.H.Stockmayer, J.S.Waugh. J.Chem.Phys.,37,1188,(1962).

(49) B.Gross, R.Kosfeld. Messtechnik, 7/8, 171, (1969).

(50) B.D.Boss, E.O.Stejskal, J.D.Ferry. J.Phys.Chem., 71, 1501,(1967).

(51) D.W.McCall, D.C.Douglass, E.W.Anderson. J.Polym.Sci., Part A-1, 1709, (1963).

(52) B.Willenberg, H.Sillescu. Ber.Bunsenges.Phys.Chem.,77,95,(1973).

(53) J.S.Murday, R.M.Cotts. J.Chem.Phys., 53, 4724, (1970).

(54) J.S.Murday, R.M.Cotts. ibid, 48, 4938, (1968).

(55) H.Hammon, H.Richtering. Ber.Bunsenges.Phys.Chem.,74,931,(1970).

(56) H.Hammon, H.Richtering, U.Zucker. ibid, 70, 1084, (1966).

(57) J.S.Murday, R.M.Cotts. Z.Naturforsch, 26a, 85, (1971).

(58) G.J.Kruger, W.Müller-Warmuth. ibid, 26a, 94, (1971).

(59) H.S.Sandhu. Can.J.Phys., 49, 1069, (1971).

(60) P.H.Oosting, N.J.Trappeniers. Physica, 51, 418, (1971).

(61) N.J.Trappeniers, C.J.Gerritsma, P.H.Oosting. Phys.Lett., 18, 256, (1965).

(62) D.E.O'Reilly. J.Chem.Phys., 52, 2804, (1970).

(63) D.E.O'Reilly. ibid, 52, 5974, (1970).

(64) E.D.Finch, et al. Arch.Biochem.Biophys., 147, 299, (1971).

(65) C.Hoheisel, H.Richtering. Z.Phys.Chem., 55, 323, (1967).

(66) K.A.Valiev, M.I.Emel'yanov. Zhurnal Strukt.Khim., 5, 7, (1964).

(67) K.J.Packer, D.J.Tomlinson. Trans.Faraday Soc., 66,1302,(1970).

(68) K.J.Packer, C.Rees, D.J.Tomlinson. Diffusion Processes, edited by J.N.Sherwood, A.V.Chadwick, W.M.Muir, F.L.Swinton, chapter 23, vol. 1, Gordon and Breach, Science Pub., Ltd., 1971.

BIBLIOGRAPHY (continued).

(69) R.L.Garwin, H.A.Reich. Phys.Rev., 115, 1478, (1959).

(70) D.W.McCall, D.C.Douglass. J.Phys.Chem., 69, 2001, (1965).

(71) B.D.Boss, E.O.Stejskal. J.Chem.Phys., 43, 1068, (1965).

(72) R.Hausser, G.Maier, F.Noack. Z.Naturforschung.,21a,1410,(1966).

(73) W.T.Higdon, J.D.Robinson. J.Chem.Phys., 37, 1161, (1962).

(74) B.D.Boss, E.O.Stejskal. J.Colloid Interface Sci.,26,271,(1968).

(75) K.J.Packer, C.Rees. ibid, 40, 206, (1972).

(76) R.E.Moll. J.Amer.Chem.Soc., 90, 4739, (1968).

(77) C.J.Clemett. J.Chem.Soc.(A), 458, (1969).

(78) A.Fratiello, D.C.Douglass. J.Mol.Spectrosc., 11, 465, (1963).

(79) C.G.Wade, J.S.Waugh. J.Chem.Phys., 43, 3555, (1965).

(80) R.S.Ehrlich, H.Y.Carr. Phys.Rev.Lett., 25, 341, (1970).

(81) J.D.Noble, M.Bloom. ibid, 14, 250, (1965).

(82) M.Lipsicas. J.Chem.Phys., 36, 1235, (1962).

(83) J.K.Tison, E.R.Hunt. ibid, 54, 1526, (1971).

(84) J.Kärger, W.Seyd, H.Pfeifer, D.Geschke. Magn.Res.Relat.Phenom., Proc.Congr.AMPERE 16th, (1970).

(85) Yu.I.Neronov, O.V.Chviruk. Russ.J.Phys.Chem., 42, 845, (1968).

(86) G.M.Panchenkov, N.N.Borisenko, V.V.Erchenkov. ibid, 43, 421, (1969).

(87) G.M.Panchenkov, N.N.Borisenko, V.V.Erchenkov. ibid, 43, 1328, (1969).

(88) G.M.Panchenkov, N.N.Borisenko, V.V.Erchenkov. ibid, 41, 484, (1967).

(89) W.R.Hackleman, P.S.Hubbard. J.Chem.Phys., 39, 2688, (1963).

(90) J.H.Rugheimer, P.S.Hubbard. ibid, 39, 552, (1963).

(91) D.W.McCall, D.C.Douglass, E.W.Anderson. Ber.Bunsenges.Phys.Chem., 67, 336, (1963).

BIBLIOGRAPHY (continued).

(92) K.T.Gillen, D.C.Douglass, M.J.R.Hoch. J.Chem.Phys.,57,5117,(1972).

(93) D.J.Tomlinson. Mol.Phys., 25, 735, (1972).

(94) H.Hamann, H.Richtering. Ber.Bunsenges.Phys.Chem., 74, 995, (1970).

(95) Yu.I.Neronov, G.M.Drabkin. Russ.J.Phys.Chem., 9, 1439, (1965).

(96) D.W.McCall, C.M.Huggins. Appl.Phys.Lett., 7, 153, (1965).

(97) D.C.Ailon, C.P.Slichter. Phys.Rev., 137, A235, (1965).

(98) D.R.Falcone, D.C.Douglass, D.W.McCall. J.Phys.Chem., 71, 2754, (1967).

(99) J.R.Gaines, K.Luszcynski, R.E.Norberg. Phys.Rev.,131,901,(1963).

(100) R.Mills. Ber.Bunsenges.Phys.Chem., 75, 195, (1971).

(101) R.Mills. J.Phys.Chem., 77, 685, (1973).

(102) M.K.Ahn, S.J.K.Jensen, D.Kivelson. J.Chem.Phys., 57,2940,(1972).

(103) J.N.Northrop, M.L.Anson. J.Gen.Physiol., 12, 543, (1928).

(104) R.H.Stokes. J.Amer.Chem.Soc., 72, 763, (1950).

(105) R.Mills, L.A.Woolf. The Diaphragm Cell, A.N.U. Press, Canberra.

(106) R.Mills. Trans.Faraday Soc., 67, 1654, (1971).

(107) J.Anderson, K.J.Saddington. J.Chem.Soc., S381, (1949).

(108) J.H.Wang. J.Amer.Chem.Soc., 73, 510, (1951).

(109) L.G.Longsworth. J.Phys.Chem., 64, 1914, (1960).

(110) A.J.Hyde Diffusion Processes, edited by J.N.Sherwood, A.V.Chadwick, W.M.Muir, F.L.Swinton, chapter 24, vol.1, Gordon and Breach, Science Pub.,Ltd.,1971.

(111) R.Mills. J.Amer.Chem.Soc., 77, 6116, (1955).

(112) R.Mills, E.W.Godbole. Aust.J.Chem., 11, 1, (1958), 12, 102, (1959).

(113) R.W.Laity. J.Phys.Chem., 63, 80, (1959).

BIBLIOGRAPHY (continued).

(114) L.Onsager. Phys.Rev., 37, 405, (1931).

(115) L.Onsager. ibid, 38, 2265, (1931).

(116) L.Onsager. Ann.New York Acad.Sci., 46, 241, (1945).

(117) R.J.Bearman. J.Phys.Chem., 65, 1961, (1961).
and other papers cited there in.

(118) S.Chapman,T.G.Cowling. The Mathematical Theory of Non Uniform Gases, University Press Cambridge, 1953.

(119) H.A.Al-Chalabi, E.McLaughlin. Mol.Phys., 19, 703, (1970).

(120) G.S.Hartley, J.Crank. Trans.Faraday Soc., 45, 801, (1949).

(121) J.G.Albright, R.Mills. J.Phys.Chem., 69, 3120, (1965).

(122) D.G.Miller. Chem.Rev., 60, 15, (1960).

(123) C.Truesdell. Irreversible Aspects of Continuum Mechanics and Transfer of Physical Characteristics in Moving Fluids, edited by H.Parkus, L.I.Sedov, p 373, Vienna, Springer, 1968.

(124) C.Truesdell. Rational Thermodynamics, pp 121, 122, 127, 139, New York, McGraw Hill, 1969.

(125) Y.Kamei, Y.Oishi. Bull.Chem.Soc.Japan, 45, 2437, (1972).

(126) Y.Oishi, Y.Kamei, A.Nishi. J.Chem.Phys., 57, 574, (1972).

(127) L.S.Darken. Amer.Inst.Min.Met.Eng.Trans., 175, 184, (1948).

(128) H.J.V.Tyrrel. J.Chem.Soc., 1599, (1963).

(129) P.C.Carman, L.H.Stein. Trans. Faraday Soc., 52, 619, (1956).

(130) J.K.Percus, G.J.Yevick. Phys.Rev., 110, 1, (1958).

(131) N.F.Carnahan, K.E.Starling. J.Chem.Phys., 51, 635, (1969).

(132) G.A.Mansoori, N.F.Carnahan, K.E.Starling, T.W.Leland. J.Chem.Phys., 54, 1523, (1971).

(133) J.L.Lebowitz. Phys.Rev., 133, A895, (1964).

BIBLIOGRAPHY (continued).

(134) J.H.Simpson, H.Y.Carr. Phys.Rev., 111, 1201, (1958).

(135) H.R. Pruppacher. J.Chem.Phys., 56, 101, (1972).

(136) A.F.Collings, R.Mills. Trans.Faraday Soc., 66, 2761, (1970).

(137) K.R.Harris, C.K.N.Pua, P.J.Dunlop. J.Phys.Chem., 74,3518, (1970).

(138) L.Eppstein. Results quoted in reference 100.

(139) J.C.Shieh, P.A.Lyons. J.Phys.Chem., 73, 3258, (1969).

(140) J.O.Hirschfelder, C.F.Curtiss, R.B.Bird.
Molecular Theory of Gases and Liquids, p.1110,
Wiley, New York, 1954.

(141) L.S.Tee, S.Gotoh, W.E.Stewart. Ind.Eng.Chem.,Fundam.,5,356,(1966).

(142) J.T.Edward. J.Chem.Educ., 47, 261, (1970).

(143) E.O.Stejskal. Rev.Sci.Instr., 34, 971, (1963).

(144) A.Allerhand. ibid, 41, 269, (1970).

(145) A.J.Strike. J.Phys(E)., 4, 251, (1971).

(146) R.S.Parker, I.Zupancic, J.Pirs. ibid, 6, 899, (1973).

(147) P.A.Johnson, A.L.Babb. J.Phys.Chem., 60, 14, (1956).

(148) A.P.Hardt, D.K.Anderson, R.Rathbun, B.W.Mar, A.L.Babb.
J.Phys.Chem., 63, 2059, (1959).

(149) C.S.Caldwell, A.L.Babb. J.Phys.Chem., 60, 51, (1956).

(150) G.R.Staker, P.J.Dunlop. J.Chem.Eng.Data, 18, 61, (1973).

(151) S.D.Christian, E.Naparko, H.E.Affsprung. J.Phys.Chem., 64, 442, (1960).

(152) D.L.Bidlack, D.K.Anderson. J.Phys.Chem., 68, 3790, (1964).

(153) L.Grunberg. Trans.Faraday Soc., 50, 1292, (1954).

(154) H.Lemonde. Ann.Phys.(Paris), 9, 539, (1938).

(155) D.K.Anderson, J.R.Hall, A.L.Babb. J.Phys.Chem., 62, 404, (1958).

(156) V.A.Kireev, J.P.Sitnikov. Zhurnal Obshch.Khim., 16, 979, (1946).

BIBLIOGRAPHY (continued).

(157) K.N.Marsh. Trans.Faraday Soc., 64, 894, (1968).

(158) B.J.Levien, K.N.Marsh. J.Chem.Thermodynamics, 2, 227, (1970).

(159) T.M.Reed, K.E.Gubbins. Applied Statistical Mechanics, p 257, McGraw-Hill, New York, 1973.

(160) G.G.Allen, P.J.Dunlop. Phys.Rev.Lett., 30, 316,(1973).

(161) T.G.Bissel, G.E.Okafor, A.G.Williamson. J.Chem.Thermodynamics, 3, 393, (1971).